STABILITY AND ACTIVITY OF A GPCR *IN VIVO* AND IN MEMBRANE MIMETIC ENVIRONMENTS

by

Andrea N. Naranjo

A dissertation submitted to the Faculty of the University of Delaware in partial fulfillment of the requirements for the degree of Doctor of Philosophy in Chemical Engineering

Fall 2014

ProQuest LLC.
789 East Eisenhower Parkway
P.O. Box 1346
Ann Arbor, MI 48106 - 1346

STABILITY AND ACTIVITY OF A GPCR *IN VIVO* AND IN MEMBRANE MIMETIC ENVIRONMENTS

by

Andrea N. Naranjo

Approved: _____
Abraham M. Lenhoff, Ph.D.
Chair of the Department of Chemical and Biomolecular Engineering

Approved: _____
Babatunde A. Ogunnaike, Ph.D.
Dean of the College of Engineering

Approved: _____
James G. Richards, Ph.D.
Vice Provost for Graduate and Professional Education

I certify that I have read this dissertation and that in my opinion it meets the academic and professional standard required by the University as a dissertation for the degree of Doctor of Philosophy.

Signed: _____

Anne S. Robinson, Ph.D.
Professor in charge of dissertation

I certify that I have read this dissertation and that in my opinion it meets the academic and professional standard required by the University as a dissertation for the degree of Doctor of Philosophy.

Signed: _____

Kelvin H. Lee, Ph.D.
Member of dissertation committee

I certify that I have read this dissertation and that in my opinion it meets the academic and professional standard required by the University as a dissertation for the degree of Doctor of Philosophy.

Signed: _____

Abraham M. Lenhoff, Ph.D.
Member of dissertation committee

I certify that I have read this dissertation and that in my opinion it meets the academic and professional standard required by the University as a dissertation for the degree of Doctor of Philosophy.

Signed: _____

Edward R. Lyman, Ph.D.
Member of dissertation committee

ACKNOWLEDGMENTS

I would not have been able to reach this far without the support of my family. Since early in my life my father cultivated my scientific curiosity and problem solving skills. My parents always made sacrifices (e.g. encouraged me to leave Ecuador to pursue my education in chemical engineering in the United States). My brother and sister always remind me of who I am and give me the strength, advice, and encouragement I need in difficult times. Along the way there were people (Ernie and Jan Dyer) and foundations (National Science Foundation) that saw potential in me and supported my education. I will be forever thankful and some day I will give back to society by encouraging people to pursue careers in science and engineering.

At North Carolina State University, Prof. Carol Hall instilled in me my passion for thermodynamics and for understanding biological phenomena at a molecular level. Prof. Anne Robinson gave me the opportunity to explore membrane protein function and molecular interactions in her laboratory; throughout my years in graduate school with patience and dedication she helped me develop as an independent researcher. I was very fortunate to have her as my advisor, as she let me explore areas where I had limited initial exposure (e.g. anisotropy), she helped become a better educator (gave me the opportunity to teach in some of her classes and supported me to pursue a higher education teaching certification), she facilitated and encouraged me to establish fruitful collaborations (i.e. Prof. John Katsaras, Prof. Edward Lyman, and Prof. Carola Wenk), and was always supportive and understanding during tough personal circumstances. I will never forget the opportunities that she created for me. I also

thank my thesis committee, Prof. Kelvin Lee, Prof. Abraham Lenhoff, and Prof. Edward Lyman, for helpful discussion and invaluable input given throughout these years.

My graduate school journey has been full of challenges and accomplishments, and I was fortunate to have the support of wonderful mentors, colleagues and friends throughout this journey. From the start my research was influenced by helpful discussions, advice and guidance from the members of Prof. Anne Robinson's laboratory. I will like to give special thanks to Dr. Emily McCusker, Prof. Michelle O'Malley, Dr. Michelle Spatara, Prof. Özge Can, Dr. David Raden, Patrick McNeely, Dr. Melissa St. Amand, Christopher O'Brien, Claire McGraw, Emily Wilkinson, Dr. Kory Blocker and Dr. Arash Foroutan. Many group members in Prof. Millicent Sullivan, Prof. Wilfred Chen, Prof. Kelvin Lee, Prof. David Colby and Prof. Norman Wagner laboratories helped me throughout the years, guiding me through techniques, instrumentation and helpful discussions, with special thanks to Dr. Peter Millili, Dr. Kory Blocker, Dr. John Larsen, Dr. Abbygail Foster, Dr. Scott Crown, Dr. Kristin Valente, and Dr. Eric Yearley. I would like to thank Prof. Maciek Antoniewicz, Prof. Wilfred Chen, Prof. Fraser Russell, Dr. Tzvetana Lazarova and Prof. Christopher Roberts for helpful discussion in the hallway or for taking the time to prepare me prior to important presentations. I would like to thank Prof. Eleftherios Papoutsakis, Prof. Eric Kmiec and the members of their laboratories for their time and guidance provided during my IGERT laboratory rotations. I will also like to thank Prof. Wilfred Chen and the members of his laboratory for welcoming me to their group meetings during the Robinson laboratory transition to Tulane University. Many thanks to Dr. Gabriele Bauer for her guidance throughout the completion of the higher education teaching

certification program. Special thanks to Kathie Young, George Whitmyre, Gary Wellmaker, Lisa Henriksen, Lisa Dougherty, Mary Malsh, Megan Argoe, Chil Alba and Susan Brook. Your help and support was critical for my time in graduate school to go smoothly.

Special thanks to my collaborators (Prof. Edward Lyman, Prof. Carola Wenk, Patrick McNeely, Dr. John Katsaras and Dr. Robert Standaert) for contributing with invaluable experiments, information and advice. Their contribution made the research presented in this thesis stronger as we strived to contribute to the G protein-coupled receptor filed by bridging biology, biophysics and computational methods. Dr. Kirk Czymmek and Dr. Jeffrey Caplan for their help with confocal imaging and protocol development.

Overall, working toward my PhD has been the most rewarding experience of my life. After so many struggles and successes, no words can explain the feeling of seeing the completion of so much work and contributing to the scientific community. I shared the ups and downs of the first three years in graduate school with some of the most amazing people I have met (Melissa L, Ale, Mercedes, Ivan, Mehmet, Jeff, Melissa SA, Abby, Andrew, Jake, Scott, Diane, Michelle, Matt, Pete, Kory, John, Özge and Chris). I had the opportunity to work with excellent high school and undergraduate students that contributed to the work described in this thesis (Amy Chevalier, Gregory D. Cousins, Esther Ayettey, and Justin Huckaby); I learnt so much from each of them, they helped me become a better mentor and made my desire to pursue a career in academia stronger. Finally, I would like to thank Patrick McNeely, I am blessed to have shared my journey through graduate school with him and I cannot wait for our next adventure together.

Dedication

To my parents (Patricio and Ana). Thank you for all the dedication, love and advice throughout my life. The values, moral, and confidence that you instilled in me have allowed me to get this far. To my beautiful mom, you will always brighten every day of my life.

TABLE OF CONTENTS

LIST OF TABLES

LIST OF FIGURES

ABSTRACT

G protein-coupled receptors (GPCRs) are integral membrane proteins involved in cellular signaling and constitute major drug targets. Despite their importance, the relationship between structure and function of these receptors is not well understood. GPCRs bind to extracellular ligands; the binding to a ligand causes a conformational change in the receptor and the interaction of the GPCR with intracellular G protein, starting a cascade of cellular events. This canonical GPCR signaling model is being constantly revised to include new experimental evidence of how allosteric ligands (that bind in a pocket distinct from the orthosteric binding pocket), lipids, and other membrane proteins modulate the GPCR signaling.

The objective of this research was twofold: 1) understanding structural and environmental factors important for GPCR expression, trafficking and function, and 2) developing *in vitro* membrane-mimetic reconstitution environments to characterize ligand-binding kinetics and lipid-receptor interactions.

The role of extracellular disulfide bonds on the trafficking and ligand-binding activity of the full-length human A_{2A} adenosine receptor ($A_{2A}R$) was examined. To this end, systematic cysteine-to-alanine mutations were conducted to replace individual and paired cysteines in three disulfide bonds present in the first two extracellular loops. Although none of the disulfide bonds were essential for the formation of plasma membrane-localized active GPCR, loss of the disulfide bonds led to changes in the distribution of the receptor within the cell and changes in the ligand-binding affinity. These results indicate that in contrast to many class A GPCRs, the

extracellular disulfide bonds of the A_{2A} receptor are not essential (including the conserved disulfide bond), but can modulate the ligand-binding activity, by either changing the conformation of the extracellular loops or perturbing the interactions of the transmembrane domains.

There is growing evidence that ligand-binding rate constants could be better predictors of drug efficacy than affinity measurements. However ligand-binding kinetics are not well characterized, as they are more challenging to measure experimentally, and rarely investigated. Using fluorescence anisotropy and $A_{2A}R$ solubilized in micelles, we determined the ligand-binding affinity and kinetics of various ligands. The determination of inhibitor dissociation constants (K_i) for six unlabeled ligands further validated the use of fluorescence anisotropy and micelle solubilized receptor for the characterization of binding affinity. We also applied fluorescence anisotropy and the analytical solution to a mass action model for two-ligand competing for one binding site, to determine the association and dissociation rate constants for three unlabeled ligands (NECA, adenosine, and ZM 241385), in competition with fluorescent ligand FITC-APEC. We identified that the different affinities between two structurally similar agonists (NECA and adenosine) result from differences in their residence time (i.e. $1/k_{off}$). Furthermore, we determined that the higher affinity of ZM 241385 results primarily from a faster association rate.

Previous studies of $A_{2A}R$ purified using the detergent dodecylmaltoside (DDM), found that a cholesterol analog was critical for ligand binding and conformational stability of the receptor. Here, we show that $A_{2A}R$ purified using a short hydrocarbon-chain lipid (1,2-dihexanoyl-sn-glycero-3-phosphocholine, DHPC) retains functionality and stability in the absence of added sterol. Additionally, longer

chain lipids (1,2-dimyristoyl-sn-glycero-3-phosphocholine, DMPC, di-14:0PC) can be added to $A_{2A}R$ purified in DHPC to form bicelles, a biologically more relevant membrane-mimetic environment. Overall, the studies and assays described in this thesis will be important as we begin to understand the emerging ligand-lipid-receptor-effector relationships.

Chapter 1

INTRODUCTION

1.1. G Protein-Coupled Receptors

G protein-coupled receptors (GPCRs), characterized by their seven α-helical transmembrane domains, are one of the largest and most diverse families of membrane proteins involved in signal transduction [1]. Because of their location at the plasma membrane and their importance in cellular signaling, GPCRs constitute major drug targets; approximately 30% of drugs on the market are known to target GPCRs [1, 2]. In 2001, 50% of all new drugs targeted GPCRs and the annual sales of these drugs exceeded $30 billion [3].

GPCRs respond to various extracellular ligands, such as hormones and neurotransmitters [4]. The binding of a ligand to a GPCR causes a conformational change of the receptor, triggering a signaling cascade and resulting in a cellular response. Ligands are classified into three main categories depending on the type of cellular response that they trigger. Agonists cause a shift in the conformation of the receptor that allows the coupling of the receptor to intracellular G proteins [3], Figure 1.1. Antagonists bind the receptors and block the binding site, while inverse agonists bind the receptors causing a shift toward an inactive conformation, thus impeding the coupling to G proteins [5].The binding site where endogenous ligands (e.g. adenosine, dopamine) bind, is known as the orthosteric binding site.

In recent years the canonical GPCR binding model has been altered to include allosteric ligands, which act away from the traditionally recognized binding site [6],

and other effectors such as kinases and arrestins [1]. It is not well understood how these recently reported GPCR-ligand-effector interactions impact GPCR signaling, and the potential of targeting these allosteric sites for the development of therapeutics has not been fully explored. Ligands can modulate the pharmacological response to treatment by combining the effects of ortho- and allosteric binding, thus fine-tuning the effects of treatment using each signaling mechanism [7]. Apart from GPCR signal modulation through allosteric ligands, other mechanisms that modulate GPCR signaling have been identified [7]; some of these mechanisms are illustrated in Figure 1.1.

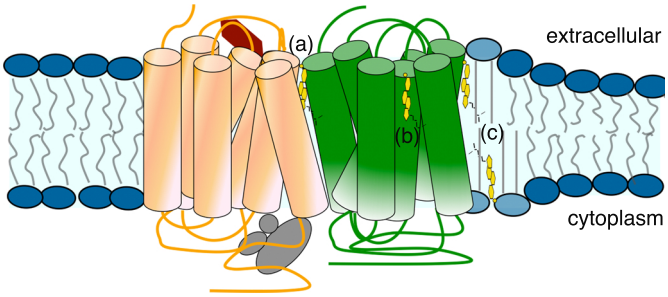

Figure 1.1 GPCR signaling modulation by the membrane environment. GPCR signal modulation can be altered through: (a) oligomerization, (b) direct GPCR-cholesterol binding, and (c) different lipid composition that affects the physical properties of the membrane (e.g. fluidity and curvature). GPCRs are shown in orange and green, cholesterols in yellow, sphingolipids in light blue, ligand in red and the intracellular G protein in gray.

The lipid environment of the plasma membrane also provides an interface that has been postulated to modify receptor activity [8, 9]. Cells derived from different tissues naturally have differing lipid compositions [10], and lipid domain composition variations have been observed within single cells as well [11]. The interaction of

GPCRs with other membrane proteins and lipids at the plasma membrane has been investigated for the past 20-30 years [8]. There is growing evidence that lipid heterogeneities in the membranes (e.g. lipid rafts) [12], direct interaction of cholesterol and other lipids, and receptor-receptor interactions can modulate GPCR signaling [3, 7, 13-16].

1.2. Adenosine Receptors

The adenosine receptors (A_1, A_3, A_{2B} and A_{2A}) are members of the family A GPCRs, and are ubiquitously expressed throughout the human body (Figure 1.2). This subfamily is one of the main targets for the treatment of neurodegenerative diseases, diabetes, inflammatory diseases, cancer and heart disease [5, 17, 18]. The adenosine receptors are known to interact with 12 marketed drugs [19], yet are the target of 88 known natural and synthetic ligands [20]. The "recognition promiscuity" of drugs with this family frequently leads to unintended physiological responses. This problem is not only inherent to GPCRs; receptors in general are the targets of 111 approved drugs, but 2278 side effects have been associated with them [7]. These side effects present an ongoing challenge to researchers, clinicians, and patients, but also represent an opportunity to improve future generations of drugs.

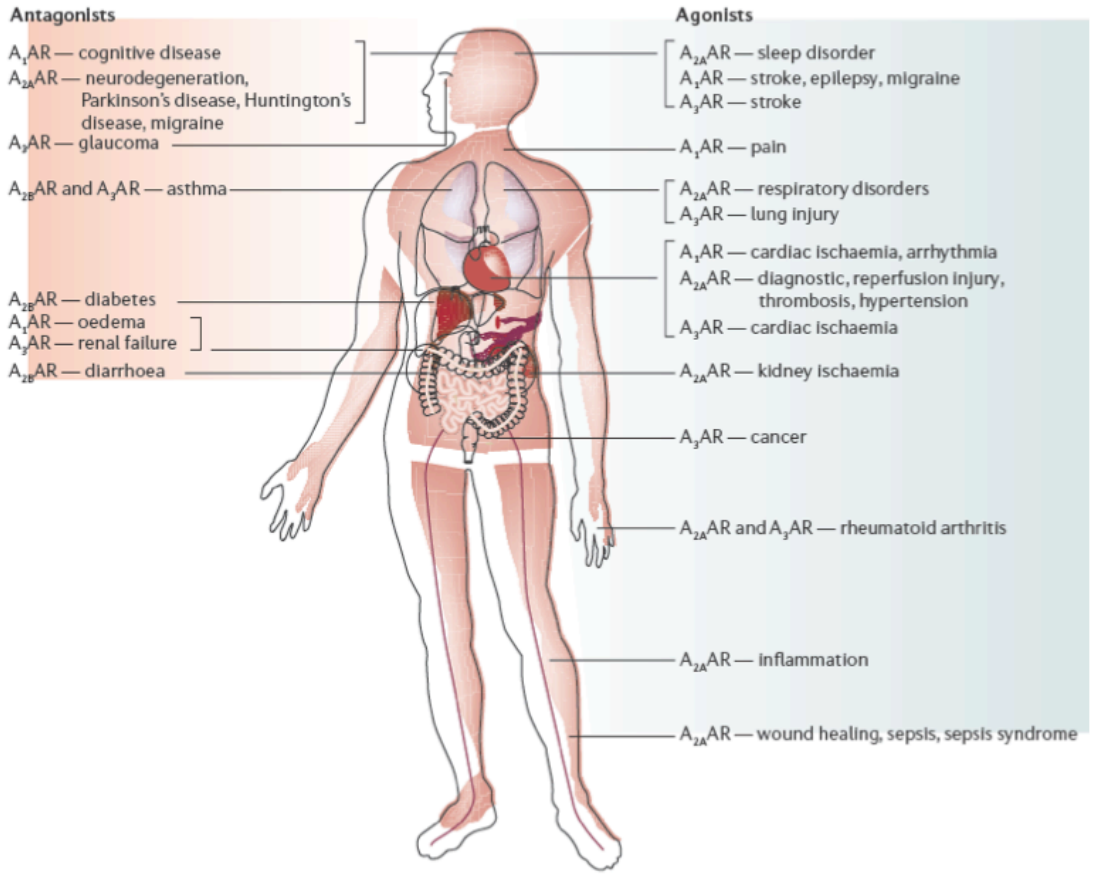

Figure 1.2 Adenosine receptors as potential therapeutic targets. Distribution of the adenosine receptors throughout the body and diseases that could potentially be treated by targeting adenosine receptors. Figure reproduced from [17] with permission (license number: 3459521281031).

The adenosine receptors (ARs) maintain a sequence homology of approximately 40%, with the highest sequence identity between A_{2A} and A_{2B} (46%), and A_1 and A_3 (46%) [21]. Despite the high sequence homology, the ARs have distinct affinities for various ligands and couple to different G proteins, whose activation regulates different membrane and intracellular proteins (e.g. adenylyl cyclase, Ca^{2+} channels, K^+ channels, and phospholipase C) [22]. Out of the four ARs, only the A_{2A}

receptor ($A_{2A}R$) expresses at high levels in heterologous systems [23] and has been extensively studied in biophysical and structural studies [24-31].

1.3. Heterologous Expression of Human GPCRs

The signaling effects of a receptor are most naturally gauged by observing phenotypic effects of modulation in the native environment. Mouse and fruit fly studies have been crucial to understand GPCR networks and the cellular pathways to disease [3, 7]. Cell culture has also been an invaluable vehicle to assess the engineering of receptors; the relatively quick turnaround and ease of experimentation has led to a number of advances in the understanding of receptor activity *in vivo* [32, 33].

In addition to *in vivo* studies, biochemical and biophysical studies are essential as complementary methods to understand the mechanisms behind receptor-ligand and receptor-receptor interaction at a molecular level. However, studying these receptors *in vitro* is very challenging due to their low expression in the native system, poor expression in heterologous hosts, difficult purification due to their hydrophobic transmembrane domains, and instability in the solubilization systems [7, 26, 34-37].

Despite these difficulties, heterologous expression of GPCRs has pressed forward over the years as the most straightforward alternative to models in native tissues or animals, and remains the most frequent means of obtaining large quantities of protein for further characterization *in vitro* [7]. Only rhodopsin has been crystallized from its native tissue with its wild type sequence; all other GPCRs have required protein engineering to stabilize the receptor or facilitate crystallization [38].

Protein engineering and expression have been performed using a variety of model cell systems, including bacteria, yeast, insect and mammalian cell lines [39-41].

Expression in all of these systems has yielded mixed results, leading to the continued use of trial and error approaches to determine the best expression system for any particular receptor [42]. When an adequate expression system is identified for a receptor of interest, these cell lines may produce sufficient protein sample for further study using powerful *in vitro* methods.

1.4. Purification of GPCRs for Structural and Biophysical Studies

Following expression, purification of membrane proteins from culture has been the major bottleneck preventing further characterization [39]. Structural determination and other biophysical studies require solubilization and purification from the cellular debris. Detergents must be tested for the solubilization and structural stabilization of the membrane protein [43, 44]. Detergent interaction could compromise the protein activity through direct interactions, or due to physical properties of micelles, as micelle dimensions are expandable and have a high degree of curvature [45]. These characteristics may not mimic the membrane environment appropriately and can pose challenges for crystal contact formation [46, 47]. The end goal of this lengthy process is to obtain a highly purified receptor that retains its native structure, dynamics, and ligand-binding functionality in order to properly mimic *in vivo* signaling activity [45].

Historically, high-resolution structures have been one ideal paradigm for understanding the mechanism of protein interactions and how the structure relates to the biological function of membrane proteins. Most discovery projects for drugs against soluble protein targets have used medicinal chemistry, directed at or guided by the crystal structures at some stage of the project [48]. Structure-based drug discovery methods have not been widely applied to GPCRs, or membrane proteins in general, due in large part to the lack of crystal structures. There have been more challenges to

structural resolution of membrane proteins than originally anticipated, in part due to the low expression level of membrane proteins in their native tissue [36], the instability of receptors in detergent solutions, and structural or conformational flexibility [45] of the purified protein. As of September 2014, there were 103,354 deposited protein structures in the Protein Data Bank (http://www.rcsb.org/pdb). Of these, fewer than 3% of the structures were of membrane-associated proteins and peptides [10, 49], corresponding to 501 unique membrane proteins (data obtained from Stephen White's website, http://blanco.biomol.uci.edu/mpstruc/listAll/list). Of these, 291 represent eukaryotic membrane proteins (data obtained from Stephen White's website). Thus, structural knowledge for membrane proteins remains far underrepresented compared to that of soluble proteins [50].

The rate of the structural determination of membrane proteins has increased in the past 14 years, and there are now high-resolution crystal structures for 29 different GPCRs, as part of the 501 aforementioned structures. For a recent review on high-resolution GPCR crystal structures refer to [51] and for a complete list of GPCRs with high resolution crystal structures refer to Stephen White's website. Some of these structures were determined using a variety of bound ligands (both agonist and antagonist), lipids, or the intracellular G protein [13, 38, 52]. The GPCR crystal structures reveal common and diverse features of the GPCRs, important characteristics of the ligand-binding pocket, GPCR motifs, possible allosteric sites, dimerization interfaces and structural conformational changes in the receptor important for G protein interaction [13, 51]. These structures, together with continuing advances in expression and crystallization of membrane proteins, will open the possibility to use

structure-based methods for the identification and design of new pharmaceuticals targeted to these membrane proteins [13, 48].

The structural knowledge gained from these experiments has opened valuable insights into the activity of receptors, but has also introduced new questions as the complexity of the signaling pathway has become clearer. The emergence of new types of ligand-receptor-effector relationships [38] and the understanding of how lipids and receptor oligomerization state modulate signaling have provided evidence for signaling mechanisms distinct from the orthosteric ligand binding site that may provide a rich source of targets for therapeutics [51]. High-resolution crystal structures that specifically capture transitional structures as the receptor enters an active signaling state [53], or through structural data of the receptors in native-like environments [45], will help address these unresolved questions. However, it is important to complement structural studies with *in vivo* and *in vitro* biophysical studies, which can provide dynamic and functional information of proteins.

The Robinson laboratory has successfully expressed the full-length human $A_{2A}R$ in yeast, *S. cerevisiae.* The successful expression of $A_{2A}R$ in yeast and the identification of a solubilization system that retains the receptor's native-like conformation and activity have enabled functional and biophysical studies of this receptor in the Robinson laboratory [23-25, 54-56], as outlined briefly below.

1.5. Successful Expression of Human $A_{2A}R$ in Yeast Cells

Many yeast strains have been utilized for the expression of human GPCRs; our lab utilizes *S. cerevisiae*. Compared to other expression systems (i.e. mammalian cells and insect cells), *S. cerevisiae* advantages include low cost, rapid growth and a well-characterized genome that can be easily manipulated [23]. Furthermore, like higher

eukaryotes, yeast possesses a compartmentalized secretory pathway and is able to perform various post-translational modifications [57].

The Robinson laboratory has successfully expressed the full-length human A_{2A} adenosine receptor in *S. cerevisiae* [23, 56]. However, the other members of the adenosine receptor subfamily (A_1, A_3, and A_{2B}) exhibit a very different trafficking pattern when expressed in *S. cerevisiae*, with most of the receptor population retained intracellularly (Figure 1.3).

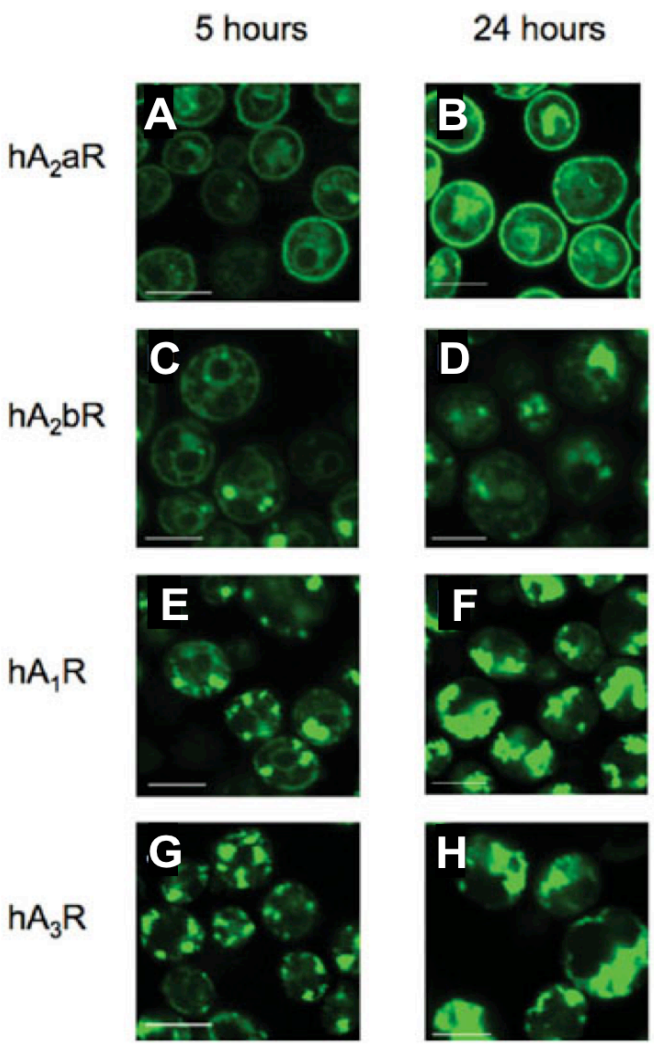

Figure 1.3 Representative confocal images of GFP-tagged human adenosine receptors in *S. cerevisiae*. Column headings denote images taken 5 hours and 24 hours post-induction with galactose. Expression of $A_{2A}R$-GFP (A-B), $A_{2B}R$-GFP (C-D), A_1R-GFP (E-F), and A_3R-GFP (G-H). Scale bar represents 5 μm. Image modified from [23] with permission (license number: 3462000288342).

O'Malley et al. observed that the receptors retained intracellularly (A_{2B}, A_1 and A_3) also activated the unfolded protein response (UPR) and heat shock response (HSR) pathways [23]. Despite the high levels of expression of $A_{2A}R$ in yeast, $A_{2A}R$ is

able to fold and traffic to the plasma membrane, passing the endoplasmic reticulum (ER) quality control. These studies indicated that A_{2B}, A_1 and A_3 expressed at high yields in *S. cerevisiae*; however, problems with the folding and/or trafficking of these receptors arose early in the secretory pathway.

1.6. Biophysical Characterization of Human $A_{2A}R$

The successful expression of the full-length human A_{2A} adenosine receptor in *S. cerevisiae* has enabled the purification of functional receptor at ~6 mg/L of culture. The high yield and purity has allowed the biophysical characterization of $A_{2A}R$ in our laboratory [24, 25, 54, 55]. These studies showed that the full-length human $A_{2A}R$ purified in dodecylmaltoside (DDM) required the cholesterol analogue cholesteryl hemisuccinate (CHS), in order to retain its α-helical content and ligand-binding activity [25]. In addition ligand-binding activity of $A_{2A}R$ increases monotonically with increasing amounts of CHS and is highest at 12 CHS monomers per mixed micelle, corresponding to a mole fraction of approximately 20% [54, 55].

Grisshammer and colleagues also described the need of CHS for the activity of a C-termimal truncated $A_{2A}R$ variant (truncated to Ala316) purified and refolded from *E. coli* [58]. Recently, specific $A_{2A}R$-cholesterol interaction sites (IS) were identified using molecular dynamics [59] and cholesterols were resolved in one of the $A_{2A}R$ crystal structures [30].

It remains unclear whether the cholesterol modulates $A_{2A}R$ activity through specific interactions or due to differences in the physical characteristics of the membrane imparted by cholesterol (e.g. curvature, fluidity, and thickness). Moving forward, it is important to understand at a molecular level the interaction between receptors and lipids.

1.6.1. Structural Features Important for the Stability and Function of $A_{2A}R$

The crystal structure of $A_{2A}R$ identified three disulfide bonds between extracellular loop 1 (ECL1) and ECL2 of the receptor [28]. It is speculated that this extensive disulfide bond network forms a rigid structure exposing the ligand-binding pocket [28]. One of the three disulfide bonds is highly conserved among many class A GPCRs [1, 21, 28], and numerous studies indicate that this disulfide bond is critical for the structural stability, expression, and function of GPCRs [1, 60]. Mutations to the conserved cysteines have shown that this covalent linkage between ECL1 and ECL2 is critical for maintaining the high-affinity ligand-binding conformation of the thyrotropin-releasing hormone receptor [61], rhodopsin [62, 63], μ opioid receptor [64], β_2 adrenergic receptor [65, 66], and A_1 adenosine receptor [67], to name a few.

The role of the disulfide bonds in the structural stability and ligand-binding activity was previously investigated in the Robinson laboratory using purified $A_{2A}R$ solubilized in micelles and the reducing agent *tris*(2-carboxyethyl)phosphine (TCEP) [24]. These studies indicated that the extracellular disulfide bonds present in $A_{2A}R$ are critical for ligand-binding activity, although they do not necessarily impart increased tertiary structure stability.

1.6.2. Importance of Ligand-Binding Kinetics

The first crystal structure of $A_{2A}R$ bound to an antagonist was published in 2008 [28]. Since then, eight structures of $A_{2A}R$ bound to various agonists and antagonists have been published [26-31]. With the availability of agonist- and antagonist-bound structures, molecular modeling can now assist in the identification of the determinants of ligand recognition and guide the design of new drugs with higher affinity [68], and improved binding kinetics. With the identification of novel drugs

that target GPCRs, measurement of ligand binding to the receptor will continue to be an essential component of the drug discovery process, in particular as we investigate the molecular determinants of binding kinetics.

Drugs are defined by three properties: their affinity to the target receptor (quantified by the equilibrium dissociation constant, K_D), the ability to bind the receptor for a sufficient time in order to induce a change in the receptor (characterized by the drug's dissociation rate constant, k_{off}), and the ability to transduce this signal inside the cell and produce the desired cellular response (i.e. the drug's efficacy) [69]. Historically, drug efficacy measurements have been used to guide drug discovery efforts in whole cells, tissues or animals [70]. Upon identification of the molecular targets of various diseases, and advances in cloning, cell-based assays, and purification of the target receptors, binding affinity optimization has guided most early-stage drug discovery efforts, with the assumption that ligand-binding affinity is a suitable surrogate for *in vivo* efficacy [70, 71].

Many efficacious drugs have been identified based on ligand affinity; however, there is recent evidence that suggests that in some cases ligand-binding kinetics could be a better predictor of the drug's efficacy and safety [70].Thus, there is great interest in developing improved methods to measure binding kinetics.

1.6.3. Membrane-Mimetic Systems

The geometry and composition of the membrane environment is critical not only for the characterization technique being used, but also for the membrane protein itself. There is growing evidence of the importance of the membrane environment for the modulation of membrane protein function [13]. Differential receptor activity has been reported in tissues or membranes with different lipid composition [13, 72],

although in these cases it remains unclear whether the interaction is directed through specific lipid-protein interactions or due to differences in the physical characteristics of the membrane (e.g. curvature, fluidity, and thickness) [13, 73]. Recent experiments have found that reconstitution of at least one receptor (β_2-adrenergic receptor) in lipid bilayers or micelles that mimic native conditions leads to a better recovery of the native signaling properties of the receptor [74]. Purified A_{2A} adenosine receptor loses its ligand-binding activity when reconstituted in DDM; however, when reconstituted in DDM with a cholesterol analogue, the receptor retains native ligand-binding affinity [25]. When this micellar system was characterized using small-angle neutron scattering, it was observed that the addition of the cholesterol analogue changed the micelle shape to become more ellipsoidal with a thickness of 32 Å, thus better reflecting the thickness of mammalian membranes [54].

During purification, due to their hydrophobic transmembrane domains, GPCRs need to be solubilized and reconstituted in membrane mimetic systems. Detergents with a hydrophobic tail of 6-12 carbon atoms are commonly used to solubilize and stabilize GPCRs [75]. Detergents are typically optically neutral, enabling characterization via spectroscopic techniques.

Even though detergents are widely used to solubilize membrane proteins, detergent micelles have proven to be less than ideal substitutes for the native membrane environment. In this simplified model system, many of the physical characteristics of native lipid bilayers (e.g. lateral pressure, membrane curvature, topological constraints and acyl chain packing) are poorly duplicated [37, 44, 45]. Even though many GPCRs are stable and retain functionality in detergent micelles, there are GPCRs and other membrane proteins that unfold and aggregate when

solubilized in detergents [44], altering their native structure and eliminating their biological function. In addition, selecting a detergent that retains membrane protein stability and function is often a matter of trial and error [37, 76]. As a result in recent years, more native-like environments such as liposomes, bicelles, and nanodiscs have been used to reconstitute membrane proteins [37, 77]. However, typically detergent micelles are often utilized for the solubilization of membrane proteins prior to the reconstitution in bicelles, liposomes or lipid cubic phases [37]. Compared to detergent micelles, bicelles, liposomes and nanodiscs have an extended planar bilayer region with a less pronounced local curvature, and for the most part are thought to represent a more native-like reconstitution system for membrane proteins. These native-like membrane environments are of interest to study receptor oligomerization and the effects of the lipid environment on GPCR signaling modulation.

1.7. Thesis Objective

Even though there have been advances in the understanding of the structure-function relationship of GPCRs, many questions remain:

- What molecular factors influence the high expression and stability of some GPCRs?
- What are the mechanisms of action of most drugs targeting GPCRs and how can one minimize the side effects associated with the drugs targeting these receptors?
- How do lipid-GPCR interactions and homo- and hetero- dimerization modulate receptor signaling?

We are interested in identifying structural characteristics of $A_{2A}R$ critical for its high expression in heterologous systems. To this end, we investigated the role that the extensive disulfide bond network plays in protein expression and function of $A_{2A}R$ (Chapter 2 and Chapter 3). Understanding the structural factors that influence receptor folding and cellular trafficking is an important step towards overcoming the limitations of the expression of human GPCRs in heterologous systems.

Taking advantage of the successful expression and purification of $A_{2A}R$, we are interested in developing methods to characterize the ligand-binding kinetics (Chapter 4). Many efficacious drugs have been identified based on ligand affinity determination; however, there is recent evidence that suggests that in some cases ligand-binding kinetics could be a better predictor of the drug's efficacy and safety [70]. Insight into the molecular interactions that govern binding kinetics will aid in the design of more effective pharmaceuticals.

Recent evidence suggests that GPCR signaling could be modulated by interactions with other membrane proteins, the lipid environment and allosteric

ligands. We aim to develop a lipid-based solubilization platform where we can study receptor-receptor and receptor-lipid interactions, and the effects that these interactions have on ligand affinity and kinetics (Chapter 5).

REFERENCES

1. Venkatakrishnan, A.J., et al., *Molecular signatures of G-protein-coupled receptors.* Nature, 2013. **494**(7436): p. 185-194.

2. Rask-Andersen, M., M.S. Almen, and H.B. Schioth, *Trends in the exploitation of novel drug targets.* Nature Reviews Drug Discovery, 2011. **10**(8): p. 579-590.

3. Thomsen, W., J. Frazer, and D. Unett, *Functional assays for screening GPCR targets.* Current Opinion in Biotechnology, 2005. **16**(6): p. 655-665.

4. Bosch, L., L. Iarriccio, and P. Garriga, *New prospects for drug discovery from structural studies of rhodopsin.* Current Pharmaceutical Design, 2005. **11**(17): p. 2243-56.

5. Li, J.N., et al., *Ligand-dependent activation and deactivation of the human adenosine A(2A) receptor.* Journal of the American Chemical Society, 2013. **135**(23): p. 8749-8759.

6. Goudet, C., et al., *Metabotropic receptors for glutamate and GABA in pain.* Brain Research Reviews, 2009. **60**(1): p. 43-56.

7. McNeely, P.M., A.N. Naranjo, and A.S. Robinson, *Structure-function studies with G protein-coupled receptors as a paradigm for improving drug discovery and development of therapeutics.* Biotechnology journal, 2012. **7**(12): p. 1451-61.

8. Chini, B. and M. Parenti, *G-protein-coupled receptors, cholesterol and palmitoylation: facts about fats.* Journal of Molecular Endocrinology, 2009. **42**(5-6): p. 371-379.

9. Lee, A.G., *Biological membranes: the importance of molecular detail.* Trends in Biochemical Sciences, 2011. **36**(9): p. 493-500.

10. Lomize, M.A., et al., *OPM: orientations of proteins in membranes database.* Bioinformatics, 2006. **22**(5): p. 623-5.

11. Ziolkowska, N.E., R. Christiano, and T.C. Walther, *Organized living: formation mechanisms and functions of plasma membrane domains in yeast.* Trends in cell biology, 2012. **22**(3): p. 151-158.

12. Lingwood, D. and K. Simons, *Lipid rafts as a membrane-organizing principle.* Science, 2010. **327**(5961): p. 46-50.

13. Oates, J. and A. Watts, *Uncovering the intimate relationship between lipids, cholesterol and GPCR activation.* Current Opinion in Structural Biology, 2011. **21**(6): p. 802-807.

14. Hanson, M.A., et al., *A specific cholesterol binding site is established by the 2.8 A structure of the human beta2-adrenergic receptor.* Structure, 2008. **16**(6): p. 897-905.

15. Pucadyil, T.J. and A. Chattopadhyay, *Role of cholesterol in the function and organization of G-protein coupled receptors.* Progress in Lipid Research, 2006. **45**(4): p. 295-333.

16. Fantini, J. and F.J. Barrantes, *Sphingolipid/cholesterol regulation of neurotransmitter receptor conformation and function.* Biochimica Et Biophysica Acta-Biomembranes, 2009. **1788**(11): p. 2345-2361.

17. Jacobson, K.A. and Z.G. Gao, *Adenosine receptors as therapeutic targets.* Nature Reviews Drug Discovery, 2006. **5**(3): p. 247-264.

18. Orru, M., et al., *Functional changes in postsynaptic adenosine A(2A) receptors during early stages of a rat model of Huntington disease.* Experimental Neurology, 2011. **232**(1): p. 76-80.

19. Knox, C., et al., *DrugBank 3.0: a comprehensive resource for 'Omics' research on drugs.* Nucleic Acids Research, 2011. **39**: p. D1035-D1041.

20. Muller, C.E. and K.A. Jacobson, *Recent developments in adenosine receptor ligands and their potential as novel drugs.* Biochimica et biophysica acta, 2011. **1808**(5): p. 1290-308.

21. Piirainen, H., et al., *Structural features of adenosine receptors: From crystal to function.* Biochimica Et Biophysica Acta-Biomembranes, 2011. **1808**(5): p. 1233-1244.

22. Ciruela, F., et al., *Adenosine receptors interacting proteins (ARIPs): Behind the biology of adenosine signaling.* Biochimica Et Biophysica Acta-Biomembranes, 2010. **1798**(1): p. 9-20.

23. O'Malley, M.A., et al., *Progress toward heterologous expression of active G-protein-coupled receptors in Saccharomyces cerevisiae: Linking cellular stress response with translocation and trafficking.* Protein Science, 2009. **18**(11): p. 2356-2370.

24. O'Malley, M.A., et al., *Analysis of Adenosine A(2)a Receptor Stability: Effects of Ligands and Disulfide Bonds.* Biochemistry, 2010. **49**(43): p. 9181-9189.

25. O'Malley, M.A., et al., *High-level expression in Saccharomyces cerevisiae enables isolation and spectroscopic characterization of functional human adenosine A2a receptor.* Journal of structural biology, 2007. **159**(2): p. 166-78.

26. Dore, A.S., et al., *Structure of the adenosine A(2A) receptor in complex with ZM241385 and the xanthines XAC and caffeine.* Structure, 2011. **19**(9): p. 1283-93.

27. Hino, T., et al., *G-protein-coupled receptor inactivation by an allosteric inverse-agonist antibody.* Nature, 2012. **482**(7384): p. 237-40.

28. Jaakola, V.P., et al., *The 2.6 angstrom crystal structure of a human A2A adenosine receptor bound to an antagonist.* Science, 2008. **322**(5905): p. 1211-7.

29. Lebon, G., et al., *Agonist-bound adenosine A2A receptor structures reveal common features of GPCR activation.* Nature, 2011. **474**(7352): p. 521-5.

30. Liu, W., et al., *Structural basis for allosteric regulation of GPCRs by sodium ions.* Science, 2012. **337**(6091): p. 232-6.

31. Xu, F., et al., *Structure of an agonist-bound human A2A adenosine receptor.* Science, 2011. **332**(6027): p. 322-7.

32. Conner, M., et al., *Systematic analysis of the entire second extracellular loop of the V-1a vasopressin receptor - Key residues, conserved throughout a G-protein-coupled receptor family, identified.* Journal of Biological Chemistry, 2007. **282**(24): p. 17405-17412.

33. Gsandtner, I. and M. Freissmuth, *A tail of two signals: The C terminus of the A(2A)-adenosine receptor recruits alternative signaling pathways.* Molecular pharmacology, 2006. **70**(2): p. 447-449.

34. Langelaan, D.N., P. Ngweniform, and J.K. Rainey, *Biophysical characterization of G-protein coupled receptor-peptide ligand binding.* Biochemistry and Cell Biology-Biochimie Et Biologie Cellulaire, 2011. **89**(2): p. 98-105.

35. Jones, J.W., et al., *Cell-free assay of G-protein-coupled receptors using fluorescence polarization.* Journal of Biomolecular Screening, 2008. **13**(5): p. 424-429.

36. Wisedchaisri, G., S.L. Reichow, and T. Gonen, *Advances in structural and functional analysis of membrane proteins by electron crystallography.* Structure, 2011. **19**(10): p. 1381-1393.

37. Allen, S.J., et al., *Expression, purification and in vitro functional reconstitution of the chemokine receptor CCR1.* Protein expression and purification, 2009. **66**(1): p. 73-81.

38. Salon, J.A., D.T. Lodowski, and K. Palczewski, *The significance of G protein-coupled receptor crystallography for drug discovery.* Pharmacological Reviews, 2011. **63**(4): p. 901-37.

39. Baneres, J.L., J.L. Popot, and B. Mouillac, *New advances in production and functional folding of G-protein-coupled receptors.* Trends in biotechnology, 2011. **29**(7): p. 314-322.

40. Sarramegna, V., et al., *Heterologous expression of G-protein-coupled receptors: comparison of expression systems from the standpoint of large-scale production and purification.* Cellular and molecular life sciences : CMLS, 2003. **60**(8): p. 1529-46.

41. Lundstrom, K., et al., *Structural genomics on membrane proteins: comparison of more than 100 GPCRs in 3 expression systems.* Journal of structural and functional genomics, 2006. **7**(2): p. 77-91.

42. Sarramegna, V., et al., *Recombinant G protein-coupled receptors from expression to renaturation: a challenge towards structure.* Cellular and Molecular Life Sciences, 2006. **63**(10): p. 1149-1164.

43. Columbus, L., et al., *Mixing and matching detergents for membrane protein NMR structure determination.* Journal of the American Chemical Society, 2009. **131**(21): p. 7320-7326.

44. Prive, G.G., *Detergents for the stabilization and crystallization of membrane proteins.* Methods, 2007. **41**(4): p. 388-97.

45. Cross, T.A., et al., *Influence of solubilizing environments on membrane protein structures.* Trends in biochemical sciences, 2011. **36**(2): p. 117-25.

46. Tate, C.G., *Practical considerations of membrane protein instability during purification and crystallisation.* Methods in molecular biology, 2010. **601**: p. 187-203.

47. Sonoda, Y., et al., *Tricks of the trade used to accelerate high-resolution structure determination of membrane proteins.* Febs Letters, 2010. **584**(12): p. 2539-2547.

48. Hubbard, R.E., *Structure-based drug discovery and protein targets in the CNS.* Neuropharmacology, 2011. **60**(1): p. 7-23.

49. Raman, P., V. Cherezov, and M. Caffrey, *The Membrane Protein Data Bank.* Cellular and molecular life sciences : CMLS, 2006. **63**(1): p. 36-51.

50. Bowie, J.U., *Solving the membrane protein folding problem.* Nature, 2005. **438**(7068): p. 581-589.

51. Katritch, V., V. Cherezov, and R.C. Stevens, *Diversity and modularity of G protein-coupled receptor structures.* Trends in Pharmacological Sciences, 2012. **33**(1): p. 17-27.

52. Rasmussen, S.G.F., et al., *Crystal structure of the beta(2) adrenergic receptor-Gs protein complex.* Nature, 2011. **477**(7366): p. 549-U311.

53. Choe, H.W., et al., *Crystal structure of metarhodopsin II.* Nature, 2011. **471**(7340): p. 651-5.

54. O'Malley, M.A., et al., *The morphology and composition of cholesterol-rich micellar nanostructures determine transmembrane protein (GPCR) activity.* Biophysical Journal, 2011. **100**(2): p. L11-L13.

55. O'Malley, M.A., et al., *Toward rational design of protein detergent complexes: determinants of mixed micelles that are critical for the in vitro stabilization of a G-protein coupled receptor.* Biophysical journal, 2011. **101**(8): p. 1938-48.

56. Niebauer, R.T. and A.S. Robinson, *Exceptional total and functional yields of the human adenosine (A2a) receptor expressed in the yeast Saccharomyces cerevisiae.* Protein expression and purification, 2006. **46**(2): p. 204-11.

57. Eckart, M.R. and C.M. Bussineau, *Quality and authenticity of heterologous proteins synthesized in yeast.* Current Opinion in Biotechnology, 1996. **7**(5): p. 525-530.

58. Weiss, H.M. and R. Grisshammer, *Purification and characterization of the human adenosine A(2a) receptor functionally expressed in Escherichia coli.* European Journal of Biochemistry, 2002. **269**(1): p. 82-92.

59. Lee, J.Y. and E. Lyman, *Predictions for cholesterol interaction sites on the A(2A) adenosine receptor.* Journal of the American Chemical Society, 2012. **134**(40): p. 16512-16515.

60. de Graaf, C., et al., *Molecular modeling of the second extracellular loop of G-protein coupled receptors and its implication on structure-based virtual screening.* Proteins-Structure Function and Bioinformatics, 2008. **71**(2): p. 599-620.

61. Perlman, J.H., et al., *A disulfide bond between conserved extracellular cysteines in the thyrotropin-releasing-hormone receptor is critical for binding.* Journal of Biological Chemistry, 1995. **270**(42): p. 24682-24685.

62. Hwa, J., et al., *Structure and function in rhodopsin: Further elucidation of the role of the intradiscal cysteines, Cys-110, -185, and -187, in rhodopsin folding and function.* Proceedings of the National Academy of Sciences of the United States of America, 1999. **96**(5): p. 1932-1935.

63. Karnik, S.S. and H.G. Khorana, *Assembly of functional rhodopsin requires a disulfide bond between cysteine residue-110 and residue-187.* Journal of Biological Chemistry, 1990. **265**(29): p. 17520-17524.

64. Zhang, P.S., et al., *Mutation of human mu opioid receptor extracellular "disulfide cysteine" residues alters ligand binding but does not prevent receptor targeting to the cell plasma membrane.* Molecular Brain Research, 1999. **72**(2): p. 195-204.

65. Dohlman, H.G., et al., *Role of Extracellular Disulfide-Bonded Cysteines in the Ligand-bonded Cysteins in the Ligand-binding Function of the Beta-2-Adrenergic Receptor* Biochemistry, 1990. **29**(9): p. 2335-2342.

66. Noda, K., et al., *The high-affinity state of the beta-2-adrenergic receptor requires unique interaction between conserved and nonconserved extracellular loop cysteines.* Journal of Biological Chemistry, 1994. **269**(9): p. 6743-6752.

67. Scholl, D.J. and J.N. Wells, *Serine and alanine mutagenesis of the nine native cysteine residues of the human A(1) adenosine receptor.* Biochemical pharmacology, 2000. **60**(11): p. 1647-1654.

68. Deflorian, F., et al., *Evaluation of molecular modeling of agonist binding in light of the crystallographic structure of an agonist-bound A(2A) adenosine receptor.* Journal of medicinal chemistry, 2012. **55**(1): p. 538-552.

69. Kenakin, T., *New concepts in pharmacological efficacy at 7TM receptors: IUPHAR Review 2.* British journal of pharmacology, 2013. **168**(3): p. 554-575.

70. Pan, A.C., et al., *Molecular determinants of drug-receptor binding kinetics.* Drug Discovery Today, 2013. **18**(13-14): p. 667-673.

71. Guo, D., et al., *Drug-target residence time-A Case for G protein-coupled receptors.* Medicinal Research Reviews, 2014. **34**(4): p. 856-892.

72. Smith, A.W., *Lipid-protein interactions in biological membranes: A dynamic perspective.* Biochimica et biophysica acta, 2012. **1818**(2): p. 172-7.

73. Phillips, R., et al., *Emerging roles for lipids in shaping membrane-protein function.* Nature, 2009. **459**(7245): p. 379-385.

74. Whorton, M.R., et al., *A monomeric G protein-coupled receptor isolated in a high-density lipoprotein particle efficiently activates its G protein.* Proceedings of the National Academy of Sciences of the United States of America, 2007. **104**(18): p. 7682-7687.

75. Zhao, X.J., et al., *Designer short peptide surfactants stabilize G protein-coupled receptor bovine rhodopsin.* Proceedings of the National Academy of Sciences of the United States of America, 2006. **103**(47): p. 17707-17712.

76. Robinson, A.S., *Production of membrane proteins : strategies for expression and isolation*2011: Wiley-VCH.

77. Orwick-Rydmark, M., et al., *Detergent-free incorporation of a seven-transmembrane receptor protein into nanosized bilayer lipodisq particles for functional and biophysical studies.* Nano letters, 2012. **12**(9): p. 4687-92.

Chapter 2

ROLE OF THE DISULFIDE BOND NETWORK ON THE TRAFFICKING OF THE HUMAN A_{2A} ADENOSINE RECEPTOR

2.1. Introduction

The crystal structure of $A_{2A}R$ identified three disulfide bonds between extracellular loop 1 (ECL1) and ECL2 of the receptor; this disulfide bond network forms a rigid structure exposing the ligand-binding pocket [1]. One of these disulfide bonds is highly conserved among many class A GPCRs [1-3] and has been shown to be critical for maintaining the high-affinity ligand-binding conformation of the thyrotropin-releasing hormone receptor [4], rhodopsin [5, 6], μ opioid receptor [7], β_2 adrenergic receptor [8, 9], and A_1 adenosine receptor [10], to name a few. Furthermore, for some GPCRs, mutating the extracellular cysteines also resulted in lower protein expression levels or reduced/abolished trafficking of the receptor to the plasma membrane. For example, mutations to the conserved cysteines in μ opioid receptor reduced the number of receptors present at the plasma membrane compared to the wild type [7]. Mutations of the cysteines in ECL1 or ECL2 of the A_1 adenosine receptor resulted in a loss of receptors at the cell surface [10]. In the aforementioned examples, the conserved disulfide bond is the only covalent link between ECL1 and ECL2, and disruption of this link likely affected the topology of the ECLs and thus the ligand-binding affinity.

Previously in the Robinson laboratory, the role of the disulfide bonds in A_{2A} adenosine receptor was investigated using reducing agents and detergent-reconstituted

receptor. Tris(2-carboxyethyl)phosphine (TCEP) treated $A_{2A}R$ displayed reduced radioligand activity compared to the wild type $A_{2A}R$ (Figure 2.1, at 0 M urea) [11]. Increasing concentrations of urea (0 – 8M) were used to perturb the structure of the wild type (WT) and disulfide-reduced receptor. At low urea concentration (0 – 1 M), the initial levels of radioactive counts remained relatively uniform for both the WT and reduced receptor (Figure 2.1), indicating no change in the ability to bind ligand, apart from the initial drop in binding activity observed for the TCEP reduced receptor. Upon incubation with more than 1 M urea, a decrease in the measured radioligand binding was observed, likely due to urea-associated unfolding [11]. At 6 M urea, most ligand-binding activity for the WT and reduced receptor was eliminated. Both the WT and TCEP reduced receptor activity loss follows a similar trend, suggesting that the tertiary structure unfolding pathways are likely analogous [11]. Overall this result indicates that the disulfide bonds in $A_{2A}R$ are critical for ligand-binding activity, but are not necessary for tertiary structure stability.

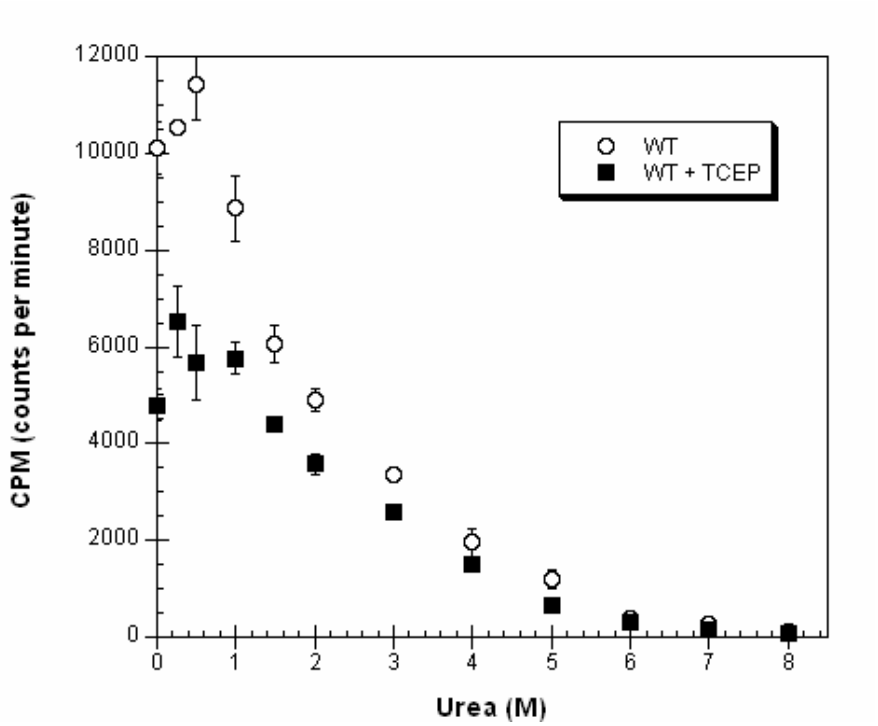

Figure 2.1 Urea denaturation of wild type A_{2A} and Tris(2-carboxyethyl)phosphine (TCEP) reduced receptor. Unfolding transition of the $A_{2A}R$ in absence or presence of the reducing agent (TCEP) was monitored using radioligand binding with 50 nM ^{3}[H] CGS 21680. Figure reproduced from [11], with permission.

In this chapter and Chapter 3 we describe a different approach to understand the role of the disulfide bond network of the human $A_{2A}R$ in the ligand-binding capability and the exceptional expression levels that have been previously reported [12-14]. To this end, mutations of the cysteines were conducted, enabling a more systematic investigation of the effects of disulfide bonds on trafficking and ligand-binding activity. The $A_{2A}R$ wild type and Cys-to-Ala constructs were expressed in mammalian cells, HEK-293. Ligand-binding and receptor distribution studies were conducted and are described in Chapter 2 and Chapter 3. Surprisingly, these data suggest that the conserved disulfide bond is not essential for the trafficking and ligand-

binding activity of this receptor. On the contrary, mutations to the cysteines in the ECLs of the $A_{2A}R$ resulted in a range of ligand-binding affinities and trafficking patterns.

2.2. Materials and Methods

2.2.1. Mutagenesis and Cloning

Human $A_{2A}R$ cDNA was a kind gift from Dr. Marlene Jacobson (Merck). Oligonucleotides used for site-directed mutagenesis and cloning were obtained from IDT (Coralville, Iowa), and are listed in Appendix A. All enzymes were purchased from New England Biolabs (Ipswich, MA). All the site-directed cysteine-to-alanine mutations were introduced in the $A_{2A}R$ gene using the pcDNA 3.1 vector and the Quick-change II XL kit (Agilent Technologies, Santa Clara, CA), following the *manufacturer's protocol.* The full-length $A_{2A}R$ coding gene was then subcloned into the vector pCEP4 or pCEP4 containing the cyan fluorescent protein (CFP) for mammalian expression. *Kpn*I and *Xho*I restriction enzymes were used for subcloning the A_{2A} gene into pCEP4.

E. coli strain DH5α was used for propagation of the cloning plasmids using Luria-Bertani media supplemented with 100 μg/ml ampicillin; cultures were incubated overnight at 37 °C and 250 rpm. Transformations of *E. coli* were performed by the heat shock method [15]. DNA was extracted from DH5α using the Wizard Plus SV Minipreps DNA Purification System from Promega (Madison, WI). All mutations were confirmed by DNA sequencing (DNA Core Facility, University of Delaware).

2.2.2. Cell Culture and Transfection

All media used for mammalian cell culture and Lipofectamine2000 were purchased from Life Technologies (Grand Island, NY). HEK-293 cells were grown in Dulbecco's Modified Eagle's Medium (DMEM) supplemented with 10% fetal calf serum at 37 °C in a humidified 5% CO_2 incubator. Transient transfections were carried out using Lipofectamine2000 following manufacturer's instructions and 800 ng of DNA per 80% confluent T-25 culture flask.

2.2.3. Expression and Trafficking Patterns

In order to confirm the expression and monitor the trafficking patterns, the $A_{2A}R$ constructs utilized for these studies contained a C-terminal-linked CFP. HEK-293 cells were imaged 36 hours after transfection. For imaging, cells were seeded at 100,000 cells per well (Nunc Lab-Tek II chambered cover glass 4-well, Thermo Scientific) and allowed to adhere overnight. Transfection efficiency was monitored using the CFP-tagged receptors; the efficiency was uniform throughout the experiments, ranging from 40%–46%.

2.2.4. Plasma Membrane and Endoplasmic Reticulum (ER) Staining

To further characterize the trafficking patterns of the $A_{2A}R$–CFP constructs, plasma membrane (WGA Alexa Fluor 555 conjugate, Molecular Probes, Eugene, OR) and endoplasmic reticulum (ER tracker green, Molecular Probes) dyes were used. For the staining experiments, transfected cells were plated at 100,000 cells per well in a 4-well imaging chamber (Nunc Lab-Tek II chambered cover glass, Thermo Scientific) coated with 12% (w/v) collagen. Cells were incubated at 37 °C in a humidified 5% CO_2 incubator overnight. The next day the cells were washed once with PBS. All aspirations and additions to the imaging wells were performed drop-wise using gel-

loading tips. 400 µL of ER tracker green solution (1 µM in PBS) was added to each well, and the plates were incubated for 20 minutes at 37 °C. 200 µL of WGA solution (2 µg/mL in PBS) was then added to each well without aspirating the ER tracker green solution. The plates were incubated for an additional five minutes at 37 °C, and the dye solutions were removed following this incubation. Next, 400 µL of 4% paraformaldehyde (in PBS) was added to each well and the plates were incubated for 10 minutes at 37 °C. After this incubation, the paraformaldehyde solution was removed, the wells were washed twice with 400 µL PBS and a final volume of 400 µL PBS was added to each well for imaging. Cells were imaged 48 hours after transfection.

2.2.5. Confocal Microscopy

Confocal images were acquired on an inverted Zeiss LSM 510 NLO laser-scanning microscope (Carl Zeiss, Inc., Germany) using a 25 mW Argon laser (LASOS, Ebersberg, Germany) and a 40x Plan-Neofluar/1.3 Oil DIC objective lens (Carl Zeiss, Inc.).

2.2.6. Analysis of Receptor Trafficking

Images of the A_{2A}R-CFP constructs, stained with the plasma membrane and ER dyes were analyzed in order to determine the distribution pattern of the different A_{2A} variants. For this purpose, while imaging, the master gain (800–900) and the laser power were kept constant. The quality of the ER and plasma membrane stains was confirmed prior to inclusion in the analysis; i.e., images where the plasma membrane dye stained the membranes of internal organelles were not used in the analysis. Images were cropped to include only one cell per file prior to the analysis.

Each file was composed of an aligned set of three 12-bit grayscale images: the CFP-tagged receptor, the plasma membrane, and the ER. See Figure 2.5 for examples; in this case, the CFP-tagged receptor is shown in cyan, the plasma membrane in red, and the ER in green to facilitate identification of the structures. For analysis, each image was subjected to thresholding to separate signal from background pixels, resulting in binary images. We used the IsoData auto-thresholding algorithm [16] that is the default thresholding algorithm in ImageJ [17]. Let S_{CFP} , S_M , S_{ER} be the set of signal pixels in the CFP-tagged receptor image, the plasma membrane image, and in the ER image, respectively. In order to compare the shapes of those three point sets, we used the directed Hausdorff distance *H(A,B)* between two point sets *A* and *B* in the plane, which is defined as follows [18]:

$$H(A,B) = \max_{a\in A} \underbrace{\min_{b\in B} ||a-b||}_{\text{nearest neighbor}}, \qquad (2.1)$$

where $||a-b||$ denotes the Euclidean distance between points *a* and *b*. The directed Hausdorff distance assigns to every point *a* in *A* its nearest neighbor in *B*, and then computes the maximum of all distances between assigned points. In order to make this distance more robust against noise and outliers causing non-representative large distances, we replace the maximum with an average and arrive at the modified directed Hausdorff distance:

$$\tilde{H}(A,B) = \text{average}_{a\in A} \ \min_{b\in B} \ ||a-b|| \quad (2.2)$$

Our goal was to quantify whether the shape of S_{CFP} was closer to the membrane shape of S_M or to the shape of the cell interior that is represented by S_{ER}. We therefore compared S_{CFP} to S_M and S_{ER} to S_M using the modified directed Hausdorff distance, and combined both quantities in a single *Hausdorff ratio* (HR):

$$\mathrm{HR}(S_{CFP}, S_M, S_{ER}) = \frac{\tilde{H}(S_{CFP}, S_M)}{\tilde{H}(S_{ER}, S_M)} \quad (2.3)$$

A large Hausdorff ratio (close to 1) indicates that the shape of S_{CFP} was similar to S_{ER}, as the average distances to the plasma membrane are similar. A small Hausdorff ratio (<0.5) indicates that the shape of S_{CFP} was more similar to the membrane shape S_M, as the average distances from the CFP-tagged receptor to the plasma membrane are overall smaller than the average distances from the ER to the plasma membrane. Due to the use of average distances as well as the use of a ratio, the Hausdorff ratio is quite robust and works well with different thresholding methods. We implemented the Hausdorff ratio computation in ImageJ [17]. This work was conducted in collaboration with Dr. Carola Wenk (Tulane University).

2.3. Results

Disulfide bonds have been shown to play a critical role in protein stability, trafficking and function for many GPCRs [3-9, 19]. To characterize the role of the specific disulfide bonds in $A_{2A}R$, we created Cys-to-Ala mutations in the three disulfide bonds that join ECL1 and ECL2 (Figure 2.2). Six single Cys-to-Ala and three double Cys-to-Ala constructs were constructed as outlined in Table 2.1.

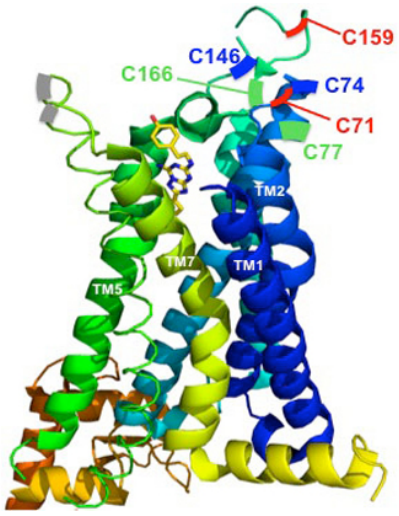

Figure 2.2 Crystal structure of $A_{2A}R$ bound to an antagonist, ZM 241385 [1]. The cysteines that form the disulfide bonds are color coded in green, red and blue. Adapted using PyMOL (The PyMOL Molecular Graphics System, Version 1.3 Schrödinger, LLC), Protein Data Bank identification code 3EML.

Table 2.1 List of the Cys-to-Ala constructs created to test the role of the disulfide bonds in the A_{2A} adenosine receptor.

Cysteine-to-Alanine constructs		
Single Cys-to-Ala constructs		Double Cys-to-Ala constructs
ECL1	ECL2	ECL1 and ECL2
C71A	C146A	C71A-C159A
C74A	C159A	C74A-C146A
C77A	C166A	C77A-C166A

2.3.1. Expression and Trafficking Patterns of $A_{2A}R$ Wild Type and Cys-to-Ala Variants

The constructs listed in Table 2.1 were transfected and expressed in HEK-293 cells as described in Materials and Methods to test how the Cys-to-Ala mutations affected the trafficking of the receptor and ligand-binding activity. Trafficking refers to the receptor movement within the cell, including insertion of new receptors into the endoplasmic reticulum membrane, movement to the plasma membrane,

internalization, recycling, and sorting of internalized receptors to lysosomes for degradation [20]. For these studies, the $A_{2A}R$ constructs were C-terminally tagged with the cyan fluorescent protein (CFP), and trafficking to the plasma membrane was analyzed by CFP fluorescence detection at the periphery of the cell via confocal microscopy. Figure 2.3 displays the typical trafficking pattern of the wild type (WT) $A_{2A}R$; a strong halo is seen at the periphery of the cell, indicating that the receptor trafficked well to the plasma membrane.

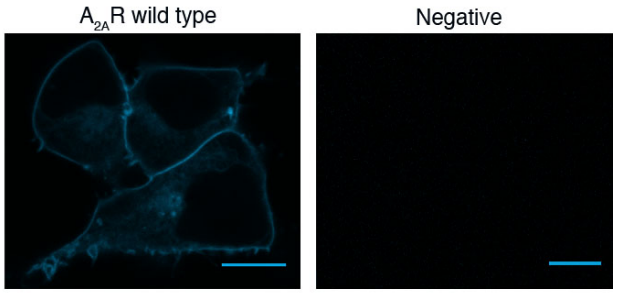

Figure 2.3 Trafficking pattern of WT $A_{2A}R$ and negative control. HEK-293 cells transiently transfected with wild type A_{2A}-CFP (left) and with an empty plasmid as a negative control (right). Scale bars, 10 μm.

The typical expression patterns of all the Cys-to-Ala variants are displayed in Figure 2.4. From these images, it appears that all $A_{2A}R$ variants trafficked to the plasma membrane. However, it is also evident that the internally localized receptor population differs between the variants and the WT $A_{2A}R$.

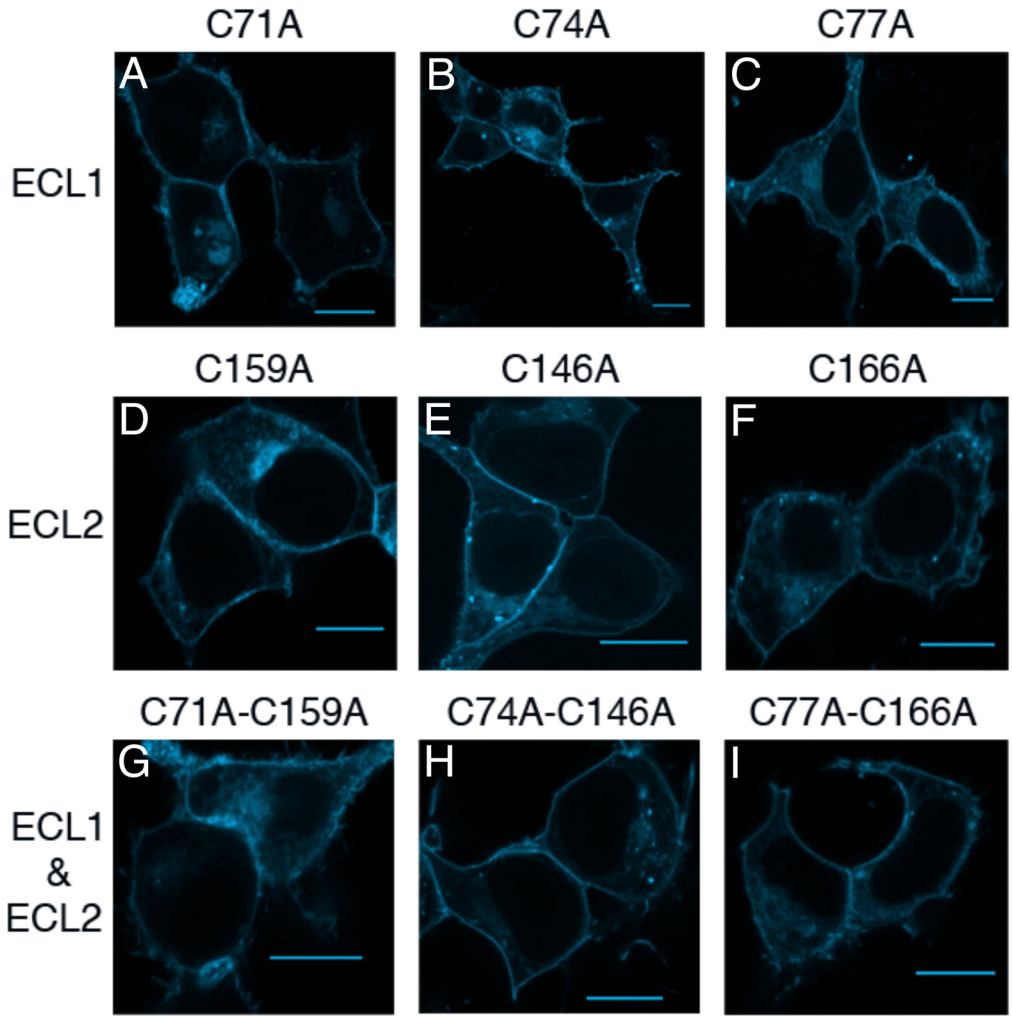

Figure 2.4 Trafficking patterns of $A_{2A}R$ Cys-to-Ala variants. HEK-293 cells transiently transfected with $A_{2A}R$-CFP constructs. A-C) $A_{2A}R$ variants with mutations in the cysteines in ECL1. D-F) Variants with mutations in the cysteines in ECL2. G-I) Variants with mutations in the cysteines in ECL1 and ECL2 that correspond to the disulfide bonds. Scale bars, 10 μm.

From these images, it is not clear whether receptors present within the cell are retained in the endoplasmic reticulum (ER), in lysosomes for degradation, or are en route to the plasma membrane. However, as our focus was on proper localization of

active receptor to the plasma membrane, we used the following methods to characterize the ligand-binding activity of the receptor once it reached the cell surface and the distribution of the receptors between the plasma membrane versus ER:

1. Comparison of the distribution of the $A_{2A}R$ variants at the plasma membrane and at the ER using plasma membrane and ER dyes.

2. Fluorescent-ligand (FITC-APEC) binding to further test if the receptor is at the plasma membrane and in its active form. Described in Chapter 3.

3. Radioligand binding to determine the affinity of the ligand to the WT and Cys-to-Ala variants. Described in Chapter 3.

Cells were stained with plasma membrane (M) and ER dyes to compare the localization of $A_{2A}R$ WT and the $A_{2A}R$ variants. At least twenty images for each A_{2A} variant were analyzed using the Hausdorff Ratio (HR), which is defined as the directed Hausdorff distance between the CFP tagged receptor and the plasma membrane divided by the directed Hausdorff distance between the ER and the plasma membrane, as described in Materials and Methods. When this ratio is low (<0.5), it indicates that the receptor was localized primarily at the plasma membrane. Ratios close to one indicate that there was a higher ER-localized receptor population. Figure 2.5 displays two examples of disparate receptor trafficking; the top image represents a cell where most of the receptor trafficked to the plasma membrane, and the bottom image represents a cell with higher levels of ER localized receptor. This difference can be seen by the clear outline of CFP at the cell periphery in Figure 2.5A compared to the diffuse CFP fluorescence throughout the ER network in Figure 2.5D. Comparison of the CFP fluorescence (Figure 2.5A and 2.5D) to that of the plasma membrane dye (2.5B or 2.5E, respectively) versus that of the fluorescence of the ER dye (2.5C and 2.5F) to that of the membrane dye confirms this analysis. Quantitatively, these

observations are reflected in the Hausdorff ratios of 0.1 for the variant that trafficked mostly to the plasma membrane, and 0.8 for the variant with higher levels of ER-localized receptor.

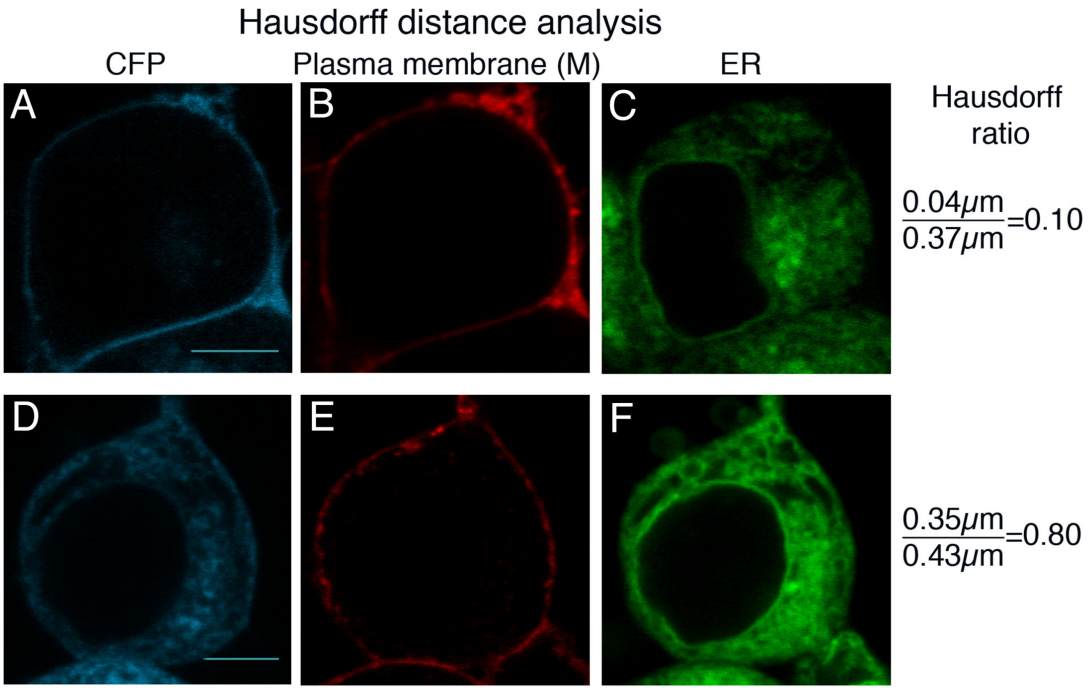

Figure 2.5 Analysis of receptor distribution within the plasma membrane and ER for two disparate examples. To quantify the receptor distribution within the cell, HEK-293 cells were transiently transfected with A_{2A}R-CFP constructs. Cells were stained using WGA plasma membrane dye (pseudocolored in red; B and E) and with ER tracker dye (pseudocolored in green; C and F). Images A-C are representative of a variant that trafficked to the plasma membrane, C74A-C146A; images D-F are representative of a variant that displayed a high ER localized receptor population, C146A. Hausdorff distance ratios were determined as described in Materials and Methods, and are shown to the right of the images. Scale bars, 10 μm.

This semi-quantitative method identified three different trafficking patterns: a higher ER retention relative to the WT $A_{2A}R$ – all the single Cys-to-Ala variants and the conserved disulfide bond variant (C77A-C166A); a similar trafficking pattern as the WT $A_{2A}R$ – C71A-C159A; and improved plasma membrane trafficking relative to the WT receptor – C74A-C146A. These different trafficking patterns are highlighted in the box plot, Figure 2.6, where the gray circles indicate the Hausdorff distance ratios for individual images of the WT and the Cys-to-Ala variants. The average values for the wild type $A_{2A}R$ and the Cys-to-Ala variants and the 95% confidence interval are listed in Table 2.2.

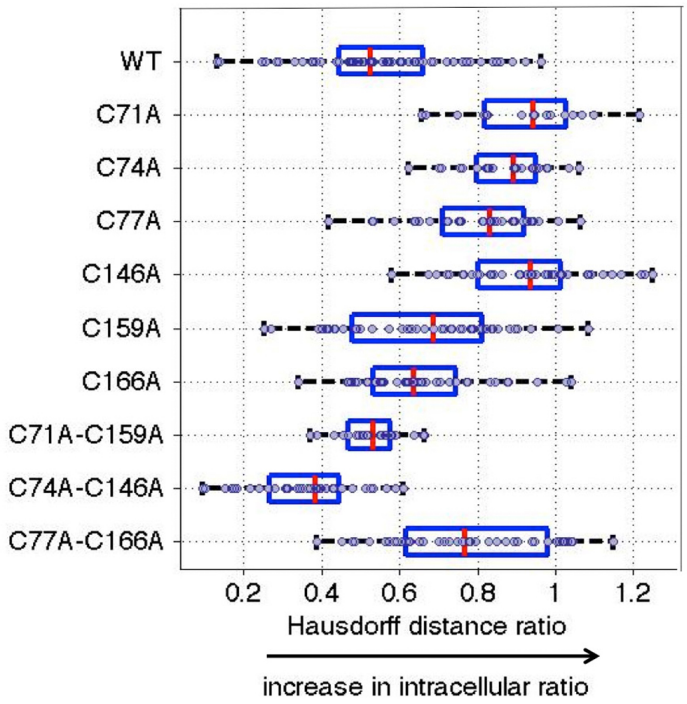

Figure 2.6 Receptor distribution within the plasma membrane and ER for WT $A_{2A}R$ and the Cys-to-Ala variants. The Hausdorff distance ratio was calculated for at least twenty images for each of the $A_{2A}R$ variants, where the gray circles represent the values calculated for each image. Box plots were used to display the data, with red lines indicating the median for each variant; the edges of the blue boxes correspond to the 25^{th} and 75^{th} percentiles.

The box plot highlights the wide range of receptor distribution observed for some of the $A_{2A}R$ variants; for example, the WT receptor had a HR ranging from 0.13-0.96. Images representative of the low and the high Hausdorff ratios for each variant are shown in Figure 2.7. Notably, the HR analysis is able to capture the variability within each variant. It should be highlighted that a correlation between the sample size

(n) and the HR variance (p=0.03, Appendix A, Figure A.1C) was observed. Taking the ratio of two independent normally distributed variables results in a Cauchy distribution and the variance of this distribution will become larger as the sample size increases; perhaps this could explain the correlation between n and HR variance. However, the sets of pixel distances (CFP to PM and ER to PM) are not normally distributed, for examples refer to Appendix A, Figure A.2, and their ratio does not result in a Cauchy distribution. The ratio distribution is mostly captured by a normal distribution and this fit was used to calculate the mean and standard error of the mean for the HR of all the variants (Table 2.2); it should be noted that these values are an approximation. Since a Cauchy distribution does not fit the HR data, it is likely that the variability observed has biological significance. To test that the HR variance is not correlated with the sample size (n) we selected at random 20 data points from the HR data set for each variant. With a constant sample size (n=20) the trend of the HR variance remained the same (Apendix A , Figure A.1B), having a strong correlation (p=0.0014) with the variance of the original HR data set ($n \geq 20$) (Apendix A, Figure A.1D). This indicates that the variance observed could be due to other parameters such as variant toxicity or conformational stability.

Table 2.2 Cellular distribution of $A_{2A}R$ WT and Cys-to-Ala variants. HEK-293 cells expressing CFP tagged $A_{2A}R$ WT and Cys-to-Ala variants, stained with plasma membrane and ER dyes. Hausdorff distance between CFP and the plasma membrane, and ER and plasma membrane were calculated. The ratio of these distances (mean±SEM), the values obtained for the 95% confidence interval, and the number of cells used for this analysis are listed in the table.

Receptor distribution: Hausdorff ratio

	mean ± SEM	95% CI	sample size
A_{2A} WT	0.55±0.02	0.50-0.60	62
C71A	0.92±0.04	0.84-1.00	20
C74A	0.87±0.02	0.82-0.92	22
C77A	0.80±0.03	0.74-0.85	33
C146A	0.93±0.02	0.88-0.98	43
C159A	0.66±0.03	0.60-0.72	45
C166A	0.66±0.02	0.61-0.71	41
C71A-C159A	0.53±0.02	0.50-0.56	24
C74A-C146A	0.36±0.02	0.32-0.41	39
C77A-C166A	0.78±0.03	0.72-0.84	42

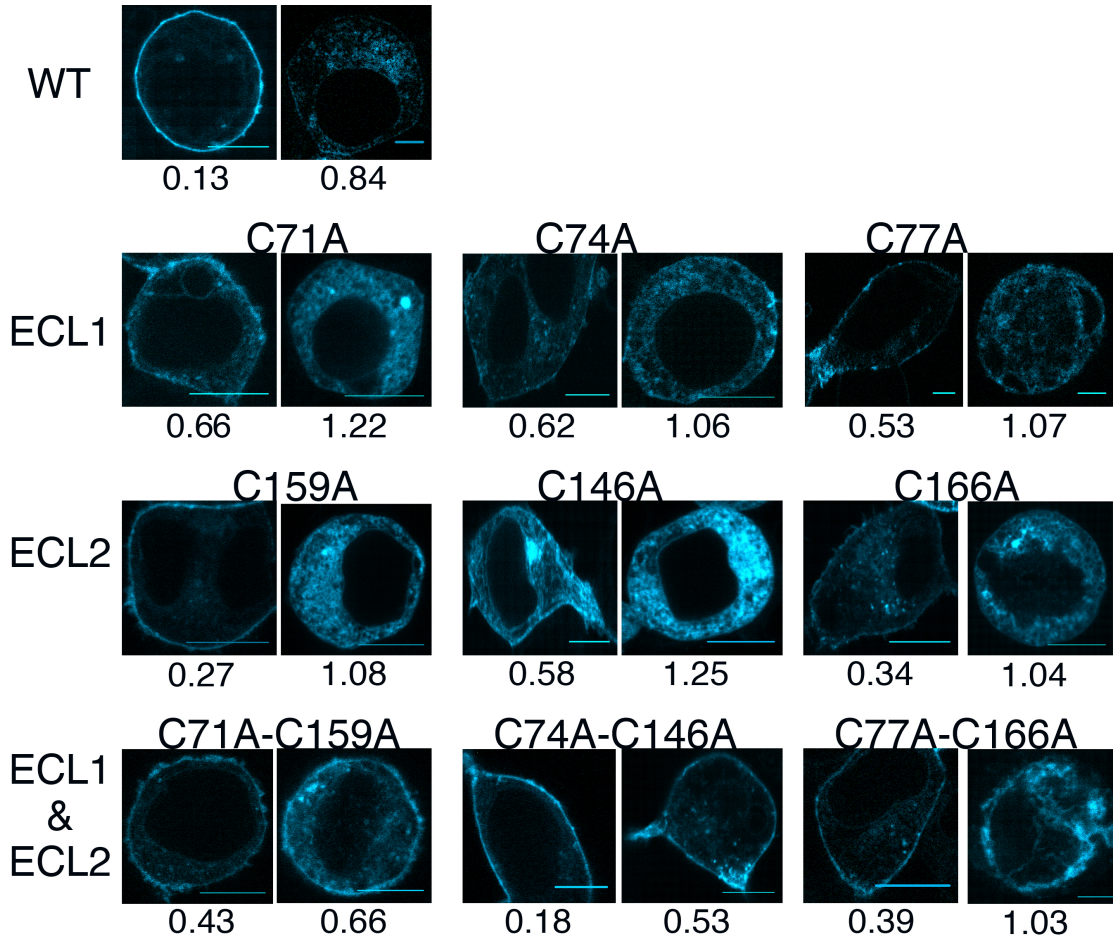

Figure 2.7 HEK-293 cells transfected with $A_{2A}R$-CFP variants. Images taken approximately 48 hours after transfection. For each variant, cells with disparate trafficking patterns are displayed to illustrate the variation in trafficking patterns within each variant. The calculated HR is displayed underneath each image. The contrast, brightness and pixel threshold for each image were adjusted for clarity. Scale bars=10µm.

2.4. Discussion and Conclusion

Tagging the WT receptor and the Cys-to-Ala constructs with CFP enabled us to confirm that the $A_{2A}R$ variants were expressed and trafficked to the plasma

membrane (Figures 2.3-2.4). Using the Hausdorff ratio (HR) analysis, a clear difference between the distribution of the WT receptor, with a HR of 0.55, and all the single Cys-to-Ala variants, with a HR range of 0.66-0.93 was observed. Overall, these studies indicate that the single Cys-to-Ala variants have significantly higher levels of ER-retained receptor (Figure 2.6 and Table 2.2).

Unpaired cysteine residues are one of the main features that are recognized by the ER quality control system [21], in particular by thiol-disulfide oxidoreductases. There are a high number of oxidoreductases in the ER, and native and non-native disulfide bonds are transiently formed in the ER until folding is complete [21, 22]. Receptor trafficking to the plasma membrane was restored and even improved in most of the double Cys-to-Ala variants, C71A-C159A (HR 0.53) and C74A-C146A (HR 0.36). Thus, our data suggest that the unpaired cysteines of the $A_{2A}R$ variants may interact with ER oxidoreductases, and are retained in the ER due to disulfide bond shuffling until a folded conformation is achieved.

In contrast to the other double cysteine variants, C77A-C166A (site of conserved disulfide bond) had a higher level of ER localized receptor (HR 0.78) compared to WT. It is unclear how the ER quality control recognizes the differences in loop structure that form upon the removal of the conserved disulfide bond, but not the removal of the other two non-conserved disulfide bonds.

REFERENCES

1. Jaakola, V.P., et al., *The 2.6 angstrom crystal structure of a human A2A adenosine receptor bound to an antagonist.* Science, 2008. **322**(5905): p. 1211-7.

2. Piirainen, H., et al., *Structural features of adenosine receptors: From crystal to function.* Biochimica Et Biophysica Acta-Biomembranes, 2011. **1808**(5): p. 1233-1244.

3. Venkatakrishnan, A.J., et al., *Molecular signatures of G-protein-coupled receptors.* Nature, 2013. **494**(7436): p. 185-194.

4. Perlman, J.H., et al., *A disulfide bond between conserved extracellular cysteines in the thyrotropin-releasing-hormone receptor is critical for binding.* Journal of Biological Chemistry, 1995. **270**(42): p. 24682-24685.

5. Hwa, J., et al., *Structure and function in rhodopsin: Further elucidation of the role of the intradiscal cysteines, Cys-110, -185, and -187, in rhodopsin folding and function.* Proceedings of the National Academy of Sciences of the United States of America, 1999. **96**(5): p. 1932-1935.

6. Karnik, S.S. and H.G. Khorana, *Assembly of functional rhodopsin requires a disulfide bond between cysteine residue-110 and residue-187.* Journal of Biological Chemistry, 1990. **265**(29): p. 17520-17524.

7. Zhang, P.S., et al., *Mutation of human mu opioid receptor extracellular "disulfide cysteine" residues alters ligand binding but does not prevent receptor targeting to the cell plasma membrane.* Molecular Brain Research, 1999. **72**(2): p. 195-204.

8. Dohlman, H.G., et al., *Role of Extracellular Disulfide-Bonded Cysteines in the Ligand-bonded Cysteins in the Ligand-binding Function of the Beta-2-Adrenergic Receptor* Biochemistry, 1990. **29**(9): p. 2335-2342.

9. Noda, K., et al., *The high-affinity state of the beta-2-adrenergic receptor requires unique interaction between conserved and nonconserved extracellular loop cysteines.* Journal of Biological Chemistry, 1994. **269**(9): p. 6743-6752.

10. Scholl, D.J. and J.N. Wells, *Serine and alanine mutagenesis of the nine native cysteine residues of the human A(1) adenosine receptor.* Biochemical pharmacology, 2000. **60**(11): p. 1647-1654.

11. O'Malley, M.A., et al., *Analysis of adenosine A(2)a receptor stability: Effects of ligands and disulfide bonds.* Biochemistry, 2010. **49**(43): p. 9181-9189.

12. Wedekind, A., et al., *Optimization of the human adenosine A2a receptor yields in Saccharomyces cerevisiae.* Biotechnol Prog, 2006. **22**(5): p. 1249-55.

13. O'Malley, M.A., et al., *High-level expression in Saccharomyces cerevisiae enables isolation and spectroscopic characterization of functional human adenosine A2a receptor.* Journal of structural biology, 2007. **159**(2): p. 166-78.

14. Niebauer, R.T. and A.S. Robinson, *Exceptional total and functional yields of the human adenosine (A2a) receptor expressed in the yeast Saccharomyces cerevisiae.* Protein Expr Purif, 2006. **46**(2): p. 204-11.

15. Sambrook, J., Fritsch, E.F., and Maniatis, T., *Molecular cloning: A laboratory manual*. 2nd ed. Vol. 1,2,3. 1989, NY: Cold Spring Harbor Laboratory Press.

16. Ridler, T.W. and S. Calvard, *Picture thresholding using an iterative selection method.* Ieee Transactions on Systems Man and Cybernetics, 1978. **8**(8): p. 630-632.

17. Schneider, C.A., W.S. Rasband, and K.W. Eliceiri, *NIH Image to ImageJ: 25 years of image analysis.* Nat Meth, 2012. **9**(7): p. 671-675.

18. Alt, H. and L.J. Guibas, *Chapter 3 - Discrete geometric shapes: Matching, interpolation, and approximation*, in *Handbook of computational geometry*, J.R. Sack and J. Urrutia, Editors. 2000, North-Holland: Amsterdam. p. 121-153.

19. de Graaf, C., et al., *Molecular modeling of the second extracellular loop of G-protein coupled receptors and its implication on structure-based virtual screening.* Proteins-Structure Function and Bioinformatics, 2008. **71**(2): p. 599-620.

20. Mundell, S. and E. Kelly, *Adenosine receptor desensitization and trafficking.* Biochimica Et Biophysica Acta-Biomembranes, 2011. **1808**(5): p. 1319-1328.

21. Ellgaard, L. and A. Helenius, *Quality control in the endoplasmic reticulum.* Nature Reviews Molecular Cell Biology, 2003. **4**(3): p. 181-191.

22. Sitia, R. and I. Braakman, *Quality control in the endoplasmic reticulum protein factory.* Nature, 2003. **426**(6968): p. 891-4.

Chapter 3

CONSERVED DISULFIDE BOND IS NOT ESSENTIAL FOR THE ADENOSINE A_{2A} RECEPTOR: EXTRACELLULAR CYSTEINES INFLUENCE RECEPTOR DISTRIBUTION WITHIN THE CELL AND LIGAND-BINDING RECOGNITION

3.1. Introduction

Unlike other class A GPCRs, such as rhodopsin and the adrenergic receptors, ECL2 of the A_{2A} adenosine receptor is mainly unstructured, with a rich disulfide bond network proposed to constrain the otherwise flexible ECL2 [1]. One of these disulfide bonds (C77-C166) is conserved in the class A GPCRs; this disulfide bond is essential for the expression, membrane trafficking and function of some GPCRs [2-9]. For example, for the closely related A_1 adenosine receptor, mutation of either cysteine of the conserved disulfide bond results in a complete loss of antagonist binding and plasma-membrane localization [10]. In contrast, mutations in the cysteines in ECL1 and ECL2, including those of the conserved disulfide bond, did not abolish plasma membrane localization of the A_{2A}R, as seen in Chapter 2. In this chapter we verified that the A_{2A}R variants trafficked to the plasma membrane and retained ligand-binding activity.

3.2. Materials and Methods

3.2.1. Cell Culture and Transfection

All media used for mammalian cell culture and Lipofectamine2000 were purchased from Life Technologies (Grand Island, NY). HEK-293 cells were grown in

Dulbecco's Modified Eagle's Medium (DMEM) supplemented with 10% fetal calf serum at 37 °C in a humidified 5% CO_2 incubator. Transient transfections were carried out using Lipofectamine2000 following manufacturer's instructions and 800 ng of DNA per 80% confluent T-25 culture flask.

3.2.2. Fluorescent Ligand Binding

For ligand binding studies, untagged receptors were used (A_{2A} constructs in pCEP4 vector). Transfected HEK-293 cells were plated at 100,000 cells per well in a 4-well imaging chamber and grown overnight. Media was removed and replaced with 70 nM FITC-APEC (NIMH synthesis program, http://nimh-repository.rti.org, NIMH Code: D-906) in PBS and incubated for 1 hour at 37 °C in a humidified 5% CO_2 incubator. Cells were imaged 36–48 hours after transfection.

3.2.3. Confocal Microscopy

Confocal images were acquired on an inverted Zeiss LSM 510 NLO laser-scanning microscope (Carl Zeiss, Inc., Germany) using a 25 mW Argon laser (LASOS, Ebersberg, Germany) and a 40x Plan-Neofluar/1.3 Oil DIC objective lens (Carl Zeiss, Inc.).

3.2.4. Radioligand Binding

Radioligand binding was performed as described previously [11]. HEK-293 cells were transfected with untagged receptors (A_{2A} constructs in pCEP4), and tested for ligand binding 48 hours after transfection. Cells from one confluent T-25 flask were washed and resuspended in the binding buffer (TME: 50 mM Tris-HCl, 10 mM $MgCl_2$ and 1 mM EDTA). Cells were then aliquoted (approximately 100,000 cells per well) into poly(ethyleneimine) (0.1% v/v) treated 96-well glass fiber filter plates

(MultiScreen-FC filter type B, Millipore, Billerica, MA). Cells were then incubated with 0–470 nM [^{3}H] CGS 21680 (Perkin Elmer, Boston, MA) for 3 hours. The binding reaction was terminated by filtration, with three washes of ice-cold TME buffer. 30 µl of scintillation solution (ULTIMA gold, Perkin Elmer) were added to each well. Ligand binding was determined via bound radioactive counts (CPMs) using a Perkin-Elmer 1450 Microbeta liquid scintillation counter. Multiple counts were taken until the values stabilized, approximately 24 hours after the addition of the scintillation solution. Non-specific binding was determined in parallel reactions using non-transfected HEK-293 cells incubated over the same ligand concentrations. All samples were run in triplicate and at least two independent biological experiments were conducted. Non-specific binding was subtracted from the total binding to determine the specific binding. Matlab (version 7.10, MathWorks, Natick, MA) was used to fit the data to the equilibrium solution of the mass action kinetic model for a single-site binding reaction:

$$C = \frac{L \times R_{\max}}{K_D + L} \tag{3.1}$$

where C is the concentration of the receptor-ligand complex (measured), L is the total radioligand concentration, R_{max} is the total number of active receptors, and K_D is the equilibrium dissociation constant. The coefficients for K_D and R_{max} were determined by averaging the minimized least square regression for the data of each experiment. The standard error of the mean (SEM) and 95% confidence intervals were determined from the sample standard deviation.

3.3. Results

In Chapter 2 we use the Hausdorff Ratio analysis to quantify the receptor distribution of the $A_{2A}R$ Cys-to-Ala variants. This analysis indicated that all the variants trafficked to the plasma membrane to some degree. Here we confirm the proper localization of active receptor to the plasma membrane, by using fluorescent-ligand (FITC-APEC) and radioligand ([^{3}H] CGS 21680) binding assays.

3.3.1. Fluorescent-Ligand Binding Activity of $A_{2A}R$ Wild Type and Cys-to-Ala Variants

Like the WT receptor, all the $A_{2A}R$ variants appeared to traffic to the plasma membrane to some degree (Figure 2.4, Chapter 2). To determine if the variants were able to bind ligand, a high affinity (K_D=57 nM) fluorescent agonist, FITC-APEC [12], was used to visualize active receptor at the cell surface. For these experiments we used HEK-293 cells expressing untagged $A_{2A}R$ variants; Figure 3.1 shows the FITC-APEC binding typically observed.

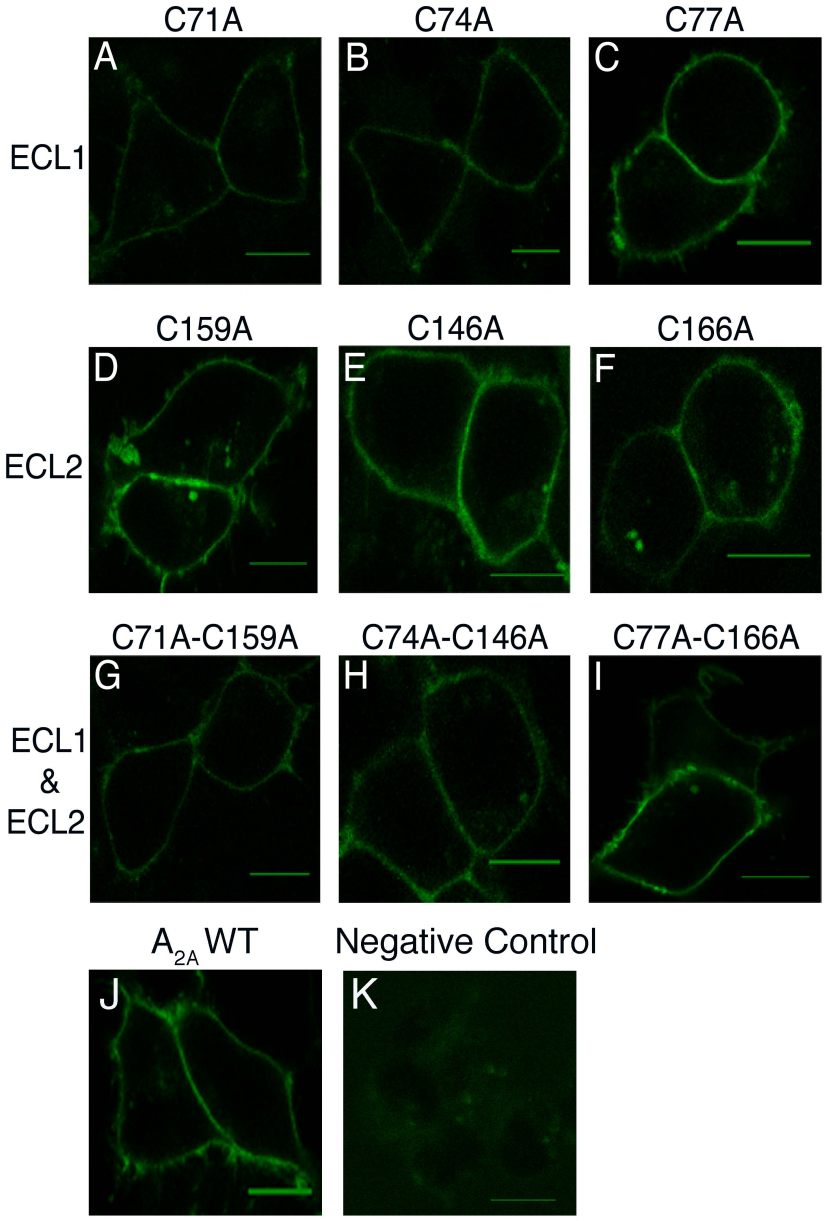

Figure 3.1 Fluorescent-ligand binding observed in the $A_{2A}R$ variants. HEK-293 cells transiently transfected with untagged $A_{2A}R$ constructs and incubated with 70nM FITC-APEC. A-C) Variants with mutations in the cysteines in ECL1. D-F) Variants with mutations in the cysteines in ECL2. G-I) Variants with mutations in the cysteines in ECL1 and ECL2, corresponding to the disulfide bonds. J-K) WT $A_{2A}R$ and negative control. Scale bars, 10 μm.

This fluorescent ligand-binding study showed that all single and double Cys-to-Ala variants were capable of binding the fluorescent ligand (Figure 3.1). This result is consistent with the observation that the single and double Cys-to-Ala variants trafficked to the plasma membrane and confirms their ligand-binding capability.

3.3.2. Saturation Binding of [^{3}H] CGS 21680 to $A_{2A}R$ Wild Type and Cys-to-Ala Variants

Radioligand binding was conducted to determine the binding affinity of the $A_{2A}R$ variants for the high-affinity agonist [^{3}H] CGS 21680 (Figure 3.2). HEK-293 cells transiently transfected with the untagged $A_{2A}R$ constructs were incubated with increasing amounts of [^{3}H] CGS 21680 and bound ligand was measured, as described in Materials and Methods.

The quantity bound receptor-ligand complexes is plotted as a function of ligand concentration for single and double Cys-to-Ala variants (Figure 3.2A), where a line shows the fit to a single-site binding model. The equilibrium dissociation constant (K_D) and the total number of active receptors per cell (R_{max}) were determined from this fit (Table 3.1).

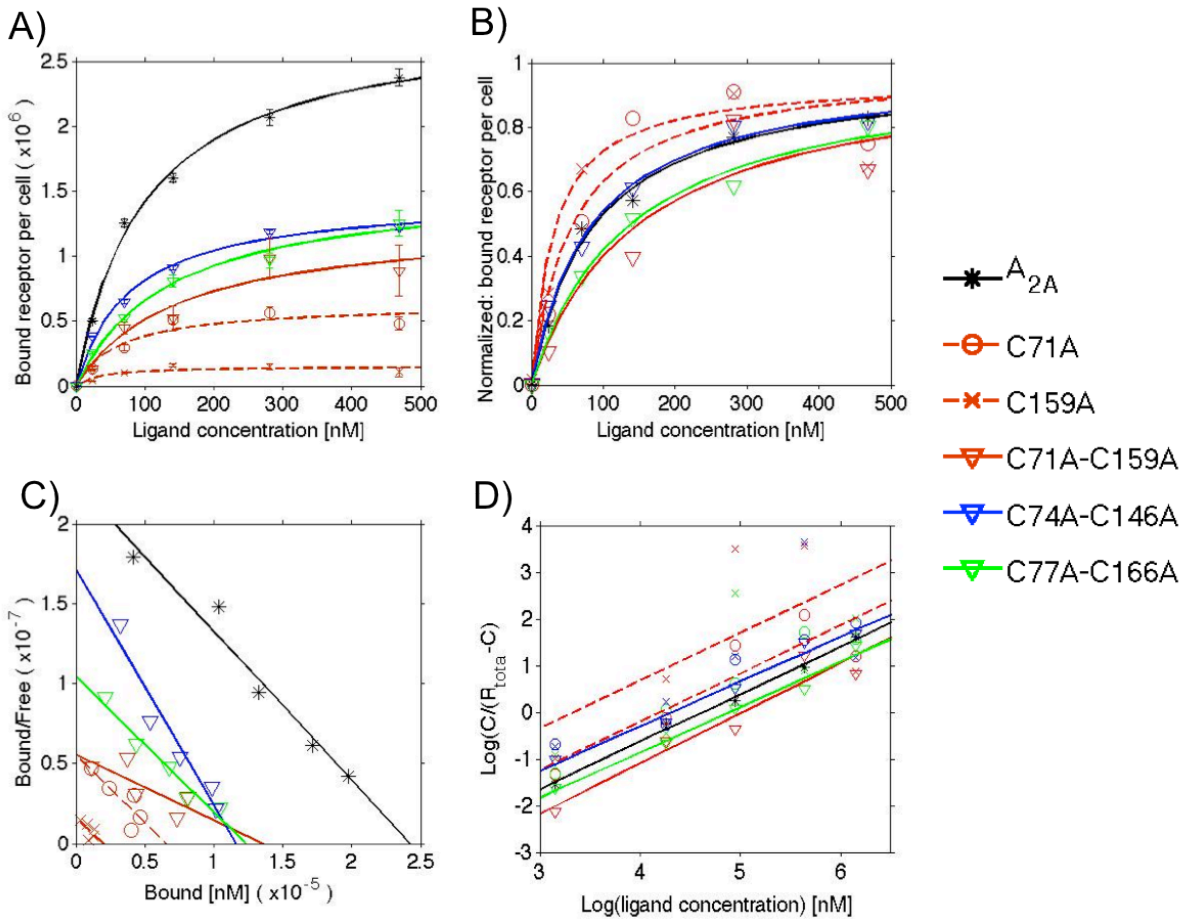

Figure 3.2 [^{3}H] CGS 21680 saturation binding to $A_{2A}R$ variants expressed in HEK-293 cells. A) Monovalent binding fit: the data points are the average of at least two independent experiments performed in triplicate. The total number of active receptors per cell (R_{max}) and the equilibrium dissociation constant (K_D) values are displayed in Table 3.1. B) Normalized monovalent binding fit: data were normalized using the R_{max} value. C) Scatchard analysis: the Scatchard analysis of [^{3}H] CGS 21680 saturation binding to HEK-293 cells expressing the $A_{2A}R$ variants was conducted according to Scatchard [13]. For the single Cys-to-Ala variants, only C71A and C159A are plotted for clarity, and dashed lines represent the fits to the data. Data for the double Cys-to-Ala variants are plotted using downward-pointing triangles and solid lines for the fits. The data for the WT $A_{2A}R$ are plotted using asterisks and a black solid line for the fit.

Normalizing the data using the R_{max} values calculated from the fits allows for easier visualization of changes in the ligand-binding affinity (K_D), as shown in Figure 3.2B. Linear transformation of the data (Scatchard analysis, Figure 3.2C) highlights that the single cysteine variants – in particular mutations in ECL2 – had the greatest impact on the total active receptor at the plasma membrane (x-axis intercept). A Hill plot (Figure 3.2D) yields a Hill coefficient equal to one, validating the use of a monovalent binding model to fit the data.

In this ligand-binding analysis, three populations with somewhat different binding affinities were identified, as follows (Table 3.1):

- C74A-C146A had similar K_D (92 nM) to the WT $A_{2A}R$ (94 nM). This variant also had improved plasma membrane trafficking relative to the WT $A_{2A}R$ (Figure 2.6, Chapter 2).

- Remarkably, the single Cys-to-Ala variants displayed modestly increased ligand-binding affinity compared to the WT receptor; despite their improved ligand-binding affinity, their higher levels of ER localization are likely a result of exposure of a free cysteine in the ECL.

- In contrast to the single cysteine variants, and uncorrelated with their plasma membrane trafficking, C77A-C166A and C71A-C159A had significantly higher K_D values (lower affinity) than the WT receptor for [^{3}H] CGS 21680.

Table 3.1 Binding parameters of $A_{2A}R$ WT and Cys-to-Ala variants. HEK-293 cells expressing untagged $A_{2A}R$ WT and Cys-to-Ala variants were incubated with increasing amount of agonist, [^{3}H] CGS 21680. Equilibrium data were fit to a monovalent binding model to determine the total number of active receptors (R_{max}) and the equilibrium dissociation constant (K_D). (+) r^2 values >0.9, and (*) r^2 values >0.84. Values represent the mean ± the standard error of the mean (SEM) for at least two independent biological experiments performed in triplicate. Sample size indicates the number of replicates measured. (^) Indicates K_D values significantly different from the wild type value, $p \leq 0.05$.

	K_D ± SEM (nM)	K_D 95% CI (nM)	R_{max} ± SEM x10^6	R_{max} % of A_{2A}	sample size
A_{2A} WT+	94.5±9.5	75.8-113.1	2.9±0.6	100	12
C71A+	61.5±11.1	39.8-83.2	0.64±0.14	22.2	6
C74A+	60.7±3.6^	53.7-67.7	1.1±0.1	38.5	6
C77A+	70.0±14.3	42.0-98.0	0.54±0.13	18.8	9
C146A+	51.7±6.3^	39.3-64.2	0.18±0.03	6.4	9
C159A*	49.8±20.9	8.7-90.8	0.16±0.01	5.6	6
C166A+	64.4±3.1^	58.4-70.4	0.44±0.12	15.3	6
C71A-C159A +	149.8±5.0 ^	140.0-159.6	1.3±0.2	44.1	6
C74A-C146A+	91.8±15.4	61.7-121.9	1.5±0.1	50.9	9
C77A-C166A+	139.8±8.9^	122.3-157.3	1.6±0.05	54.4	6

3.4. Discussion

The results presented in Chapter 2 and Chapter 3 indicate that the conserved disulfide bond (C77-C166) is not essential for the expression and ligand-binding activity of the $A_{2A}R$. In contrast, by mutating the cysteines in ECL1 and ECL2, including those of the conserved disulfide bond, we were able to access a range of ligand-binding affinities (from 52-150 nM) and only somewhat reduced trafficking to the plasma membrane.

3.4.1. Receptor Ligand-Binding Activity and Thermodynamic Stability

Even though the single Cys-to-Ala variants exhibited higher levels of ER localized receptors compared to the WT, they were able to bind fluorescent and radiolabeled ligands with affinity close to WT (Figure 3.1A-F and Figure 3.2). It is possible that these variants could still form two disulfide bonds between ECL1 and ECL2, achieving a non-native conformation with higher affinity to the ligand than the WT receptor (Figure 3.2B and Table 3.1).

Our data suggest that only two disulfide bonds are needed to maintain the most active conformation of $A_{2A}R$. Mutations to C71-C159 and C77-C166 had a somewhat negative impact on the ligand-binding affinity (Figure 3.2B and Table 3.1). In contrast, mutations to C74-C146 had no effect on ligand affinity, further suggesting that this disulfide bond is not necessary for the folding and activation of this receptor. However, the disulfide bond between C74-C146 could be important for the interactions with other ligands not tested in the current study (e.g. antagonists and other agonists) or for ligand-binding kinetics.

In vitro studies of $A_{2A}R$ where purified receptor was denatured using urea showed that WT receptor and TCEP reduced receptor underwent a similar unfolding transition; however, ligand binding was significantly decreased in the TCEP reduced receptor (Figure 2.1, Chapter 2) [14]. Taken together with our *in vivo* studies, these data indicate that the disulfide bonds in $A_{2A}R$ are more critical for maintaining the active conformation of the receptor than for achieving a more stable structural conformation [14].

It has been reported that the recognition of misfolded proteins by the quality control system in the ER is correlated with the thermodynamic stability of the protein or altered folding kinetics [15-17]. Since mutation to C74-C146 improved the

receptor trafficking to the plasma membrane (Figure 2.6 and Table 2.2, in Chapter 2), it is possible that in this case the removal of the disulfide bond between C74 and C146 improved receptor stability, assembly efficiency, and thus, trafficking**.** Our results suggest that in $A_{2A}R$ the disulfide bonds restrict the active conformation of the receptor. However, this constrained active conformation may not be the more stable conformation, as seen with the loss of the C74-C146 bond, which improved the trafficking of the receptor. One possible explanation that is consistent with our results is that during evolution $A_{2A}R$ was optimized for function rather than for folding and assembly, as previously suggested by Ellgaard and Helenius to explain the poor native trafficking efficiency of some proteins, including CFTR and the δ opioid receptor [16].

The range of ligand-binding affinities observed with the $A_{2A}R$ variants (52–150 nM) suggests that the disulfide bonds may regulate the active conformation of this receptor and that different active conformations could be achieved with various cysteine mutations. It is unclear whether the disulfide bonds are important to maintain the active conformation of the ECLs, or of residues in the transmembrane domains encompassing the ligand-binding pocket.

3.4.2. Importance of Disulfide Bonds in Ligand Recognition

There is growing evidence that ECL2 is important for ligand recognition in class A GPCRs [7]. In many GPCRs, this region is not well conserved in length, amino acid composition, and number of disulfide bonds [9, 18]. In contrast, there exists high structural similarity among GPCR transmembrane domains [19]. This can be observed within the adenosine receptor (AR) family, which share high sequence homology of the residues in the transmembrane domains, with low homology in the ECL regions, as seen in Figure 3.3. It has been postulated that interactions that

determine AR subtype selectivity are localized to the more diverse upper and extracellular regions of the binding pocket [20]. In contrast, the lower portion of the ligand-binding pocket is believed to determine the strength of ligand binding [21].

Figure 3.3 Sequence alignment of the human adenosine receptors. The yellow highlight denotes the approximate boundary of the extracellular loops, and the cysteines in ECL1 and ECL2 are highlighted in blue. Asterisks indicate fully conserved residues, colons indicate conservation between groups of strongly similar properties, and periods indicate conservation between groups of weakly similar properties. UniProt was used for sequence alignment [22].

From the $A_{2A}R$ crystal structures, NMR, molecular modeling and mutagenesis studies, the details of the ligand-binding pocket of the ARs are becoming clearer. In $A_{2A}R$, ECL2 forms a random coil structure with a very short α-helical segment at the end of the loop [19]. This segment could form critical aromatic π-stacking interactions between F168 and the heterocyclic core of various $A_{2A}R$ agonists and antagonists [19, 21, 23-27]. Additionally, this small α-helical segment contains E169, which could form important polar interactions with various ligands and with H264 in ECL3 [25]. ECL2 has another α-helical segment, above F168 and E169, Figure 3.4. This helix contains the positively charged residues K150 and K153, which can play a role in initial ligand recognition and movement to the binding site [Supplement of 25, 28]. Additionally, in molecular modeling studies, the carboxyl group of the agonist CGS 21680 is in contact with K153 through ionic interactions [25].

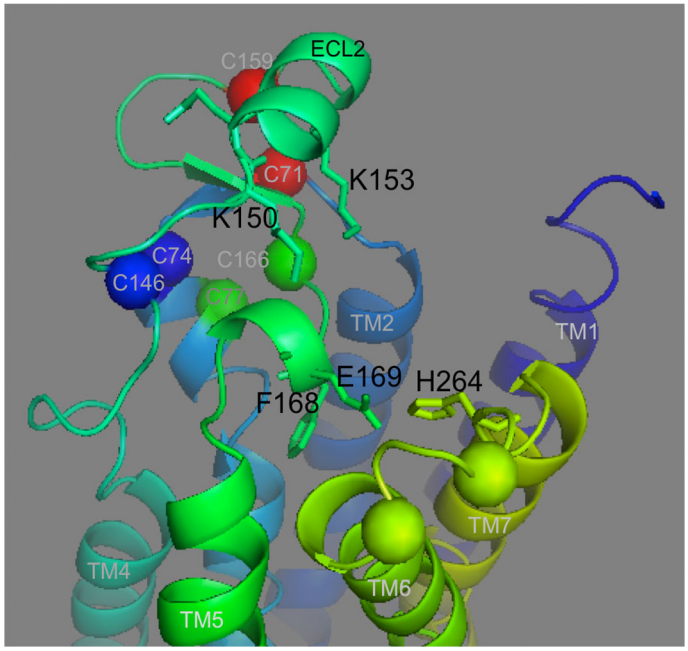

Figure 3.4 Residues in ECL2 important for ligand recognition and binding. Cysteines are indicated as spheres, and color-coded to note the corresponding disulfide bonds. Residues in the ECLs important for ligand binding are indicated as sticks. Adapted using PyMOL, Protein Data Bank identification code 4EIY.

Our data suggest that only two disulfide bonds are needed to retain ligand-binding affinity, C71-C159 and C77-C166, and therefore these two disulfide bonds may be critical for restricting the conformation of the two helices in the ECL2. Furthermore, mutations to C71-C159 and C77-C166 had the highest impact on the ligand-binding affinity of $A_{2A}R$, which could be due to an increased flexibility of ECL2 in the absence of these disulfide bonds, resulting in a conformation where F168, E169, K150 or K153 are not in direct contact with the ligand. It is likely that the disulfide bonds restrict the conformation of the ECLs, and that for the incoming ligand, each ECL topology represents a signature for each receptor [6].

The four ARs contain a conserved phenylalanine (F168) residue in ECL2, and E169 is conserved in $A_{2A}R$, $A_{2B}R$ and A_1R, as seen in Figure 3.3. Therefore, these residues could also form important contacts with the ligand in the other ARs. A_1R and A_3R have only the one conserved disulfide bond linking ECL1 and ECL2. $A_{2B}R$ has a rich concentration of cysteines, and could potentially form two disulfide bonds between ECL1 and ECL2. Since the disulfide bond network is different among the ARs, the interactions between the residues important for ligand binding (e.g. F168 and E169) and the ligand could vary due to a difference in loop topology, restricted by the disulfide bonds. The different disulfide bond networks present in the ARs could help explain why the ARs have different affinities for the same ligand.

3.5. Conclusion

The ECL regions are challenging to capture in crystal structures due to their flexibility; therefore, mutagenesis and functional studies continue to provide insight into the importance of these flexible regions. Our results suggest that the disulfide bond network in $A_{2A}R$ is important for maintaining the active topology of the ECLs. By mutating the cysteines in the ECLs, we were able to access various active conformations. None of the cysteine residues mutated in this study, including the conserved cysteines, were essential for A_{2A} adenosine receptor trafficking and ligand-binding activity. Our results also indicate that the disulfide bonds do not contribute to the assembly of the most stable conformation, as the removal of C74-C146 improves folding efficiency and trafficking to the plasma membrane, attributes that have been linked to conformational stability. This suggests that a widely accepted concept in the biophysical community, that disulfide bonds contribute to protein stability, may not

always be the case, in particular with proteins with an extensive disulfide bond network, such as $A_{2A}R$.

3.6. Acknowledgements

Emily C. McCusker, a previous graduate student, established the foundation for the work described in Chapter 2 and Chapter 3. Many undergraduate students contributed to this work: Amy Chevalier was essential in the development of the plasma membrane and ER staining protocol and she took many of the confocal images. Esther Ayettey took many of the FITC-APEC binding confocal images and also conducted some of the plasma membrane and ER staining experiments. Gregory D. Cousins developed the algorithm used for the HR analysis of the confocal images. Dr. Kirk Czymmek and the BioImaging Center at the Delaware Biotechnology Institute assisted with the development of the staining protocol and obtaining the confocal images.

REFERENCES

1. Jaakola, V.P., et al., *The 2.6 angstrom crystal structure of a human A2A adenosine receptor bound to an antagonist.* Science, 2008. **322**(5905): p. 1211-7.

2. Dohlman, H.G., et al., *Role of Extracellular Disulfide-Bonded Cysteines in the Ligand-bonded Cysteins in the Ligand-binding Function of the Beta-2-Adrenergic Receptor* Biochemistry, 1990. **29**(9): p. 2335-2342.

3. Karnik, S.S. and H.G. Khorana, *Assembly of functional rhodopsin requires a disulfide bond between cysteine residue-110 and residue-187.* Journal of Biological Chemistry, 1990. **265**(29): p. 17520-17524.

4. Noda, K., et al., *The high-affinity state of the beta-2-adrenergic receptor requires unique interaction between conserved and nonconserved extracellular loop cysteines.* Journal of Biological Chemistry, 1994. **269**(9): p. 6743-6752.

5. Perlman, J.H., et al., *A disulfide bond between conserved extracellular cysteines in the thyrotropin-releasing-hormone receptor is critical for binding.* Journal of Biological Chemistry, 1995. **270**(42): p. 24682-24685.

6. Zhang, P.S., et al., *Mutation of human mu opioid receptor extracellular "disulfide cysteine" residues alters ligand binding but does not prevent receptor targeting to the cell plasma membrane.* Molecular Brain Research, 1999. **72**(2): p. 195-204.

7. Venkatakrishnan, A.J., et al., *Molecular signatures of G-protein-coupled receptors.* Nature, 2013. **494**(7436): p. 185-194.

8. Hwa, J., et al., *Structure and function in rhodopsin: Further elucidation of the role of the intradiscal cysteines, Cys-110, -185, and -187, in rhodopsin folding and function.* Proceedings of the National Academy of Sciences of the United States of America, 1999. **96**(5): p. 1932-1935.

9. de Graaf, C., et al., *Molecular modeling of the second extracellular loop of G-protein coupled receptors and its implication on structure-based virtual screening.* Proteins-Structure Function and Bioinformatics, 2008. **71**(2): p. 599-620.

10. Scholl, D.J. and J.N. Wells, *Serine and alanine mutagenesis of the nine native cysteine residues of the human A(1) adenosine receptor.* Biochemical pharmacology, 2000. **60**(11): p. 1647-1654.

11. O'Malley, M.A., et al., *High-level expression in Saccharomyces cerevisiae enables isolation and spectroscopic characterization of functional human adenosine A2a receptor.* Journal of structural biology, 2007. **159**(2): p. 166-78.

12. McCabe, R.T., P. Skolnick, and K.A. Jacobson, *2-[2-[4-[2-[2-[1,3-Dihydro-1,1-bis (4-hydroxyphenyl)-3-oxo-5-isobenzofuranthioureidyl]ethylaminocarbonyl]ethyl]pheny l] ethylamino]-5'--ethylcarboxamidoadenosine (FITC-APEC): A Fluorescent Ligand For A-Adenosine Receptors.* Journal of fluorescence, 1992. **2**(4): p. 217-223.

13. Scatchard, G., *The attractions of proteins for small molecules and ions* Annals of the New York Academy of Sciences, 1949. **51**(4): p. 660-672.

14. O'Malley, M.A., et al., *Analysis of adenosine A(2)a receptor stability: Effects of ligands and disulfide bonds.* Biochemistry, 2010. **49**(43): p. 9181-9189.

15. Krebs, M.P., et al., *Quality control of integral membrane proteins.* Trends in Biochemical Sciences, 2004. **29**(12): p. 648-655.

16. Ellgaard, L. and A. Helenius, *Quality control in the endoplasmic reticulum.* Nature Reviews Molecular Cell Biology, 2003. **4**(3): p. 181-191.

17. Nagy, J.K. and C.R. Sanders, *Destabilizing mutations promote membrane protein misfolding.* Biochemistry, 2004. **43**(1): p. 19-25.

18. Seibt, B.F., et al., *The second extracellular loop of GPCRs determines subtype-selectivity and controls efficacy as evidenced by loop exchange study at A(2) adenosine receptors.* Biochemical pharmacology, 2013. **85**(9): p. 1317-1329.

19. Piirainen, H., et al., *Structural features of adenosine receptors: From crystal to function.* Biochimica Et Biophysica Acta-Biomembranes, 2011. **1808**(5): p. 1233-1244.

20. Li, J.N., et al., *Ligand-dependent activation and deactivation of the human adenosine A(2A) receptor.* Journal of the American Chemical Society, 2013. **135**(23): p. 8749-8759.

21. Jaakola, V.P., et al., *Ligand Binding and Subtype Selectivity of the Human A(2A) Adenosine Receptor Identification and Characterization of Essential Amino Acid Residues.* Journal of Biological Chemistry, 2010. **285**(17): p. 13032-13044.

22. Apweiler, R., et al., *Activities at the Universal Protein Resource (UniProt).* Nucleic Acids Research, 2014. **42**(D1): p. D191-D198.

23. Lane, J.R., et al., *A novel nonribose agonist, LUF5834, engages residues that are distinct from those of adenosine-like ligands to activate the adenosine A(2a) receptor.* Molecular pharmacology, 2012. **81**(3): p. 475-487.

24. Xu, F., et al., *Structure of an agonist-bound human A2A adenosine receptor.* Science, 2011. **332**(6027): p. 322-7.

25. Deflorian, F., et al., *Evaluation of molecular modeling of agonist binding in light of the crystallographic structure of an agonist-bound A(2A) adenosine receptor.* Journal of medicinal chemistry, 2012. **55**(1): p. 538-552.

26. Lebon, G., et al., *Agonist-bound adenosine A2A receptor structures reveal common features of GPCR activation.* Nature, 2011. **474**(7352): p. 521-5.

27. Dore, A.S., et al., *Structure of the adenosine A(2A) receptor in complex with ZM241385 and the xanthines XAC and caffeine.* Structure, 2011. **19**(9): p. 1283-93.

28. Liu, W., et al., *Structural basis for allosteric regulation of GPCRs by sodium ions.* Science, 2012. **337**(6091): p. 232-6.

Chapter 4

USING FLUORESCENCE ANISOTROPY TO CHARACTERIZE BINDING AFFINITY AND KINETICS OF UNLABELED LIGANDS

4.1. Introduction

The first high-resolution crystal structure for a G protein-coupled receptor (GPCR), rhodopsin, was published in 2000 [1]. For approximately a decade after the rhodopsin structure was published our knowledge of how drugs interact with GPCRs was based on rhodopsin homology models, apart from site-directed mutagenesis and radioligand-binding experiments [2]. Now there are high-resolution crystal structures for 29 GPCRs out of approximately 850 GPCRs in the human genome; 300 of them are considered potential drug targets [3, 4]. More GPCR structures will continue to advance *in silico* drug discovery, with the goal of designing more effective therapeutics.

As described in Chapter 1, Section 1.6.2, drug efficacy determination historically has guided drug discovery efforts in whole cells, tissues or animals [5]. Identification of the molecular targets of various diseases coupled with advances in cloning, cell-based assays, and purification of the target receptors has led to the widely accepted practice of binding affinity optimization to guide most early-stage drug discovery efforts [5, 6]. The success of this approach is predicated on the assumption that ligand-binding affinity is a suitable surrogate for *in vivo* efficacy.

Many efficacious drugs have been identified based on ligand affinity determination [5]; however, there is recent evidence to suggest that in some cases

ligand-binding kinetics could be a better predictor of a drug's potential efficacy and safety [5]. For example, the residence time ($RT=1/k_{off}$) of $A_{2A}R$ agonists was correlated to the efficacy of the drug, while affinity was not [7]. For many GPCRs, lead compounds are identified based on inhibitor dissociation constant (K_i), calculated from data measured predominantly under equilibrium conditions, and the binding kinetics are usually not considered [6, 7]. Awareness and experimental evidence of the importance of binding kinetics is increasing and there is great interest in the development of assays to measure ligand-binding kinetics.

Drug efficacy will continue to be the main attribute for selecting a drug as a therapeutic. However, knowledge of the ligand-binding kinetics can allow the design of drugs with the desired association and dissociation rates; long residence time could be desired for allergy medicines, while drugs with shorter residence time could be desired for conditions where on-target toxicity is a problem [6].

Taking advantage of the successful expression of full-length human $A_{2A}R$ in yeast and the successful purification of functional receptor in micelles (DDM/CHAPS/CHS) [8, 9], we developed a fluorescence anisotropy-based *in vitro* method to characterize the ligand-binding affinity and kinetics of unlabeled ligands.

4.2. Using Fluorescence Polarization to Measure Ligand-Binding Affinity

In contrast to traditional radioligand-binding assays, in fluorescence anisotropy (FA) (also referred to as fluorescence polarization) assays the unbound ligand does not need to be separated, but it does contribute to the signal [10]. FA assays rely on the difference in molecular rotational mobility between the bound and unbound ligand [11, 12], Figure 4.1.

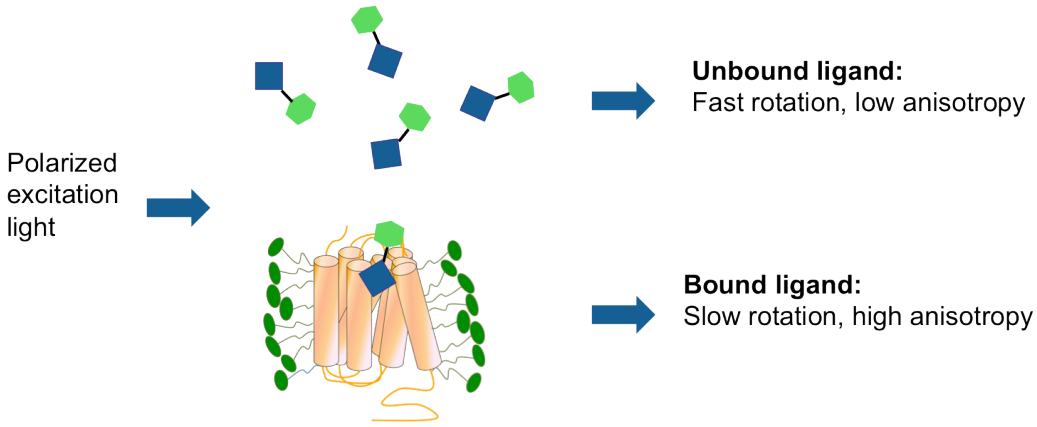

Figure 4.1 Principle behind fluorescence anisotropy assay. Due to the difference in molecular volume, bound and unbound ligands have different rotation, leading to different anisotropy values.

Linear polarized light is used to excite the sample, allowing the specific excitation of fluorophores properly aligned with the excitation light [13]. Emission is detected parallel and perpendicular to the excitation light. Free or unbound ligand will rotate freely, leading to a lower anisotropy signal. In contrast, bound ligand will have a slower rotation, leading to a higher anisotropy signal [11].

FA has been used to characterize the ligand binding of various GPCRs, including the CCR1 [3], MC5 receptor [10], A_{2A} adenosine receptor [11], β_1 adrenergic receptor [14], and M_1 muscarinic receptor [12], to name a few.

Prystay et al. validated a fluorescence polarization binding assay by comparing the results to values calculated from traditional radioligand saturation binding assays. Six different GPCRs were tested; the K_D and B_{max} calculated from the fluorescence polarization analysis were in agreement with values obtained from radioligand-binding experiments [10]. Kecskés et al. also used a fluorescence polarization assay to measure the K_i of eleven $A_{2A}R$ specific and non-specific ligands; all K_i values matched

the values calculated using radioligand-binding assays [11]. These studies highlight the potential of fluorescence polarization assays as an alternative and potentially more versatile approach to measuring ligand-binding affinity than radioligand-binding assays. To date, few studies have used FA to measure ligand-binding kinetics for GPCRs.

4.3. Materials and Methods

4.3.1. Expression and Purification of A_{2A} from Yeast Membrane Preparations

Full-length human $A_{2A}R$ was expressed in *Saccharomyces cerevisiae* cells, BJ5464, using the multi-integrating pITy-$A_{2A}R$-His_{10} plasmid, as previously described [9]. Both the lipid and detergent purification protocols started from cell pellets, which were collected via centrifugation of a 600 ml culture 24 hours after induction. Aliquots of 50 ml cell culture at an optical density (OD_{600}) of approximately 22-25 were collected by centrifugation (3,220 g) and frozen at -80 °C. Freezing cell pellets at a consistent optical density and starting the detergent solubilization step from membrane preparations instead of crude cell lysis improved reproducibility and purity of the purification.

Cell pellets were thawed using 22 ml of Buffer A (10% glycerol, 50 mM sodium phosphate monobasic and 300 mM sodium chloride at pH 8, supplemented with 1 mM phenylmethanesulfonyl fluoride (PMSF) and complete EDTA-free protease inhibitor tablets (Roche Applied Science, Indianapolis, IN)). Cells were then combined with 0.5 mm zirconia/silica beads (BioSpec, Bartlesville, OK) and lysed using a vortex for six-60 second pulses, placing the cells on ice for 60 seconds between pulses. The beads were then removed using Kontes separation columns.

Samples were placed on ice and probe-sonicated (Branson 450 set at 50% power) twice, for 20 seconds. The lysate was centrifuged at 3,220 g for 30 min at 4 °C to remove unlysed cells and cellular debris. The supernatant was then centrifuged at 100,000 g for 45 minutes at 4 °C, to remove most soluble proteins. The crude membranes (pellet) were resuspended in Buffer A and membranes were homogenized using a Potter-Elvehjem tissue homogenizer. After homogenization the following detergents were added: 2% (w/v) DDM + 1% (w/v) 3-(3-cholamidopropyl) dimethylammoniopropane sulfonate (CHAPS) + 0.2% (w/v) CHS (from Anatrace, Maumee, OH).

The membrane was solubilized overnight at 4ºC. The following morning, insoluble matter was removed via centrifugation at 80,000 g for 1 hr at 4 ºC. Supernatant (approximately 20 ml) was supplemented with one protease inhibitor tablet, 1 mM PMSF and 15 mM imidazole to prevent non-specific binding to the nickel resin. This solubilized membrane mixture was then added to pre-equilibrated Ni-NTA Superflow resin (Qiagen, Valencia, CA), and samples were incubated for at least 3 hours at 4 °C in an end-over-end mixer to allow binding to the nickel resin. Unbound material was removed by low speed centrifugation, followed by low-concentration imidazole washes to reduce non-specific binding using buffer A containing 0.2% (w/v) DDM + 0.1% (w/v) CHAPS + 0.02% (w/v) CHS. The washes contained increasing amounts of imidazole (20 mM, 30 mM and 50 mM imidazole, respectively). Each imidazole wash was incubated for 20 minutes at 4 °C in an end-over-end mixer, followed by low speed centrifugation and removal of the supernatant. To elute A_{2A}R-His_{10} from the nickel resin, samples were incubated at 4 °C for 1 hour with Buffer A, 500 mM imidazole and 0.2% (w/v) DDM + 0.1% (w/v) CHAPS +

0.02% (w/v) CHS. PD-10 desalting columns (GE Healthcare, Pittsburgh, PA) were used per manufacturer instructions to remove imidazole and salt ions using the elution buffer, Buffer B (50 mM phosphate at pH 7 and 0.2% (w/v) DDM + 0.1% (w/v) CHAPS + 0.02% (w/v) CHS). A_{2A}R-DCC (DDM/CHAPS/CHS) samples were stored at 4 °C and used within one week.

4.3.2. Protein Purity and Concentration

Samples were separated via SDS-PAGE on a 12% Tris-Glycine gel (ThermoFisher Scientific, Rockford, IL), and protein bands were detected via staining with Sypro Ruby (Life Technologies, Carisbad, CA). Protein concentration was determined using UV absorbance at 280 nm as described in [9], and protein purity was quantified from the gel stain image using FIJI [15]. All A_{2A}R samples used in these studies had a purity of 90% or higher (Table 5.1, Chapter 5).

4.3.3. Fluorescence Anisotropy Assay

Ligand-binding affinity and kinetics were measured using the agonist FITC-APEC (NIMH synthesis program, http://nimh-repository.rti.org, NIMH Code: D-906) [16]. Measurements were conducted in half size Corning Costar 96-well half area black polystyrene plates (catalog # 3875, Corning Incorporated, Acton, MA) using a Synergy H1 plate reader (BioTek, Winooski, VT) at an excitation wavelength of 480–485 nm and emission wavelength of 520–528 nm. All measurements were taken at a constant gain (75); for assays at low fluorescent ligand concentration (0.5–1 nM) readings were also taken at a higher gain (100). Scatter measurements prior to the addition of fluorescent ligand were taken for all samples and subtracted as described below. All unlabeled ligands were purchased from Tocris.

Equilibrium Measurements

Solubilized $A_{2A}R$ was incubated with FITC-APEC until equilibrium was reached (approximately two to three hours at room temperature, depending on the concentration of FITC-APEC). Empty micelles were also incubated with FITC-APEC as a negative control; non-specific binding was measured using 10 μM NECA. The parallel and perpendicular fluorescence emission of the solubilized $A_{2A}R$ and empty micelles were measured prior to the addition of FITC-APEC to account for scatter. Prior to calculating anisotropy (Equation 4.1), the fluorescence signal due to scatter was subtracted from the parallel and perpendicular fluorescence intensity of samples containing FITC-APEC.

$$A = \frac{F_{\parallel} - F_{\perp}}{F_{\parallel} + 2F_{\parallel}} \times 1000 \quad (4.1)$$

where A is anisotropy in milli-anisotropy units (mA), $F_{\parallel}$ and $F_{\perp}$ are the parallel and perpendicular emission fluorescence intensities, respectively.

To calculate the maximum anisotropy (A_{max}) value for FITC-APEC bound to micelle solubilized $A_{2A}R$, the receptor concentration was varied from 0–1.6 μM, while varying the concentration of FITC-APEC from 0.5–100 nM. To calculate the minimum anisotropy (A_{min}), empty micelles and excess competitor (10 μM NECA) were used. All ligand dilutions were prepared so that 2 μL of labeled ligand were added per sample; this assured that DMSO was 2% of the sample and guaranteed consistency between experiments. Usually DMSO concentrations up to 5% had no effect on the anisotropy signal observed [14].

Scatter data were taken prior to the addition of the fluorescent ligand. $A_{2A}R$-DCC and control samples were incubated with FITC-APEC for two hours at room temperature, protected from light prior to measurements.

For competition binding experiments A_{2A}R-DCC samples, diluted to 800 nM, were incubated with 30nM FITC-APEC and the appropriate amount of competitor for 4 hours (~ $3.5/k_{off}$ [17]) at room temperature and protected from light. At this receptor concentration, both controls (empty micelles and A_{2A}R-DCC incubated with 10 μM NECA) had similar anisotropy values (Figure 4.2). We tested six unlabeled ligands: NECA, adenosine, CGS 21680, Bay 606583, ZM 241385 and SCH442416.

Kinetic Measurements

For FITC-APEC association kinetic measurements, A_{2A}R-DCC (diluted to 800 nM) and empty micelles were incubated with 30 nM FITC-APEC with and without competitor (NECA, adenosine and ZM 241385). Measurements were taken every 8 seconds at room temperature until equilibrium was reached.

4.4. Data Analysis

4.4.1. Calculating Receptor-Ligand Complexes from Anisotropy Data

The measured anisotropy signal is a weighted average of that due to bound ligand, corresponding to the maximum anisotropy signal (A_{max}), and unbound ligand, corresponding to the minimum anisotropy signal (A_{min}). Once the A_{max} and A_{min} are determined (Figure 4.2), the receptor-ligand complex (RL) can be calculated using the following equation [10]:

$$A = A_{max}\frac{RL}{L_T} + A_{min}\frac{L_f}{L_T} \quad (4.2)$$

where the only unknown is RL, the receptor-ligand complex. L_T is the concentration of total labeled ligand added; L_f is the free ligand ($L_f = L_T - RL$). A is the measured

anisotropy signal; A_{min} and A_{max} are the maximum and minimum anisotropy values determined experimentally for the system.

Once the concentration of the RL complexes are calculated, Scatchard plot analysis [18] was used to calculate the affinity (K_D) of FITC-APEC to $A_{2A}R$ in DCC micelles.

$$\frac{RL}{L_f} = \frac{-RL}{K_D} + \frac{B_{max}}{K_D} \tag{4.3}$$

where RL is the concentration of the receptor-ligand complex (calculated using Equation 4.2), B_{max} is the total number of available binding sites, L_f is the free labeled ligand concentration. B_{max} and K_D are calculated from the slope and y-axis intercept of the line. B_{max} was used to calculate α (the fraction of purified receptor that bound the agonist FITC-APEC).

4.4.2. Inhibitor Dissociation Constants

In competition experiments, the labeled ligand competes with increasing concentration of unlabeled ligand. From these experiments the half-maximal inhibition (IC_{50}) can be calculated using Equation 4.4. To calculate the IC_{50}, the maximum (Y_{max}) and minimum (Y_{min}) anisotropy values were determined, corresponding to the anisotropy values without competitor and with the highest competitor concentration. A is the measured anisotropy as a function of increasing concentration of inhibitor (I). The inhibitor dissociation constant (K_i) can then be calculated using Equation 4.5 (Cheng-Prusoff equation [19]), where L and K_D are the ligand concentration and the equilibrium dissociation constant of the labeled ligand.

$$A = Y_{min} + \frac{Y_{max}\text{-}Y_{min}}{1+10^{I\text{-}IC50}} \quad (4.4)$$

$$K_i = \frac{IC_{50}}{1+\frac{L}{K_D}} \quad (4.5)$$

4.4.3. Kinetic Measurements

Single-phase exponential association (Equation 4.6) and dissociation (Equation 4.7) equations have been used to calculate the association and dissociation rate constants of labeled ligands from anisotropy data [11], with the goal of obtaining the equilibrium dissociation constant, $K_D=k_{off}/k_{on}$. For association data,

$$A = Y_{max}\left(1\text{-}e^{Kx}\right) \quad (4.6)$$

A is the measured anisotropy; Y_{max} is the maximum value of the kinetic association curve. Note that this will not be the same as A_{max} observed for equilibrium data. K is the observed rate constant, K_{obs}. For dissociation data,

$$A = (A_0\text{-}NS)e^{\text{-}Kx} + NS \quad (4.7)$$

A is the measured anisotropy; A_0 is the initial anisotropy value prior to competitor addition, NS is the asymptotic value for the anisotropy as time approaches infinity, associated with non-specific binding. K is the dissociation rate constant, k_{off}. K_{obs} and k_{off} are then related to the labeled ligand concentration ($K_{obs}= k_{on}[L]+k_{off}$) to calculate k_{on} and K_D.

Apart from the exponential approximation, we used the analytical solution to a mass action model for one ligand and a single-site binding reaction to fit the FITC-APEC association kinetic data [17]. Equation 4.8 is the elementary equation for the two chemical species, receptor (R) and ligand (L); both species bind to form receptor-ligand complexes (C).

$$R + L \leftrightarrow C \tag{4.8}$$

The rate equations for the concentration of receptor-ligand complexes, ligand and receptor are given by Equations 4.9-4.11. R, L, and C are the concentrations of each species, k_{on} and k_{off} are the association and dissociation rate constants, respectively. The rate equations are constrained by the conservation of mass.

$$\frac{dC}{dt} = k_{on}RL\text{-}k_{off}C \tag{4.9}$$

$$\frac{dR}{dt} = \text{-}k_{on}RL + k_{off}C \tag{4.10}$$

$$\frac{dL}{dt} = \text{-}k_{on}RL + k_{off}C \tag{4.11}$$

Solving these coupled differential equations yields Equation 4.12, defining the amount of receptor-ligand complexes (C) as a function of time:

$$C = \frac{k_{on}NL}{K_A}(1\text{-}\exp(\text{-}K_A t)) \tag{4.12}$$

$$K_A = k_{on}L + k_{off} \tag{4.13}$$

where N is the total number of available binding sites ($N=\alpha R_T$).

We used the analytical solution to a mass action model for two ligands and a single-site binding reaction to fit the FITC-APEC and competitor association kinetic data [17]. Equations 4.14 and 4.15 are the elementary equations for the three chemical species, receptor (R), labeled ligand (L) and competitor (I); these three species bind to form receptor-labeled ligand complexes (C_L), and receptor-competitor complexes (C_I).

$$R + L \leftrightarrow C_L \tag{4.14}$$

$$R + I \leftrightarrow C_I \tag{4.15}$$

The rate equations for the concentration of C_L and C_I are given by Equations 4.16 and 4.17. R, L, I, C_L and C_I are the concentrations of each species, k_1 and k_2 are

the association and dissociation rate constants of the labeled ligand, determined from Equation 4.12. k_3 and k_4 are the association and dissociation rate constants of the competitor. The rate equations are constrained by the conservation of mass.

$$\frac{dC_L}{dt} = k_1 RL - k_2 C_L \tag{4.16}$$

$$\frac{dC_I}{dt} = k_3 RI - k_4 C_I \tag{4.17}$$

Solving these differential equations yields Equation 4.18, defining the amount of receptor- labeled ligand complexes (C_L) as a function of time [17]:

$$C_L = \frac{k_1 NL}{K_F - K_s}\left(\frac{k_4(K_F - K_S)}{K_F - K_S} + \frac{k_4 - K_F}{K_F}\exp(-K_F t) - \frac{k_4 - K_s}{K_S}\exp(-K_S t)\right) \tag{4.18}$$

$$K_A = k_1 L + k_2 \tag{4.19}$$

$$K_B = k_3 I + k_4 \tag{4.20}$$

$$K_F = 0.5\left(K_A + K_B + \sqrt{(K_A - K_B)^2 + 4k_1 k_3 LI}\right) \tag{4.21}$$

$$K_S = 0.5\left(K_A + K_B - \sqrt{(K_A - K_B)^2 + 4k_1 k_3 LI}\right) \tag{4.22}$$

where N is the total number of available binding sites ($N=\alpha R_T$).

Matlab (version 7.10, MathWorks, Natick, MA) was used to fit the data; all functions used are in Appendix B.

4.5. Results

4.5.1. Fluorescence Anisotropy as a Tool to Measure Ligand-Binding Affinity

In fluorescence anisotropy (FA) assays, the unbound ligand contributes to the anisotropy signal (see Figure 4.2). This characteristic of FA assays introduces some

advantages and disadvantages that need to be considered during assay development. For these studies we use full-length human $A_{2A}R$ solubilized in micelles [9] and the fluorescent ligand FITC-APEC [16].

Classical saturation binding assays involving a constant receptor concentration and increasing amounts of labeled ligand need to be designed with care when using FA, as increasing concentrations of unbound ligand decreases the measured anisotropy signal [10], Figure 4.2. Hence, by necessity, FA assays often operate in the ligand-depleted regime. Figure 4.2 illustrates the decrease of FA signal as the fluorescent ligand concentration increases for any given receptor concentration.

To calculate the maximum anisotropy value (A_{max}) of FITC-APEC bound to $A_{2A}R$ in DDM/CHAPS/CHS micelles ($A_{2A}R$-DCC), the receptor concentration was varied from 0–1.6 μM, while varying the concentration of FITC-APEC from 0.5–100 nM. The highest anisotropy signal (A_{max}= 226.8±5.8 mA, n=3) was attained using 0.5–10 nM FITC-APEC (Figure 4.2). The minimum anisotropy value (A_{min}=103.2±2.0 mA, n=5) was determined using empty DCC micelles.

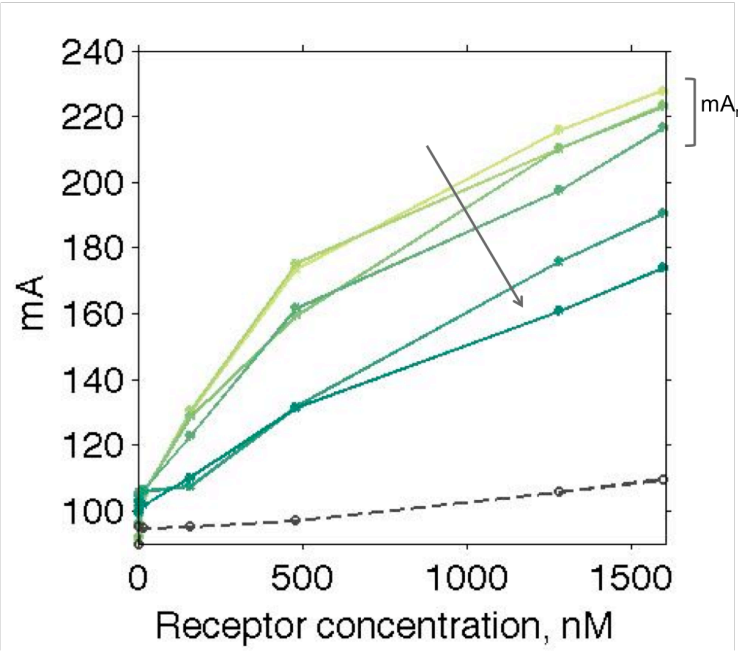

Figure 4.2 Maximum and minimum anisotropy values for FITC-APEC binding to A_{2A}R-DCC. Binding was monitored by increases in FA. Various concentrations of receptor were incubated with increasing fluorescent ligand concentrations (0.5 nM–100 nM); the arrow indicates the decrease in anisotropy as the ligand concentration increases (0.5, 1, 10, 30, 70, and 100 nM). The maximum anisotropy signal was achieved at 0.5–10 nM FITC-APEC. Non-specific binding was measured using 10 μM NECA, dashed line.

At low ligand concentration (0.5 nM and 1 nM), the signal due to scatter (measured prior to the addition of FITC-APEC to the sample) represented approximately 21% of the total parallel and perpendicular fluorescence emission signal of the sample after addition of FITC-APEC. We were able to correct for this by subtracting the parallel and perpendicular signal due to scatter from the parallel and

perpendicular emission of the sample after addition of FITC-APEC. This scatter correction improved the data quality and reproducibility at low concentrations of the fluorescent ligand. Above 10 nM FITC-APEC the scatter represented less than 2% of the emitted signal. The arrow in Figure 4.2 indicates a decrease in the anisotropy signal as the FITC-APEC concentration increases from 0.5 nM to 100 nM. This decrease in anisotropy is due to the contribution of increasing amounts of free ligand.

Classical receptor saturation experiments can be conducted using FA; however, it requires the measurement of the maximum (A_{max}), minimum (A_{min}) and displaced (A_{dis}) anisotropy of the system. Once these values are determined, the receptor–ligand complexes (RL) can be calculated [10]. Note that at approximately 800 nM total receptor concentration, A_{min} equals A_{dis} (Figure 4.2) and Equation 4.2 can be used to calculate RL.

To calculate the equilibrium dissociation constant (K_D) we incubate the solubilized receptor with increasing amounts of FITC-APEC. We used the data for 160 nM and 480nM receptor concentration for the Scatchard plot analysis, as they best approximate the excess ligand regime. K_D=22.34 nM and α=0.056 were calculated from the Scatchard plot analysis, Figure 4.3C.

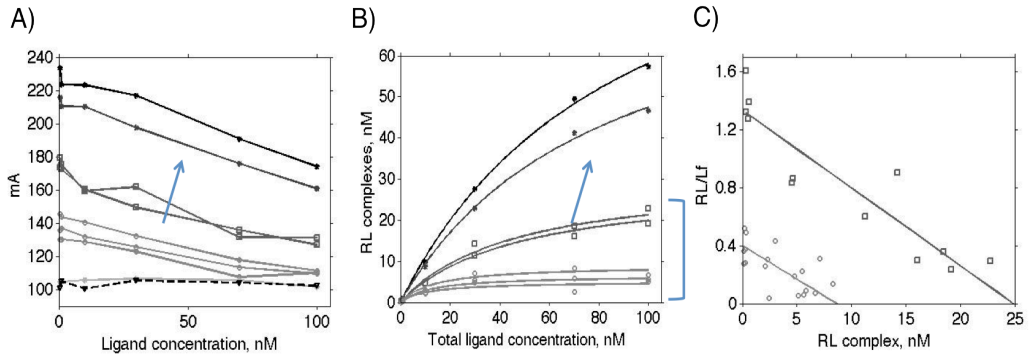

Figure 4.3 Receptor saturation experiments using FA. A) Anisotropy raw data: $A_{2A}R$ at different concentrations (16–1600 nM) were incubated with increasing concentrations of FITC-APEC. Measurements were taken after equilibrium was reached. Arrow indicates increasing concentration of receptor (16, 160, 480, 1280 and 1600 nM). B) Mathematical transformation from anisotropy to receptor-ligand complexes. Arrow indicates increasing receptor concentration. C) Scatchard analysis was conducted for the 160 nM (open circles) and 480 nM (open squares) receptor concentration data, to more closely reflect the excess ligand regime. Scatchard analysis resulted in a K_D=22.34±2.2 nM (± SEM, n=5) and α=0.056±0.004 (± SEM, n=5).

Inhibitor dissociation constants were determined for six unlabeled ligands: adenosine, CGS 21680, NECA, SCH 442416, ZM 241685 and Bay 606583 (an A_{2B} specific agonist) (Figure 4.4). In order to minimize scatter and maximize anisotropy signal, the experiments were performed using 800 nM receptor and 30 nM FITC-APEC. Increasing amounts of unlabeled ligands were added to solutions containing receptor and FITC-APEC, as described in Materials and Methods (Section 4.4.2). The values for IC_{50} and K_i (Table 4.1) were then determined from fits to the equilibrium anisotropy values as described by equations (4.4) and (4.5).

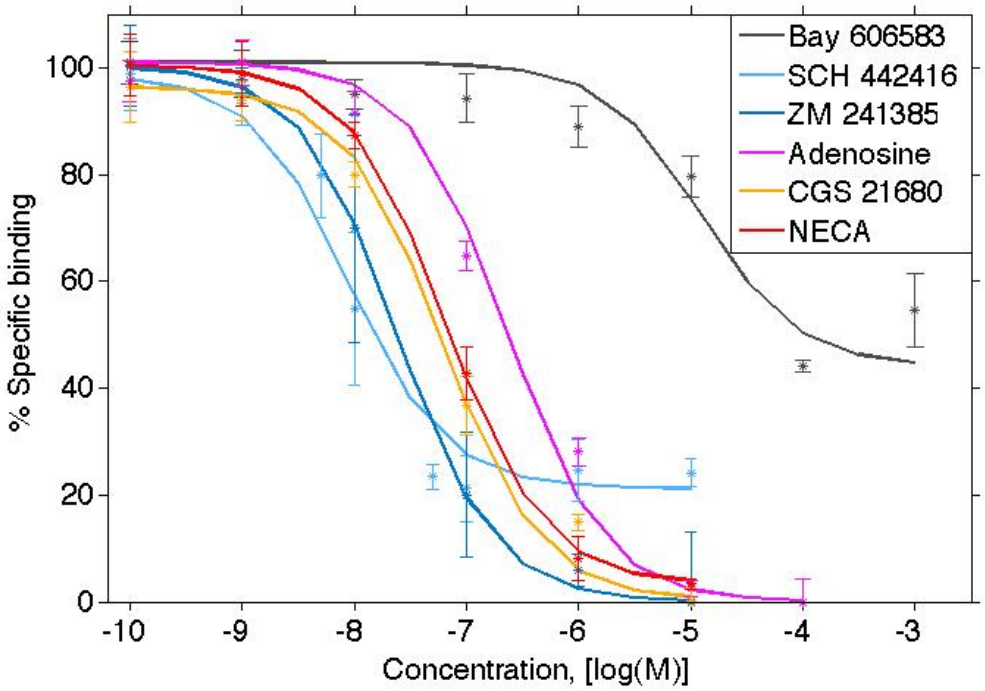

Figure 4.4 Competition of 30 nM FITC-APEC and increasing concentration of unlabeled ligand: Bay 606583 (dark gray), SCH 442416 (in light blue), ZM 241685 (in blue), adenosine (magenta), CGS 21680 (yellow) and NECA (red). Data are plotted as % of initial specific FA value. Data represent the mean ± standard deviation from two independent experiments performed in duplicate (n=4). Lines represent the fit to Equation 4.4, where IC_{50} values were determined by averaging the minimized least square regression for the data of each experiment. IC_{50} values are listed in Table 4.1.

Table 4.1 Half-maximal inhibition values (IC_{50}) for Bay 606583, SCH 442416, ZM 241685, adenosine, CGS 21680 and NECA. Inhibitor dissociation constants (K_i) were calculated using Equation 4.5. Data represent the mean and the 95% confidence interval. The symbols (*, ^, #) indicate ligands with IC_{50} and K_i values that are not significantly different ($p>0.05$).

	IC_{50} (95% CI) nM	K_i (95% CI) nM
Bay 606583	12.0 (1.24–22.8) x 10^3	5132.9 (360.3–9905.4)
SCH 442416	9.4 (4.5–14.3)	4.0 (1.7–6.3)^
ZM 241385	23.6 (15.7–31.6)	10.1 (6.1–14.1)^
Adenosine	227.5 (172.1–283.0)	97.1 (65.4–128.8)
CGS 21680	62.3 (58.7–65.9)*	26.6 (20.6–32.6)#
NECA	67.1 (57.7–76.4)*	28.6 (21.2–36.0)#

4.5.2. Ligand-Binding Kinetics

Two approaches were used to fit the FITC-APEC association and dissociation experiments:

- Exponential approximation where the observed association rate constant (k_{obs}) was calculated from the association data (Figure 4.5A) and k_{off} was calculated from the dissociation curve (Figure 4.5B);
- The analytical solution to a mass action model for one ligand and a single-site binding reaction [17], where the analytical solution requires a known B_{max}.

Ligand-binding association experiments were performed using 800 nM receptor and 30 nM FITC-APEC (Figure 4.5A). Dissociation experiments were performed using 1 μM competitor (ZM 241385 and adenosine) (Figure 4.5B).

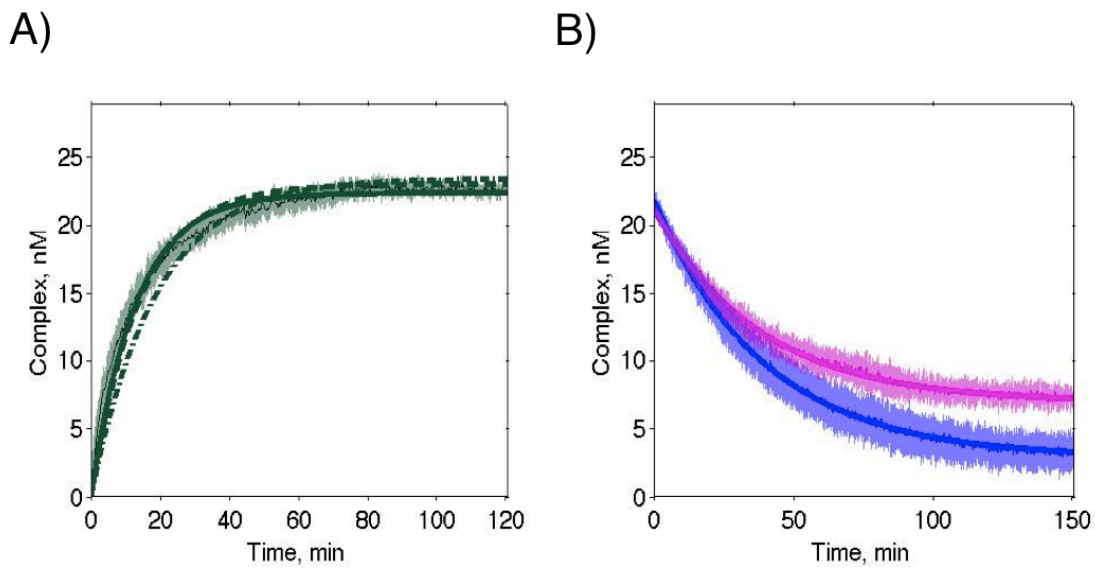

Figure 4.5 FITC-APEC association and dissociation experiments. A) Binding of 30 nM FITC-APEC to $A_{2A}R$ in DCC micelles. The thin green line represents the mean and the shaded green area represents the standard deviation of two independent experiments performed in triplicate. The analytical solution and B_{max} determined from equilibrium data (Figure 4.3) were used to fit the FITC-APEC association data; the green solid line indicates the fit. k_{off}=0.0391±0.0023 $min^{-1}$and k_{on}=0.0014±0.0001 min^{-1} nM^{-1} (±SEM, n=6) were calculated yielding a K_D=29.0±2.8 nM. The dash-dot line indicates a fit where the k_{off} was fixed to the value obtained from the exponential dissociation fit. B) Dissociation of 30 nM FITC-APEC using 1 µM ZM 241385 (blue) and 1µM Adenosine (magenta). The thin blue and magenta lines represent the mean and the shaded blue and magenta areas represents the standard deviation of two independent experiments performed in duplicate. Exponential fits for the association and dissociation experiments are indicated by the solid green (A) and blue and magenta lines (B). k_{off}=0.0255±0.0010 min^{-1} (±SEM, n=8), k_{on}=0.0018±0.0001 min^{-1} nM^{-1} (±SEM, n=6) were calculated (K_D=14.0 ± 1.1 nM).

Exponential fits for the association and dissociation data yielded FITC-APEC association and dissociation rate constants of 0.0018 min^{-1} nM^{-1} (0.0016–0.0021 min^{-1} nM^{-1}, 95% confidence interval) and 0.0255 min^{-1} (0.0236–0.0274 min^{-1}, 95%

confidence interval), respectively (Figure 4.5A and 4.5B). An equilibrium dissociation constant of 14.0 nM (11.8–16.1 nM, 95% confidence interval) was calculated from these kinetic data. Typically, the analytical solution has not been used to determine k_{on} and k_{off}, as it requires the determination of B_{max}. To implement this approach, we used the value for B_{max} determined from equilibrium data (Figure 4.3C). Using this constraint, the analytical solution approach was used to determine the k_{on} and k_{off} from the association data, and yielded association and dissociation rates of 0.0014 min^{-1} nM^{-1} (0.0011–0.0016 min^{-1} nM^{-1}, 95% confidence interval) and 0.0391 min^{-1} (0.0346–0.0436 min^{-1}, 95% confidence interval) (Figure 4.5A). An equilibrium dissociation constant of 29.0 nM (23.4–34.5 nM, 95% confidence interval) was calculated from these kinetic data. The association and dissociation rates calculated from the two fits were significantly different ($p<0.05$) (Table 4.2). However, the equilibrium dissociation constant values differ only by a factor of 1.7.

Table 4.2 FITC-APEC association and dissociation rate constants calculated using exponential approximation and analytical solution. Equilibrium dissociation constant (K_D) calculated via Scatchard is also listed.

	k_{on} (95% CI) nM^{-1} min^{-1}	k_{off} (95% CI) min^{-1}	K_D (95% CI) nM
Exponential approximation	0.0018 (0.0016–0.0021)	0.0255 (0.0236–0.0274)	14.0 (11.8–16.1)
Analytical solution	0.0014 (0.0011–0.0016)	0.0391 (0.0346–0.0436)	29.0 (23.4–34.5)
Scatchard analysis	----	----	22.34 (18.0–26.7)

To examine the effects of two ligands competing for the same binding site, receptor was diluted to 800 nM and incubated with 30 nM FITC-APEC with and

without three ligand competitors (ZM 241385, NECA and adenosine) until equilibrium was reached. Competition association experiments were conducted using two concentrations of competitor: ZM 241385 (16 nM and 65 nM), NECA (65 nM and 320 nM) and adenosine (65 nM and 320 nM). For clarity, only the experiments using 65 nM of competitor are plotted in Figure 4.6. We used the analytical solution to a mass action model for two ligands and a single-site binding reaction [17] to fit the competitive association data to calculate the association and dissociation rate constants for ZM 241385, NECA and adenosine.

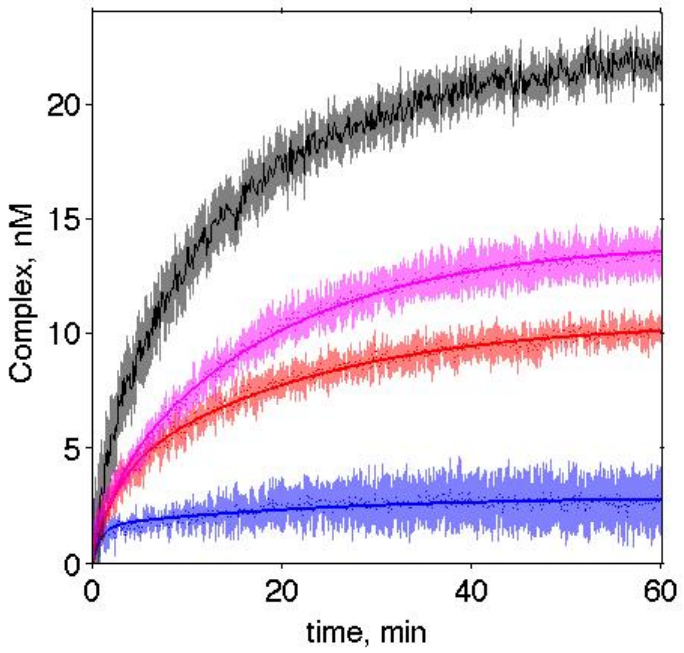

Figure 4.6 Competition association experiments. Binding of 30 nM FITC-APEC without any competitor (black), and with 65 nM of competitor: ZM 241385 (blue), NECA (red) and adenosine (magenta). Data are plotted as points and the shaded areas represent the standard deviation of two independent experiments performed in duplicate, n=4. The association and dissociation rates calculated for ZM 241385, NECA and adenosine are listed in Table 4.3.

Table 4.3 The association and dissociation rates of the unlabeled ligands were calculated from two sets of experiments performed using different competitor concentrations (16 nM and 65 nM ZM 241385; 65 nM and 320 nM NECA; 65 nM and 320 nM adenosine), n=8. The symbols (*, ^, #, +) indicate ligands with k_{on}, k_{off}, residence time ($RT=1/k_{off}$), and K_D (k_{off}/k_{on}) values that are not significantly different ($p>0.05$). Values in black were calculated using the FITC-APEC k_{on} and k_{off} values determined using the analytical solution (Table 4.2) and values in orange were calculated using the FITC-APEC k_{on} and k_{off} values determined using exponential approximations (Table 4.2). Values underlined represent cases where the exponential and analytical fits were statistically different ($p<0.05$), however these values differ by only a factor of 2.

	k_{on} (95% CI) min^{-1} nM^{-1}	k_{off} (95% CI) min^{-1}	RT (95% CI) min	K_D (95% CI) nM
ZM 241385	0.0174 (0.0101–0.0247) 0.0219 (0.0147–0.0290)	0.0774 (0.0513–0.1035)^ 0.0444 (0.0314–0.0573)^	12.9 (8.6–17.3)^ 22.5 (16.0–29.1)^	4.5 (2.1–6.8) 2.0 (1.1–2.9)
Adenosine	0.0031 (0.0022–0.0040)* 0.0034 (0.0025–0.0043)*	0.1764 (0.1389–0.2138) 0.0817 (0.0706–0.0928)	5.7 (4.5–6.9) 12.2 (10.6–13.9)+	57.1 (37.0–77.2)# 23.9 (17.1–30.8)#
NECA	0.0032 (0.0018–0.0045)* 0.0041 (0.0026–0.0056)*	0.0955 (0.0650–0.1260)^ 0.0548 (0.0413–0.0684)^	10.5 (7.1–13.8)^ 18.2 (13.7–22.7)^+	30.2 (14.3–46.1)# 13.5 (7.5–19.5)#

4.6. Discussion

Currently the majority of ligand-binding assays are conducted using radiolabeled ligand [11, 12]; due to the high cost, radioactive waste disposal, and health hazards [11, 14], alternatives to radioligand-binding assays are of interest. Multiple laboratories have validated the use of FA or fluorescence polarization for the characterization of ligand-binding affinity [11]; however, FA assays are limited by the availability of suitable fluorescent ligands [6, 11]. Due to this limitation, FA potential for high-throughput screening has not been widely applied.

The contribution of unbound ligand to the FA signal observed can potentially complicate the analysis of classical saturation curves [11], in particular because of a decrease in anisotropy as the free ligand concentration increases; to balance the

anisotropy signal from bound and free ligand, FA-based assays typically operate in the ligand depletion regime, as approximately 20% of the fluorescence ligand should bind the receptor to obtain a significant change in the anisotropy signal [14]. Another difficulty of FA-based assays is the contribution of scatter, especially if using membrane preparations. Here, using micelle solubilized $A_{2A}R$ we were able to apply two approaches to calculate the equilibrium dissociation constant from fluorescence anisotropy data:

- Scatchard plot analysis
- Determination of K_D using 1-phase exponential association and dissociation equations. Data were fit to exponential approximations.

These two approaches have been used previously to calculate the K_D values of fluorescent ligands from FA data [10, 11].

We also have used the analytical solution to fit the FITC-APEC association data (Figure 4.5A). The association and dissociation rate constants for FITC-APEC determined using an exponential approximation and the analytical solution were also used to calculate K_D (Table 4.2). The values of the equilibrium dissociation constant calculated using three approaches (Table 4.2) are a factor of 2–4 lower than the value initially reported for this fluorescent ligand (57 nM) [16]. However, this previous result was for $A_{2A}R$ in striatal tissue membrane preparations of bovine brain compared to our purified receptor in micelles. As expected, the K_D value obtained from the analytical solution is not significantly different from the K_D value calculated from Scatchard analysis, as the B_{max} value determined from the Scatchard analysis was used to fit the analytical solution.

The Scatchard plot analysis revealed that B_{max} in this system (FITC-APEC binding to $A_{2A}R$ in micelles) represents 5.6% of the total protein concentration. This

result unveils interesting characteristics about this system and potentially GPCRs in general.

- 100% of $A_{2A}R$ purified in DCC micelles bound an antagonist (xanthine) affinity chromatography column. However, only 17% of the purified receptor bound [^{3}H] CGS 21680 (a high affinity agonist) [9]
- FITC-APEC appears to bind a small percentage (5.6%) of the purified receptor population

Discrepancies between the B_{max} obtained from XAC affinity column and agonist radioligand binding ([^{3}H] CGS 21680) were attributed to possible limitations with the radioligand-binding in a filter-based assay [9]. Here we see a similar decrease in the B_{max} by using another agonist (FITC-APEC) and a homogeneous FA-based ligand-binding assay. Often saturation binding experiments are conducted using agonist and whole cells or membrane preparations; and often B_{max} is assumed to represent R_T [20]. The results from the Scatchard analysis indicate that the total number of purified receptors (R_T) may not equal B_{max}. This observation requires more testing to determine if this apparent discrepancy in active receptor number is seen in biological membranes or if it is a characteristic of this detergent micelle system.

It is plausible that FITC-APEC is binding only to a small percentage of the purified receptor, indicating that this fluorescent ligand is recognizing a particular conformation of the receptor. There is evidence of the existence of multiple active states (R*) and that ligands can stabilize distinct conformations, resulting in diverse downstream responses [4]. Furthermore, there is evidence that inverse agonists preferentially bind the inactive state of the receptor (R), while agonists preferentially bind the activated state (R*) [21-23], and neutral antagonists demonstrated equal affinity for both states [7, 23]. For example, using $A_{2A}R$ (with a C-terminal truncation

of 96 residues) purified from *E. coli,* lower number of binding sites (one-tenth) where measured when using the agonists [^{3}H] NECA compared to the number of binding sites measured using the antagonist [^{3}H] ZM 241385 [24].

It is also speculated that G proteins are required to stabilize the fully active conformation of the receptor [21]. It should be noted that caffeine, XAC and ZM 241385, often labeled as antagonist, have been identified as inverse agonists [22]. This highlights the discrepancies currently present in GPCR literature, as characterizing ligands as antagonist or inverse agonist often requires the measurement of the intracellular response to the ligand, and the result depends on the signaling pathway tested.

There is evidence in literature indicating that $A_{2A}R$ dimers are the functional signaling receptor species [25]. Furthermore, recent mouse studies indicate that ligands had different affinity to $A_{2A}R$ depending upon the oligomerization state of $A_{2A}R$ with different receptors [26]. In the Robinson laboratory (see Patrick McNeely's PhD thesis), we have evidence that antagonist addition facilitates dimer dissociation. Together, this evidence points to the possibility that different receptor conformations may have differential ligand recognition. Moving forward, it is important to determine experimentally why FITC-APEC recognizes only 5.6% of the DCC solubilized receptor and confirm this observation in other *in vivo* model systems. It appears that the mechanism of ligand-receptor interaction that better describes the B_{max} observed in this system (i.e. binding of fluorescent agonist FITC-APEC to $A_{2A}R$ solubilized in micelles) is better described by the "conformation-selection" mechanism [6].

$$R \leftrightarrow R^* \leftrightarrow R^*L \tag{4.23}$$

This mechanism describes the equilibrium between two conformations of the receptor (R and R^*) in the absence of ligand. The ligand specifically binds only the R^* conformation to form R^*L complex.

It is important to note that even though the exponential approximation and the analytical solution fit the FITC-APEC association data, the residuals indicate that there is a portion of the data not being captured by the fits (Figure 4.5A). It is possible that the undershoot and overshoot observed using these fits are due to varying rate constants, or the interconversion between the R and R* conformations. The receptor saturation experiments and Scatchard analysis (Figure 4.3) validated the use of a one-site binding model to fit the data, therefore a two-site binding model was not considered. Diffusion limitations were also not considered as diffusion controlled rates constant range between 6 and 600 nM^{-1} min^{-1} [27], at least two orders of magnitude faster than the rates measured for $A_{2A}R$ solubilized in detergent micelles (Table 4.2 and 4.3).

Magnani and colleges report a slow interconversion between the R and R* conformations, as it was not observed over a period of 14 hours [24]. Because the rates between R and R^* are slow relative to the ligand binding to R^* it is likely that during the course of our experiments (2-4 hours) only limited interconversion between the R and R* conformations took place.

Using the binding affinity of FITC-APEC to $A_{2A}R$ in micelles determined from Scatchard plot analysis, we were able to calculate the inhibitor dissociation constants (K_i) for six unlabeled ligands (Table 4.4). Table 4.4 compares these values to K_i values reported in literature. ZM 241385 and SCH 442416 are antagonists known to have high affinity (K_D<10nM) for $A_{2A}R$. NECA, adenosine and CGS 21680 are agonists

with high affinity for $A_{2A}R$. The K_i values we determined from FA competition association experiments are in agreement with values published in literature (Table 4.4). Bay 606583 has been reported as a specific agonist for A_{2B} (EC_{50} 2.83 nM) [28]. However, we detected modest affinity of Bay 606583 to $A_{2A}R$ (K_i=5.1 μM). Hill slopes between -0.8 and -1.0 were determined for all the ligands tested (except for Bay 606583, with a Hill slope equal to 0.3), indicating that the labeled and unlabeled ligand compete for the same binding site [14]. The curve for Bay 606583 has a shallower slope, potentially indicating that the binding does not follow the law of mass action for one binding site. However, these data are hard to interpret because a clear bottom plateau was not achieved [29]. A two-site binding model did not improve the fit to the data (based on the R-square values) and led to a site with a similar IC50 value as the one-site binding fit (12.7×10^3 nM) and another site with an IC50 value outside of the range of the data (708 M); for these reasons the two-site binding fit was disregarded [29].

All ligands that compete for the same binding site should reach the same bottom plateau [29]. It is unclear why SCH 442416 does not reach the same bottom plateau; the Hill slope indicates competition for one binding site, however the labeled and unlabeled ligand achieve a new equilibrium with a plateau at a higher value than the rest of the ligands. It could be possible that SCH 442416 is binding to both receptor conformations (R and R*) resulting in depletion of the unlabeled ligand prior to achieving the observed experimental plateau.

Table 4.4 K_i values calculated using FA and $A_{2A}R$ solubilized in micelles[a]. K_i values reported in literature are listed in the second column[b].

	K_i (95% CI) [a] nM	K_i [b] nM
Bay 606583	5132.9 (360.3–9905.4)	-
SCH 442416	4.0 (1.7–6.3)^	4.1[11]
ZM2 41385	10.1 (6.1–14.1)^	1.6 [11]
Adenosine	97.1 (65.4–128.8)	45 [in supplemental information of 21]
CGS 21680	26.6 (20.6–32.6)#	27 [11]
NECA	28.6 (21.2–36.0)#	20 [11]

Because the rates between R and R^* are slow relative to the ligand binding to R^*, the dissociation rate constant will equal R^*L dissociation rate constant [6]. Using the "conformation-selection" model and the B_{max} determined via Scatchard plot analysis allowed us to perform ligand-binding kinetic analysis using the analytical solution for two-ligand competitive binding [17]. The association and dissociation rate constants that we calculated using this analytical solution compare favorably to values that have been reported in literature (Table 4.5) for a slightly different system ($A_{2A}R$ in membrane preparations tested at 5 ºC using an inverse agonist, [^{3}H] ZM 241385) [7].

Table 4.5 Comparison of kinetic binding constant with values reported in literature [7].

	k_{on} [a] min^{-1} nM^{-1}	k_{on} [b] min^{-1} nM^{-1}	k_{off} [a] min^{-1}	k_{off} [b] min^{-1}	K_D [a] nM	K_D [b] nM
ZM 241385	0.0174	0.028 [7]	0.0774	0.03 [7]	4.5	0.9 [7]
Adenosine	0.0031	--	0.1764	--	57.1	--
NECA	0.0032	0.0005 [7]	0.0955	0.03 [7]	30.2	58 [7]

[a] k_{on}, k_{off} and K_D values calculated using FA, FITC-APEC and $A_{2A}R$ solubilized in micelles. Measurement conducted at room temperature.
[b] k_{on}, k_{off} and K_D values calculated for $A_{2A}R$ in HEK293 membrane preparation. Measurement conducted using [^{3}H] ZM 241385 at 5ºC [7].

It is important to note that the measurements in [7] were conducted at 5 ºC while our measurements were conducted at room temperature, which could explain the faster kinetics observed in our system. However, similar K_D values were obtained and importantly, the kinetic trends are consistent, i.e. the dissociation rate constants for NECA and ZM 241385 are not statistically different. Differences in the association rate constants underlie the differences observed in the K_D values.

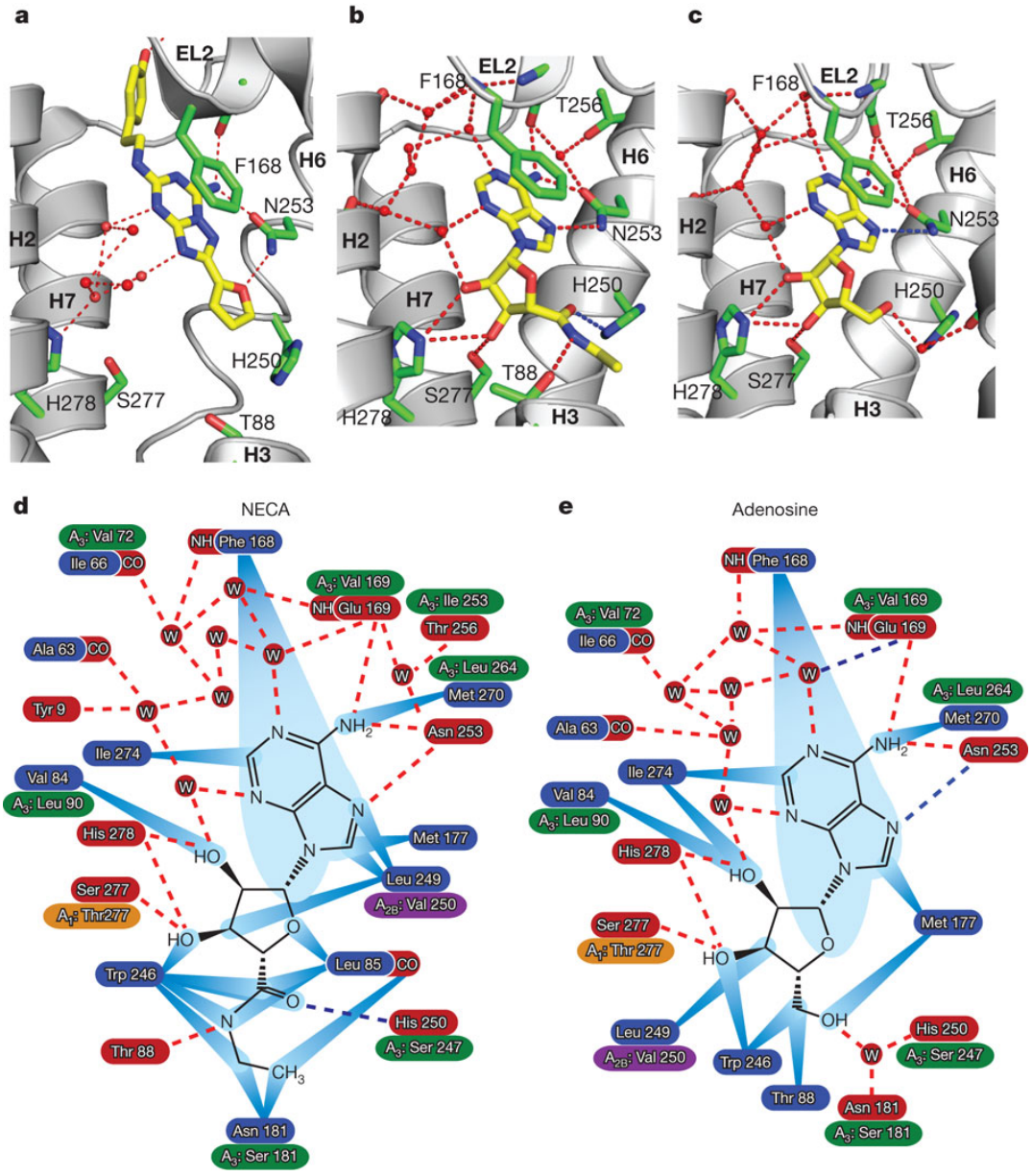

Figure 4.7 Receptor-ligand interactions. Structures of the human $A_{2A}R$ bound to A) ZM 241385 (PDB code: 3EML), B) NECA (PDB code: 2YDV), and C) adenosine (PDB code: 2YDO). Amino acid residues interacting with D) NECA and E) adenosine are highlighted: van der Waals interactions (blue), hydrogen bonds (red). Residues not conserved within the adenosine receptor family are indicated in orange for A_1, purple for A_{2B}, and in green for A_3. Figure reproduced from [21], with permission (license number: 3473440028858).

Recent structures of $A_{2A}R$ bound to ZM 241385, NECA, and adenosine have highlighted differences between the active and inactive receptor conformation [21, 22, 30, 31]. Binding of agonists NECA and adenosine cause an inward shift of helices 3, 5, and 7 (as seen in Figure 4.7), accompanied by a contraction of the ligand-binding pocket and the opening of the cleft where the G protein can bind. Inverse agonists stabilize the inactive state of the receptor, characterized by the presence of the ionic lock [22].

The adenine ring of NECA and adenosine superimpose almost exactly. Similar interactions are observed by the triazolotriazine ring in ZM 241385 [21], Figure 4.7. Many of the interactions with the upper portion of the ligand-binding pocket and extracellular loop 2 (ECL2) are conserved between agonist and inverse agonist (i.e. hydrogen bonding with Glu169 (ECL2) and Asn 253 (helix 6), and π-stacking with Phe 168 (ECL2)).

One of the main differences between these agonists and ZM 241385 arises from contacts made by ribose and furan groups, respectively. The ribose ring in NECA and adenosine is located deep in the binding pocket, making polar contacts (hydrogen bonding) with conserved residues in helix 7 (Ser 277 and His 278) and non-polar interactions (van der Waals) with residues in helix 3 and 6 [21]. ZM 241385 does not reach this far into the binding pocket, and does not interact with Ser 277 and His 278, indicating that these residues may be important for the activation of $A_{2A}R$ [21, 22]. The fact that ZM 241385 is not found deep in the binding pocket could in part explain the faster association rate of this ligand (Table 4.5).

The GPCR family has the ability to bind ligands of diverse shapes, sizes and chemical properties [4], and often similar ligands (e.g. NECA and adenosine) can bind

with different affinity to the same receptor. Using fluorescence anisotropy we determined the main difference between these similar ligands is their residence time, while the association rate was not statistically different. The difference in residence time then translates to a higher affinity of NECA to $A_{2A}R$. Furthermore, we identified that the higher affinity of ZM 241385 results mostly from a faster association rate.

4.7. Conclusion

We were able to apply FA to measure affinity and kinetics of ligands targeting the full-length human $A_{2A}R$. The K_i values for six unlabeled ligands were determined and are in agreement with values reported in literature. The K_i values calculated from the inhibition association experiments deviated from values reported in literature by only a factor of 1-6. This indicates that the micelle-solubilized receptor retains a binding affinity comparable to the affinity of the receptor in more complex systems (i.e. membrane preparations).

Furthermore, the analytical solutions for single-site binding models fit the FITC-APEC association kinetic data and the two-ligand kinetic association data. It is important to note that FA assays generally operate in the ligand depletion regime; here we validated the application of this analytic approach for characterizing the binding kinetics of $A_{2A}R$ ligands, further expanding the use of FA assays.

Currently, the molecular determinants of ligand-receptor binding kinetics remain poorly understood [5]. In combination with mutagenesis studies, structural data and molecular dynamic simulations, this *in vitro* system could aid in the rational design of drugs (with the desired binding kinetics) that target the human A_{2A} adenosine receptor.

4.8. Acknowledgements

The work presented in this chapter was motivated and guided by molecular dynamic and computer simulations. The work started with the purpose of validating experimentally molecular dynamic simulations (conducted in Dr. Edward Lyman's group) that indicated a difference in residence time of NECA and adenosine. Patrick McNeely conducted computer simulations to guide the two-ligand competition experiments. Based on these simulations the optimal competitor ligand concentrations were chosen.

REFERENCES

1. Palczewski, K., et al., *Crystal structure of rhodopsin: A G protein-coupled receptor.* Science, 2000. **289**(5480): p. 739-45.

2. Zhukov, A., et al., *Biophysical mapping of the adenosine A(2A) receptor.* Journal of medicinal chemistry, 2011. **54**(13): p. 4312-4323.

3. Allen, S.J., et al., *Expression, purification and in vitro functional reconstitution of the chemokine receptor CCR1.* Protein expression and purification, 2009. **66**(1): p. 73-81.

4. Venkatakrishnan, A.J., et al., *Molecular signatures of G-protein-coupled receptors.* Nature, 2013. **494**(7436): p. 185-194.

5. Pan, A.C., et al., *Molecular determinants of drug-receptor binding kinetics.* Drug Discovery Today, 2013. **18**(13-14): p. 667-673.

6. Guo, D., et al., *Drug-target residence time-A case for G protein-coupled receptors.* Medicinal Research Reviews, 2014. **34**(4): p. 856-892.

7. Guo, D., et al., *Functional efficacy of adenosine A2A receptor agonists is positively correlated to their receptor residence time.* British journal of pharmacology, 2012. **166**(6): p. 1846-1859.

8. Niebauer, R.T. and A.S. Robinson, *Exceptional total and functional yields of the human adenosine (A2a) receptor expressed in the yeast Saccharomyces cerevisiae.* Protein expression and purification, 2006. **46**(2): p. 204-11.

9. O'Malley, M.A., et al., *High-level expression in Saccharomyces cerevisiae enables isolation and spectroscopic characterization of functional human adenosine A2a receptor.* Journal of structural biology, 2007. **159**(2): p. 166-78.

10. Prystay, L., M. Gosselin, and P. Banks, *Determination of equilibrium dissociation constants in fluorescence polarization.* Journal of Biomolecular Screening, 2001. **6**(3): p. 141-150.

11. Kecskes, M., et al., *Novel Alexa Fluor-488 labeled antagonist of the A(2A) adenosine receptor: Application to a fluorescence polarization-based receptor binding assay.* Biochemical pharmacology, 2010. **80**(4): p. 506-511.

12. Huwiler, K.G., et al., *A fluorescence anisotropy assay for the muscarinic M1 G-protein-coupled receptor.* Assay and Drug Development Technologies, 2010. **8**(3): p. 356-366.

13. James, N.G. and D.M. Jameson, *Steady-state fluorescence polarization/anisotropy for the study of protein interactions.* Fluorescence Spectroscopy and Microscopy: Methods and Protocols, 2014. **1076**: p. 29-42.

14. Allen, M., J. Reeves, and G. Mellor, *High throughput fluorescence polarization: A homogeneous alternative to radioligand binding for cell surface receptors.* Journal of Biomolecular Screening, 2000. **5**(2): p. 63-69.

15. Schindelin, J., et al., *Fiji: an open-source platform for biological-image analysis.* Nat Meth, 2012. **9**(7): p. 676-682.

16. McCabe, R.T., P. Skolnick, and K.A. Jacobson, *2-[2-[4-[2-[2-[1,3-Dihydro-1,1-bis (4-hydroxyphenyl)-3-oxo-5-isobenzofuranthioureidyl]ethylaminocarbonyl]ethyl]pheny l] ethylamino]-5'--ethylcarboxamidoadenosine (FITC-APEC): A Fluorescent Ligand For A-Adenosine Receptors.* Journal of fluorescence, 1992. **2**(4): p. 217-223.

17. Motulsky, H.J. and L.C. Mahan, *The kinetics of competitive radioligand binding predicted by the law of mass-action.* Molecular pharmacology, 1984. **25**(1): p. 1-9.

18. Scatchard, G., *The attractions of proteins for small molecules and ions* Annals of the New York Academy of Sciences, 1949. **51**(4): p. 660-672.

19. Cheng, Y. and W.H. Prusoff, *Relationship between inhibition constant (K1) and concentration of inhibitor which causes 50 per cent inhibition (I50) of an enzymatic-reaction.* Biochemical pharmacology, 1973. **22**(23): p. 3099-3108.

20. Lauffenburger, D.A. and J.J. Linderman, *Receptors: Models for binding, trafficking, and signaling*1993: Oxford University Press.

21. Lebon, G., et al., *Agonist-bound adenosine A2A receptor structures reveal common features of GPCR activation.* Nature, 2011. **474**(7352): p. 521-5.

22. Dore, A.S., et al., *Structure of the adenosine A(2A) receptor in complex with ZM241385 and the xanthines XAC and caffeine.* Structure, 2011. **19**(9): p. 1283-93.

23. Bennett, K.A., et al., *Pharmacology and structure of isolated conformations of the adenosine A(2A) receptor define ligand efficacy.* Molecular pharmacology, 2013. **83**(5): p. 949-958.

24. Magnani, F., et al., *Co-evolving stability and conformational homogeneity of the human adenosine A(2a) receptor.* Proceedings of the National Academy of Sciences of the United States of America, 2008. **105**(31): p. 10744-10749.

25. Canals, M., et al., *Homodimerization of adenosine A2A receptors: qualitative and quantitative assessment by fluorescence and bioluminescence energy transfer.* Journal of neurochemistry, 2004. **88**(3): p. 726-34.

26. Orru, M., et al., *Striatal pre- and postsynaptic profile of adenosine A(2A) receptor antagonists.* Plos One, 2011. **6**(1).

27. Alberty, R.A. and G.G. Hammes, *Application of the Theory of Diffusion-controlled Reactions to Enzyme Kinetics.* The Journal of Physical Chemistry, 1958. **62**(2): p. 154-159.

28. http://www.tocris.com/.

29. Mailman, R.B. and B. J., *Lesson 5: Competitive binding data with one class of receptors.* 1997.

30. Jaakola, V.P., et al., *The 2.6 angstrom crystal structure of a human A2A adenosine receptor bound to an antagonist.* Science, 2008. **322**(5905): p. 1211-7.

31. Liu, W., et al., *Structural basis for allosteric regulation of GPCRs by sodium ions.* Science, 2012. **337**(6091): p. 232-6.

Chapter 5

A_{2A} ADENOSINE RECEPTOR PURIFICATION AND FUNCTIONALITY IN A PURE PHOSPHOLIPID SOLUBILIZATION SYSTEM

5.1. Introduction

As described in Chapter 1, Section 1.1 and 1.6, the interaction of GPCRs with other membrane proteins and lipids at the plasma membrane has been investigated for the past 20-30 years [1]. There is growing evidence that lipid heterogeneities in the membranes (e.g. lipid rafts) [2], as well as direct interaction of cholesterol and other lipids can modulate GPCR signaling [3-5].

With the vision of establishing a pure lipid system in the absence of a detergent solubilization step, we used a short hydrocarbon chain lipid (1,2-dihexanoyl-sn-glycero-3-phosphocholine, DHPC) to solubilize and purify the A_{2A}R. After purification with DHPC, long-chain lipids (1,2-dimyristoyl-sn-glycero-3-phosphocholine, DMPC, di-14:0PC) were added to form bilayered micelles or bicelles. Compared to detergent micelles, bicelles have an extended planar bilayer region with a less pronounced local curvature, and for the most part, bicelles are thought to represent a more native-like reconstitution system for membrane proteins [6-8]. This bilayered micelle system can be aligned in the presence of an external magnetic field [9-13], making it an especially useful model membrane platform for nuclear magnetic resonance (NMR) studies, enabling the investigation of GPCR activity in morphologies with different degrees of intrinsic curvature [14] and different lipid compositions.

5.2. Materials and Methods

5.2.1. Expression and Purification of $A_{2A}R$ from Yeast Membrane Preparations

Full-length human $A_{2A}R$ was expressed in *Saccharomyces cerevisiae* cells, BJ5464, using the multi-integrating pITy-$A_{2A}R$-His_{10} plasmid, as previously described [15]. Both the lipid and detergent purification protocols started from cell pellets, which were collected via centrifugation of a 600 ml culture 24 hours after induction. Aliquots of 50 ml of culture at an optical density (OD_{600}) of approximately 22-25 were collected by centrifugation (3,220 g) and frozen at -80 °C. Freezing cell pellets at a consistent optical density and starting the detergent solubilization step from membrane preparations instead of crude cell lysis improved reproducibility and the purity of the purified protein.

Cell pellets were thawed and washed with 22 ml of Buffer A (10% glycerol, 50 mM sodium phosphate monobasic and 300 mM sodium chloride at pH 8, supplemented with 1 mM phenylmethanesulfonyl fluoride (PMSF) and complete EDTA-free protease inhibitor tablets (Roche Applied Science, Indianapolis, IN)). Cells were then combined with 0.5 mm zirconia/silica beads (BioSpec, Bartlesville, OK) and lysed using a vortex for six-60 second pulses, placing the cells on ice for 60 seconds between pulses. The beads were then removed using Kontes separation columns. Samples were placed on ice and probe-sonicated (Branson 450 set at 50% power) twice, for 20 seconds. The lysate was centrifuged at 3,220 g for 30 min at 4 °C to remove unlysed cells and cellular debris. The supernatant was then spun at 100,000 g for 45 minutes at 4 °C, to remove most soluble proteins. The crude membranes (pellet) were resuspended in Buffer A and membranes were homogenized using a Potter-Elvehjem tissue homogenizer. After homogenization one of the following

detergent/lipid combinations were added: 6.25% (w/v) DHPC (Avanti Polar Lipids, Alabaster, AL), 2% (w/v) DDM + 1% (w/v) 3-(3-cholamidopropyl) dimethylammoniopropane sulfonate (CHAPS) + 0.2% (w/v) CHS (all from Anatrace, Maumee, OH), or 2% (w/v) DDM. 6.25% (w/v) DHPC corresponds to 138 mM, approximately 10 times the critical micellar concentration of DHPC (11-16 mM) [16].

The membrane was solubilized overnight at 4 ºC. The following morning, insoluble matter was removed via centrifugation at 80,000 g for 1 hr at 4 ºC. Supernatant (approximately 20 ml) was supplemented with one protease inhibitor tablet, 1 mM PMSF and 15 mM imidazole to prevent non-specific binding to the nickel resin. This solubilized membrane mixture was then added to pre-equilibrated Ni-NTA Superflow resin (Qiagen, Valencia, CA), and samples were incubated for at least 3 hours at 4 °C in an end-over-end mixer to allow binding to the nickel resin. Unbound material was removed by low speed centrifugation, followed by low-concentration imidazole washes to reduce non-specific binding using buffer A containing one of the following detergent/lipid combinations: 0.8% (w/v) DHPC, 0.2% (w/v) DDM + 0.1% (w/v) CHAPS + 0.02% (w/v) CHS, or 0.2% (w/v) DDM. The washes contained increasing amounts of imidazole (20 mM, 30 mM and 50 mM imidazole, respectively). Each imidazole wash was incubated for 20 minutes at 4 °C in an end-over-end mixer, followed by low speed centrifugation and removal of the supernatant. To elute A_{2A}R-His_{10} from the nickel resin, samples were incubated at 4 °C for 1 hour with Buffer A, 500 mM imidazole and one of the following detergent/lipid combinations: 0.8% (w/v) DHPC, 0.2% (w/v) DDM + 0.1% (w/v) CHAPS + 0.02% (w/v) CHS, or 0.2% (w/v) DDM. PD-10 desalting columns (GE Healthcare, Pittsburgh, PA) were used per manufacturer instructions to remove

imidazole and salt ions using the elution buffer, Buffer B (50 mM phosphate at pH 7 and one of the following detergent/lipid combinations: 0.8% (w/v) DHPC, 0.2% (w/v) DDM + 0.1% (w/v) CHAPS + 0.02% (w/v) CHS, or 0.2% (w/v) DDM). Purified protein samples were stored at 4 °C.

5.2.2. Addition of DMPC to Form Bicelles

DMPC (1,2-dimyristoyl-sn-glycero-3-phosphocholine) was purchased from Avanti Polar Lipids. 1 ml of an 8 wt/v% DMPC and 1 wt/v% DHPC mixture was prepared by first mixing the lipids prior to the addition of phosphate buffer. The mixture was vortexed and incubated at 4 ºC for 15 minutes. This solution remained cloudy, as the lipids were not completely solubilized. Samples were then cycled between room temperature and -20 ºC until a clear solution was achieved. At this stage, the clear lipid solution was added at a 1:1 volume ratio to $A_{2A}R$ purified in DHPC; the solution remained clear. The final DMPC/DHPC molar ratio was equal to 3.

5.2.3. Protein Purity, Concentration and Biophysical Characterization

Samples were separated via SDS-PAGE on a 12% Tris-Glycine gel (ThermoFisher Scientific, Rockford, IL), and protein bands were detected via staining with a high-sensitivity Coomassie G-250 (MP Biomedicals, Santa Ana, CA) protocol (Blue Silver) [17] or Sypro Ruby (Life Technologies, Carisbad, CA). For Western blotting, mouse anti-A_{2A} primary antibody was used (Santa Cruz Biotechnology, Santa Cruz, CA, catalogue # 32261) at 1:5000 dilution. Alexa Fluor 488 goat anti-mouse (Life Technologies, Carisbad, CA, catalogue # A11029) or horseradish peroxidase (HRP)-conjugated goat anti-mouse (Abcam, Cambridge, MA, catalogue # 97265)

polyclonal secondary antibodies were used at a 1:5000 dilution. For chemiluminescent detection Luminata Forte Western HRP substrate was used (EMD Millipore, Billerica, MA). Fluorescence or chemiluminescence signal was detected using the BioSpectrum imaging system (UVP, Upland, CA). Protein concentration was determined using UV absorbance at 280 nm as described in [15], and protein purity was quantified from the gel stain image using FIJI [18]. A detailed description of the CD and fluorescence data collection and analysis is given elsewhere [15].

5.2.4. Ligand Binding of Reconstituted $A_{2A}R$

Radioligand Binding

Ligand binding of purified receptors has been described previously [15], with minor modifications. Briefly, after the 50 mM imidazole wash, approximately 50 µl of settled resin was collected and resuspended in Buffer B. Approximately 2 µl of A_{2A}-His_{10}-containing resin was added per well to a poly(ethyleneimine) (0.1% v/v) treated 96-well plate (glass fiber type B filters, Millipore). Samples were incubated with increasing amounts of tritiated CGS 21680 (Perkin Elmer, Waltham, MA) for 4 hours. Non-specific binding was determined by addition of 0.5 mM cold ligand, SCH 442416 (Tocris Bioscience, Ellisville, MO), to the samples at each concentration of tritiated ligand. Specific binding was determined by subtracting these controls from the counts obtained from the sample data. Binding was measured using a Perkin-Elmer 1450 Microbeta liquid scintillation counter. All samples were run in triplicate and samples from at least two independent purifications were used. The data were fit to a single-site binding model (Equation 5.1) using Matlab (version 7.10, MathWorks, Natick, MA).

$$C = \frac{B_{max} \times L}{K_D + L} \quad (5.1)$$

where C is the concentration of the receptor-ligand complex (in counts per minute, CPM), L is the total radioligand concentration, B_{max} represents the total number of active receptors (in counts per minute, CPM), and K_D is the equilibrium dissociation constant. The value for K_D was determined by averaging the K_D value obtained for each experiment, determined by minimizing the least squares. The standard error of the mean (SEM) and 95% confidence intervals were determined from the sample standard deviation.

Fluorescence Anisotropy

Ligand-binding activity over time was monitored using the agonist FITC-APEC (NIMH synthesis program, http://nimh-repository.rti.org, NIMH Code: D-906) [19]. Solubilized $A_{2A}R$ was incubated with 70 nM FITC-APEC until equilibrium was reached, approximately one hour at room temperature. Empty micelles or bicelles were also incubated with 70 nM FITC-APEC as a negative control. For the fluorescence anisotropy measurements we used 480-485 nm excitation and 520-528 nm emission wavelengths, using a Synergy H1 plate reader (BioTek, Winooski, VT) or a PC1 spectrofluorimeter (ISS, Champaign, IL) for detection. The parallel and perpendicular fluorescence emission of the solubilized $A_{2A}R$ and empty micelles/bicelles was measured prior to the addition of FITC-APEC to account for scatter. Prior to calculating the anisotropy value (mA) (Equation 5.2), the average fluorescence signal due to scatter was subtracted from the parallel and perpendicular fluorescence intensity of samples containing 70 nM FITC-APEC.

$$mA = \frac{F_{\parallel} - F_{\perp}}{F_{\parallel} + 2F_{\parallel}} \quad (5.2)$$

where anisotropy is reported in milli-anisotropy units (mA), $F_{\parallel}$ and $F_{\perp}$ are the parallel and perpendicular fluorescence intensity, respectively.

5.3. Results and Discussion

5.3.1. Choice of Membrane-Mimetic System

Detergents with a hydrophobic tail of 6-12 carbon atoms are commonly used to solubilize, stabilize and crystallize GPCRs [20]. Here, to establish a pure lipid solubilization system, with no traces of detergents, we used the short hydrocarbon chain lipid DHPC (1,2-dihexanoyl-sn-glycero-3-phosphocholine) to purify the full-length human A_{2A} adenosine receptor. Short hydrocarbon chain lipids (DHPC and 1,2-diheptanoyl-sn-glycero-3-phosphocholine (di:07PC)) have been used to solubilize or reconstitute a wide range of β-strand and α-helical membrane proteins expressed in *E. coli* and cell-free systems [21]. DHPC and di:07PC spontaneously assemble into micelles due to their short hydrocarbon chains and large head groups, thus effectively acting as biologically relevant detergents [16, 22] with minimal deleterious effects on membrane proteins [23]. Presently, however, the mechanisms by which lipids facilitate purification are not well understood. For example, it is speculated that short hydrocarbon chain lipids disrupt membranes by interacting with the native membrane lipids rather than the membrane protein itself, in effect leaving the protein surrounded by a thin shell of its native lipids after purification [16, 24]. For these studies we used DHPC to purify $A_{2A}R$ and compare the results to those for $A_{2A}R$ purified in DDM (with and without the cholesterol analog CHS).

5.3.2. $A_{2A}R$ Solubilized in DHPC and DDM

Yeast BJ5464 cells expressing the human A_{2A} receptor ($A_{2A}R$) were grown and membrane preparations were carried out as described in the Materials and Methods. Samples of $A_{2A}R$ extracted and purified from cellular membranes using detergents/lipids were separated via gel electrophoresis, and protein bands were detected using Blue Silver (a high-sensitivity Coomassie protocol) or Sypro Ruby, and Western analysis using anti-$A_{2A}R$ antibodies. DHPC purification results were compared to those from the detergent purification of $A_{2A}R$ using DDM, 3-(3-cholamidopropyl) dimethylammoniopropane sulfonate (CHAPS) and cholesteryl hemisuccinate (CHS), Figure 5.1A and 5.1B. Sypro Ruby staining (Figure 5.1A) revealed a pronounced band at approximately 40 kDa, which corresponds to $A_{2A}R$ monomers, and whose identity was confirmed by Western analysis (Figure 5.1B) and mass spectrometry of protein isolated from the gel. $A_{2A}R$ exists in monomeric and multimeric forms [25-27]; these higher order oligomers can be observed in the gel stain and Western Blot, Figure 5.1A and 5.1B. Treatment with Tris-(2-carboxyethyl)phosphine (TCEP) as a reducing agent was used to confirm that the higher molecular weight oligomers were not disulfide-linked (Appendix C).

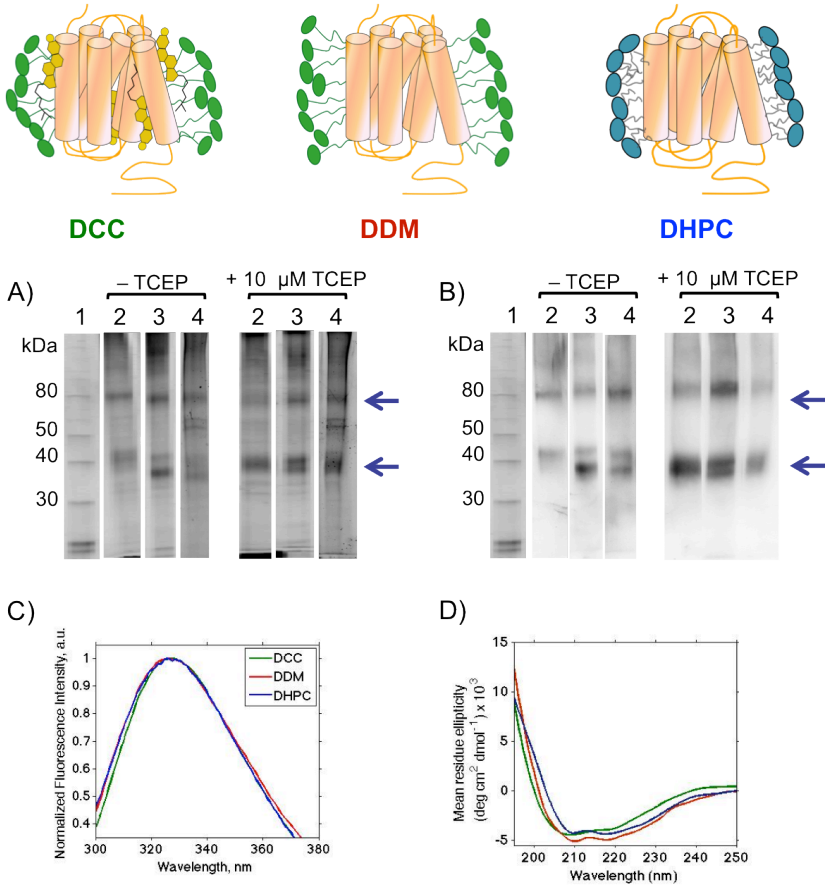

Figure 5.1 $A_{2A}R$ solubilized in various micellar environments. $A_{2A}R$ protein bands were separated via SDS-PAGE using a 12% Tris-Glycine gel, stained with Sypro Ruby (A) and blotted in a nitrocellulose membrane for Western blot detection with an anti-A_{2A} primary antibody (B). Lane (1) contains MagicMark protein standard, with molecular weights indicated on the left. Lane (2) is $A_{2A}R$ purified from membrane preparations using DCC (0.1% DDM, 0.1% CHAPS, and 0.02% CHS). Lane (3) is $A_{2A}R$ purified from membrane preparations using DDM (0.1%). Lane (4) is $A_{2A}R$ purified from membrane preparations using the short hydrocarbon chain lipid (0.8% DHPC). Samples were also incubated with 10 µM TCEP. Arrows indicate the $A_{2A}R$ monomer and oligomers. C) Fluorescence spectroscopy of purified $A_{2A}R$ confirmed that the receptor is in a hydrophobic environment. The data points represent the average from three different purifications. D) CD spectrum verified that the structural conformation of $A_{2A}R$ purified using DCC, DDM and DHPC is α-helical.

DHPC was able to directly solubilize the membrane preparations and extract $A_{2A}R$, as observed via protein gels and Western Blot, Figure 5.1A and 5.1B. Moreover, DHPC was more effective in solubilizing the plasma membrane and organelle membranes, as mitochondrial membrane proteins were identified as contaminants (Appendix C).

We conducted GC/MS analysis to determine levels of residual ergosterol in the purified samples. Approximately 360 nM of ergosterol was detected in $A_{2A}R$ solubilized in DDM/CHAPS/CHS (DCC), corresponding to an $A_{2A}R$ to ergosterol molar ratio of 3:1. No ergosterol was detected in the A_{2A}DDM and A_{2A}DHPC samples (Appendix C). These results could indicate that DHPC is more effective in solubilizing the membranes and stripping ergosterol. This observation contradicts the speculation that short hydrocarbon chain lipids purify membrane proteins, leaving the protein surrounded by a thin shell of its native lipids after purification [16, 24]. It is typically observed that detergents vary in their efficacy to solubilize membranes, and other contaminants are often observed as a function of the detergent used [8]; nevertheless, the absence of ergosterol in the DHPC purification and the presence of ergosterol in the DCC purification were unexpected.

Table 5.1 Purity and concentration of $A_{2A}R$ solubilized in various micellar environments. The images from the gel stains were used to calculate the protein purity using FIJI. Protein concentration was determined via UV absorbance at 280 nm. The mean and the standard error of the mean are reported for at least five independent purifications.

	Protein purity (%)	Protein concentration μg/ml (mg per L of culture)	Sample size
$A_{2A}R$-DCC	90.1 ± 1.2	63.0 ± 2.5 (4.4)	7
$A_{2A}R$-DDM	91.7 ± 0.9	55.0 ± 3.3 (3.9)	5
$A_{2A}R$-DHPC	73.4 ± 3.5	88 ± 18.9 (6.2)	6

Table 5.1 summarizes the concentration and purity of $A_{2A}R$ purified using detergents and short hydrocarbon chain lipids. A final protein concentration of 0.088 mg/ml (corresponding to 6.2 mg/L of culture) was determined for the DHPC purification via UV absorbance at 280 nm. Higher purity was observed for the DDM purification.

5.3.3. DHPC Maintains Native-Like Conformation

Initial biophysical characterization using intrinsic fluorescence and circular dichroism (CD) indicated that $A_{2A}R$ was incorporated in DHPC micelles and retained its α-helical content; these results were compared with those for $A_{2A}R$ in DCC and $A_{2A}R$ in DDM, Figure 5.1C and Figure 5.1D. The intrinsic fluorescence spectrum of $A_{2A}R$ solubilized in DHPC had a maximum at 327.6±1.3 nm, indicating that the receptor is situated in a hydrophobic environment, in a compact and native-like fold, similar to that observed for DCC and DDM (Figure 5.1C). CD analysis showed that $A_{2A}R$ in DHPC micelles is predominantly α-helical, with two minima around 208 and 222 as expected for $A_{2A}R$, similar to that reported in DCC [15], Figure 5.1D.

5.3.4. $A_{2A}R$ DHPC Radioligand Binding

To determine whether the DHPC-purified $A_{2A}R$ was functional, ligand-binding activity was measured using the tritiated agonist CGS 21680. The ligand binds to $A_{2A}R$ in a saturable manner, similar to that of DCC (Figure 5.2). However, it should be noted that the data for $A_{2A}R$ solubilized in DHPC did not reach saturation within the concentration range of tritiated ligand used (up to 300 nM). The data were fit using a single-site binding model, determining an equilibrium dissociation constant (K_D) of 378 nM for $A_{2A}R$ solubilized in DHPC (Figure 5.2). The 95% confidence interval for the K_D value was not calculated due to the high uncertainty associated with the B_{max} value. These data indicate that $A_{2A}R$ solubilized in DHPC has a lower affinity for the ligand than $A_{2A}R$ solubilized in DCC. We have previously reported a K_D value of 66 ± 4 nM for DCC-purified receptor, while no significant binding was detected for the DDM-purified receptor [15]; a representative ligand-binding curve for $A_{2A}R$-DCC is displayed in Figure 5.2. Even though $A_{2A}R$-DHPC has lower affinity to the ligand than $A_{2A}R$-DCC, the K_D value for DHPC-purified $A_{2A}R$ compares favorably to values in literature, where a range of 2.34-632 nM is reported for $A_{2A}R$ and CGS 21680 in various systems [28-31]. Thus, the variability in K_D may depend on the membrane-mimetic environments that the protein resides in, apart from changes in pH, temperature, and ion concentrations [32].

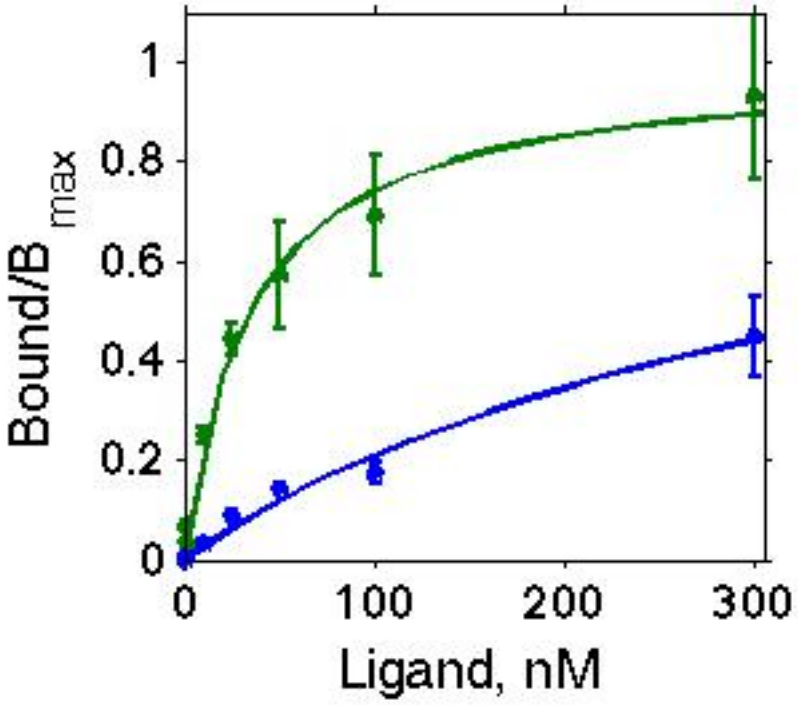

Figure 5.2 Ligand binding of [^{3}H] CGS 21680 to $A_{2A}R$ in DCC (green) and in DHPC (blue) micelles. Data were normalized using the B_{max} values. The data points show the average of three different $A_{2A}R$-DHPC purifications run in duplicate or triplicate (n=7); a K_D of 378 nM was calculated after fitting the data to a single-site binding model (line).

There are previous reports of the importance of cholesterol in the function of $A_{2A}R$, it is intriguing that DHPC retains the ligand-binding activity and native-like conformation of $A_{2A}R$ in the absence of cholesterol. The differences observed in the ligand-binding affinity of $A_{2A}R$ solubilized in DCC versus DHPC could be due to differences of these two micellar environments or the presence of native lipids that were retained throughout the purification. The DCC purification had large amounts of CHS, and ergosterol was identified in this $A_{2A}R$ sample. Cholesterol is known to generate a tighter packing of lipid hydrocarbon chains [33]; therefore it is possible that

DCC micelles provide a more rigid environment for $A_{2A}R$, while DHPC micelles provide a more flexible environment. In an NMR study Wüthrich and co-workers observed that the hydrocarbon tails of DHPC form close contacts with the hydrophobic region of OmpX [34]. This close interaction was hypothesized to play a role in stabilizing the protein's fold. Moreover, data from $A_{2A}R$ crystal structures show phospholipids bound to the cholesterol consensus motif [35] or forming other close contacts with the protein, potentially stabilizing the structure of the protein and enabling its function [36].

However, the previous hypothesis that short hydrocarbon chain lipids interact primarily with the native lipids during the protein extraction process–thus retaining some of the native lipids during the purification [16, 37], may not be supported since we did not detect the presence of ergosterol in this sample. Further studies targeting other lipids should take place to confirm this. It is not clear why DDM does not support the ligand-binding activity of $A_{2A}R$, whereas DHPC does. Furthermore, it is unknown if the presence of ergosterol in $A_{2A}R$-DCC has an effect on the observed ligand-binding activity.

5.3.5. $A_{2A}R$ Fluorescent-Ligand Binding

Ligand-binding activity was also characterized using the fluorescent agonist FITC-APEC [19]. Fluorescence anisotropy was measured to confirm the binding of the fluorescent ligand to $A_{2A}R$ solubilized in the different micellar environments. To compare the ligand binding of FITC-APEC to $A_{2A}R$ solubilized in DCC, DDM and DHPC, the receptor concentration was diluted to 1.1 μM; measurements were taken within three days after the purification (Figure 5.3).

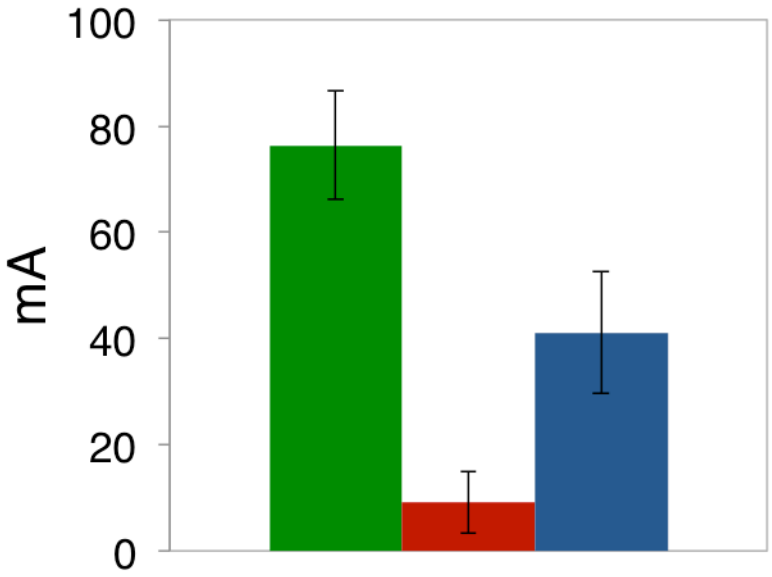

Figure 5.3 Ligand-binding characterization using fluorescence anisotropy. Binding of 70 nM FITC-APEC to 1.1 μM $A_{2A}R$ solubilized in DCC (green), DDM (red), and DHPC (blue). Measurements were taken within five days after purification. Empty micelles were used as a negative control and the anisotropy values were subtracted from micelles containing $A_{2A}R$.

$A_{2A}R$ in DDM exhibited low levels of ligand-binding activity, while $A_{2A}R$-DCC and $A_{2A}R$-DHPC bound the fluorescent ligand. The ligand-binding results obtained using anisotropy are consistent with the results obtained using [^{3}H] CGS 21680 (Figure 5.2 and [15]).

Although there are differences in the ligand-binding activity of $A_{2A}R$ purified in detergent and in lipid micelles (Figure 5.2 and Figure 5.3), it remains unclear whether these differences can be ascribed to the conformation of the receptor in the different solubilization systems. An important result of the lipid purification protocol was that cholesterol was not needed for the protein to retain its α-helical content and ligand-binding activity.

Many studies have indicated that cholesterol is important for $A_{2A}R$ ligand-binding activity [15, 38], for its signaling pathway selectivity [39], and for its coupling to Gs (the corresponding Gα-subunit) [40]. The results presented here indicate that $A_{2A}R$ is active in DHPC, but perhaps in a different conformation, with less affinity to the ligands tested. Importantly, DHPC can be used for the solubilization of $A_{2A}R$, and enables an all-lipid reconstitution system with no possible trace of detergent. Addition of long hydrocarbon chain lipids will enable the control of the membrane constituents and physical characteristics, allowing the study of the structure and function of GPCRs in the context of their lipid environment.

5.3.6. Addition of DMPC to Form Bicelles

One of the most extensively researched bicellar lipid mixtures is composed of the short hydrocarbon chain lipid DHPC in conjunction with the much-studied, long hydrocarbon-chain lipid, 1,2-dimyristoyl-sn-glycero-3-phosphocholine (DMPC, di-14:0PC) [12, 23, 41-43]. This DMPC/DHPC mixture is tunable, assuming a number of morphologies (e.g. bilayered micelles, unilamellar vesicles, multilamellar vesicles, perforated lamellae, ribbon-meshed lamellae) depending on the total lipid concentration, the molar ratio of DMPC-to-DHPC, net charge, and temperature [14, 44]. In these mixtures, the long hydrocarbon chain DMPC lipids make up the planar surface of the bilayer, while the short hydrocarbon chain DHPC lipids form the high curvature regions of the membrane. Some of these spontaneously-formed morphologies can be aligned in the presence of an external magnetic field [9-13]. Over the years bicelles have been widely used in nuclear magnetic resonance (NMR) studies, and have been used successfully to characterize GPCRs (e.g. β2 adrenergic receptor and chemokine CXCR1 receptor) [45, 46] by X-ray scattering and NMR

spectroscopy. However, prior to reconstitution in bicelles, GPCRs are solubilized using detergents [47]; for example, the aforementioned receptors, β2 adrenergic and chemokine CXCR1, were first solubilized using DDM and dodecylphosphocholine, respectively. By adding DMPC directly to $A_{2A}R$ solubilized in DHPC, we circumvent the detergent addition step.

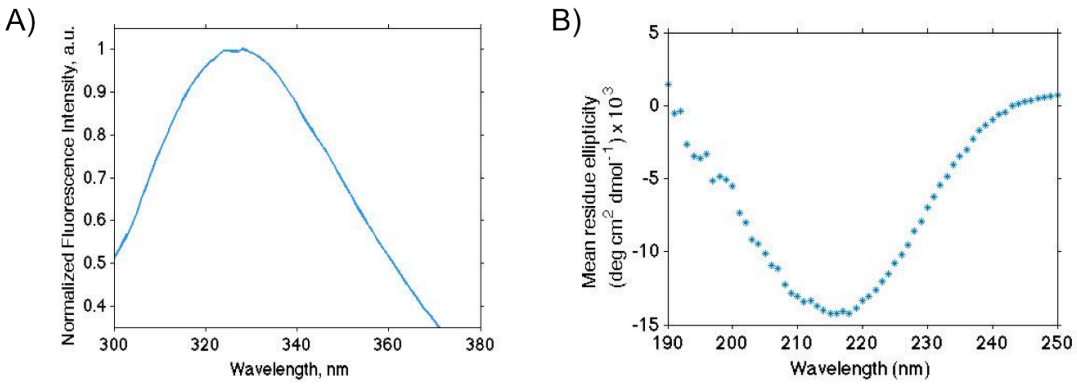

Figure 5.4 Initial characterization of $A_{2A}R$ reconstituted in bicelles. A) Fluorescence spectroscopy of $A_{2A}R$ reconstituted in DMPC/DHPC bicelles confirmed that the receptor is in a hydrophobic environment. B) CD spectrum verified that the structural conformation of $A_{2A}R$ in DMPC/DHPC bicelles is α-helical.

Initial biophysical characterization using intrinsic fluorescence and circular dichroism (CD) indicated that $A_{2A}R$ reconstituted in bicelles retained native-like structure (Figure 5.4). The intrinsic fluorescence of $A_{2A}R$ in bicelles has a peak at 328.9±1.1 nm; $A_{2A}R$ solubilized in DHPC had a maximum at 327.6±1.3 nm (Figure 5.1C). This slight shift in the fluorescence maximum could imply minor differences in the structural conformation of the receptor and its local environment. However, both

data sets indicate that the tryptophan residues of the protein reside in a hydrophobic environment.

CD analysis was used as a semi-quantitative measure of whether the receptor reconstituted in DMPC/DHPC was predominantly α-helical (Figure 5.4B), similar to the DHPC-purified protein (Figure 5.1D). The signal from empty DMPC/DHPC bicelles obfuscated some of the signal between 195-220 nm. The data, however, show that $A_{2A}R$ in DMPC/DHPC bicelles is predominantly α-helical.

Fluorescence anisotropy was used to confirm the ligand-binding activity of $A_{2A}R$ solubilized in bicelles. Figure 5.5 shows the results for $A_{2A}R$ purified in DHPC and upon reconstitution in DMPC/DHPC bicelles. This initial ligand-binding analysis indicates that $A_{2A}R$ in bicelles retains ligand-binding activity. The increase in fluorescence anisotropy observed between $A_{2A}R$ in DHPC and that of $A_{2A}R$ reconstituted in bicelles could be partially due to the increase in molecular volume of bicelles. Further characterization of these systems could potentially highlight affinity and kinetic differences of the receptor in the different reconstitution environments.

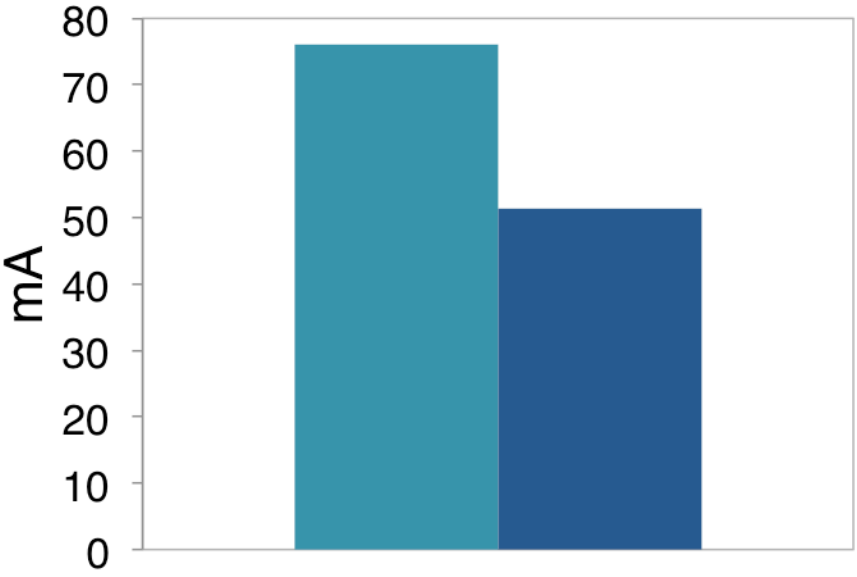

Figure 5.5 Ligand-binding characterization using fluorescence anisotropy. Binding of 70 nM FITC-APEC to $A_{2A}R$ reconstituted in DMPC/DHPC bicelles (light blue) and $A_{2A}R$ purified using DHPC (blue). Empty bicelles and DHPC micelles were used as a negative control and the anisotropy values were subtracted from bicelles/micelles containing $A_{2A}R$.

5.4. Conclusion

Purifying GPCRs in their active conformation remains a grand challenge, and finding agents that can purify and stabilize a wide range of GPCRs is of current interest. We have successfully used the short hydrocarbon chain lipid (1,2-dihexanoyl-sn-glycero-3-phosphocholine, DHPC) to solubilize and purify the full-length human $A_{2A}R$ in high yield (6.2 mg per liter of culture) and in active form.

In DHPC the receptor was able to bind ligand, retained its α-helical content and maintained the functional stability, equivalent to the stability imparted by the detergent system in the presence of a cholesterol analog. Using the short-chain lipid DHPC we did not need a sterol to retain ligand-binding activity (Figure 5.2 and Figure

5.3) and α-helical content (Figure 5.1D), indicating that $A_{2A}R$ in DHPC is in an active conformation, albeit one with less affinity for the ligands tested in this study. Understanding the mechanistic differences between the two purification systems (i.e. the need of cholesterol in DDM micelles) will shed light on GPCR allosteric signal modulation by cholesterol and other lipids, in general.

Our results from GC/MS analysis showed that DHPC stripped the ergosterol, indicating that perhaps this short-chain lipid may also strip other lipids during the purification as well, in contrast with previous hypotheses that indicate that short hydrocarbon chain lipids leave the protein surrounded by a thin shell of its native lipids [16, 24]. On the other hand, DCC-purified $A_{2A}R$ retained detectable levels of ergosterol; DCC is commonly used for the purification and solubilization of GPCRs (see table in Appendix C highlighting GPCR solubilization and reconstitution systems). It remains to be investigated how the presence of ergosterol in the $A_{2A}R$-DCC purification affects the ligand-binding activity and stability.

The DHPC purification system alleviates the need for detergents, which investigators have traditionally made great efforts to remove prior to the reconstitution of membrane proteins into biomimetic membrane systems [48-51]. Additionally, the present lipid purification system allowed the facile incorporation of long hydrocarbon chain lipids (DMPC). Initial characterization of $A_{2A}R$ reconstituted in DHPC/DMPC bilayered micelles indicated that the receptor retained its α-helical content and ligand-binding activity.

5.5. Acknowledgements

The work presented in this chapter was conducted in collaboration with Dr. John Katsaras and Dr. Robert Standaert.

REFERENCES

1. Chini, B. and M. Parenti, *G-protein-coupled receptors, cholesterol and palmitoylation: facts about fats.* Journal of Molecular Endocrinology, 2009. **42**(5-6): p. 371-379.

2. Lingwood, D. and K. Simons, *Lipid rafts as a membrane-organizing principle.* Science, 2010. **327**(5961): p. 46-50.

3. Oates, J. and A. Watts, *Uncovering the intimate relationship between lipids, cholesterol and GPCR activation.* Current Opinion in Structural Biology, 2011. **21**(6): p. 802-807.

4. Hanson, M.A., et al., *A specific cholesterol binding site is established by the 2.8 A structure of the human beta2-adrenergic receptor.* Structure, 2008. **16**(6): p. 897-905.

5. McNeely, P.M., A.N. Naranjo, and A.S. Robinson, *Structure-function studies with G protein-coupled receptors as a paradigm for improving drug discovery and development of therapeutics.* Biotechnology journal, 2012. **7**(12): p. 1451-61.

6. Tapaneeyakorn, S., et al., *Solution- and solid-state NMR studies of GPCRs and their ligands.* Biochimica et biophysica acta, 2011. **1808**(6): p. 1462-75.

7. Maler, L., *Solution NMR studies of peptide-lipid interactions in model membranes.* Molecular Membrane Biology, 2012. **29**(5): p. 155-176.

8. Allen, S.J., et al., *Expression, purification and in vitro functional reconstitution of the chemokine receptor CCR1.* Protein expression and purification, 2009. **66**(1): p. 73-81.

9. Sanders, C.R., 2nd and G.C. Landis, *Reconstitution of membrane proteins into lipid-rich bilayered mixed micelles for NMR studies.* Biochemistry, 1995. **34**(12): p. 4030-40.

10. Prosser, R.S., et al., *Lanthanide chelates as bilayer alignment tools in NMR studies of membrane-associated peptides.* Journal of magnetic resonance, 1999. **141**(2): p. 256-60.

11. Nieh, M.P., et al., *Magnetically alignable phase of phospholipid "bicelle" mixtures is a chiral nematic made up of wormlike micelles.* Langmuir : the ACS journal of surfaces and colloids, 2004. **20**(19): p. 7893-7.

12. Katsaras, J., et al., *Rarely observed phase transitions in a novel lyotropic liquid crystal system.* Physical review letters, 1997. **78**(5): p. 899-902.

13. Tjandra, N. and A. Bax, *Direct measurement of distances and angles in biomolecules by NMR in a dilute liquid crystalline medium.* Science, 1997. **278**(5340): p. 1111-4.

14. Harroun, T.A., et al., *Comprehensive examination of mesophases formed by DMPC and DHPC mixtures.* Langmuir : the ACS journal of surfaces and colloids, 2005. **21**(12): p. 5356-61.

15. O'Malley, M.A., et al., *High-level expression in Saccharomyces cerevisiae enables isolation and spectroscopic characterization of functional human adenosine A2a receptor.* Journal of structural biology, 2007. **159**(2): p. 166-78.

16. Hauser, H., *Short-chain phospholipids as detergents.* Biochimica Et Biophysica Acta-Biomembranes, 2000. **1508**(1-2): p. 164-181.

17. Candiano, G., et al., *Blue silver: A very sensitive colloidal Coomassie G-250 staining for proteome analysis.* Electrophoresis, 2004. **25**(9): p. 1327-1333.

18. Schindelin, J., et al., *Fiji: an open-source platform for biological-image analysis.* Nat Meth, 2012. **9**(7): p. 676-682.

19. McCabe, R.T., P. Skolnick, and K.A. Jacobson, *2-[2-[4-[2-[2-[1,3-Dihydro-1,1-bis (4-hydroxyphenyl)-3-oxo-5-isobenzofuranthioureidyl]ethylaminocarbonyl]ethyl]pheny l] ethylamino]-5'--ethylcarboxamidoadenosine (FITC-APEC): A Fluorescent Ligand For A-Adenosine Receptors.* Journal of fluorescence, 1992. **2**(4): p. 217-223.

20. Zhao, X.J., et al., *Designer short peptide surfactants stabilize G protein-coupled receptor bovine rhodopsin.* Proceedings of the National Academy of Sciences of the United States of America, 2006. **103**(47): p. 17707-17712.

21. Patching, S.G., *NMR structures of polytopic integral membrane proteins.* Molecular Membrane Biology, 2011. **28**(6): p. 370-97.

22. Prive, G.G., *Detergents for the stabilization and crystallization of membrane proteins.* Methods, 2007. **41**(4): p. 388-97.

23. Sanders, C.R. and F. Sonnichsen, *Solution NMR of membrane proteins: practice and challenges.* Magnetic resonance in chemistry : MRC, 2006. **44 Spec No**: p. S24-40.

24. Shivanna, B.D. and E.S. Rowe, *Preservation of the native structure and function of Ca2+-ATPase from sarcoplasmic reticulum: solubilization and reconstitution by new short-chain phospholipid detergent 1,2-diheptanoyl-sn-phosphatidylcholine.* The Biochemical journal, 1997. **325 (Pt 2)**: p. 533-42.

25. Vidi, P.A., et al., *Adenosine A(2A) receptors assemble into higher-order oligomers at the plasma membrane.* FEBS letters, 2008. **582**(29): p. 3985-90.

26. Canals, M., et al., *Homodimerization of adenosine A2A receptors: qualitative and quantitative assessment by fluorescence and bioluminescence energy transfer.* Journal of neurochemistry, 2004. **88**(3): p. 726-34.

27. Lukasiewicz, S., et al., *Fluorescence studies of homooligomerization of adenosine A2A and serotonin 5-HT1A receptors reveal the specificity of receptor interactions in the plasma membrane.* Pharmacological reports : PR, 2007. **59**(4): p. 379-92.

28. Johansson, B., et al., *The binding of the adenosine A2 receptor selective agonist [3H]CGS 21680 to rat cortex differs from its binding to rat striatum.* European journal of pharmacology, 1993. **247**(2): p. 103-10.

29. Jiang, Q., et al., *Mutagenesis reveals structure-activity parallels between human A2A adenosine receptors and biogenic amine G protein-coupled receptors.* Journal of medicinal chemistry, 1997. **40**(16): p. 2588-95.

30. Jarvis, M.F., et al., *[3H]CGS 21680, a selective A2 adenosine receptor agonist directly labels A2 receptors in rat brain.* The Journal of pharmacology and experimental therapeutics, 1989. **251**(3): p. 888-93.

31. Niebauer, R.T. and A.S. Robinson, *Exceptional total and functional yields of the human adenosine (A2a) receptor expressed in the yeast Saccharomyces cerevisiae.* Protein expression and purification, 2006. **46**(2): p. 204-11.

32. Lauffenburger, D.A. and J.J. Linderman, *Receptors: Models for binding, trafficking, and signaling*1993: Oxford University Press.

33. Soubias, O. and K. Gawrisch, *The role of the lipid matrix for structure and function of the GPCR rhodopsin.* Biochimica et biophysica acta, 2012. **1818**(2): p. 234-40.

34. Fernandez, C., et al., *Lipid-protein interactions in DHPC micelles containing the integral membrane protein OmpX investigated by NMR spectroscopy.* Proceedings of the National Academy of Sciences of the United States of America, 2002. **99**(21): p. 13533-7.

35. Jaakola, V.P., et al., *The 2.6 angstrom crystal structure of a human A2A adenosine receptor bound to an antagonist.* Science, 2008. **322**(5905): p. 1211-7.

36. Liu, W., et al., *Structural basis for allosteric regulation of GPCRs by sodium ions.* Science, 2012. **337**(6091): p. 232-6.

37. Kessi, J., et al., *Short-chain phosphatidylcholines as superior detergents in solubilizing membrane proteins and preserving biological activity.* Biochemistry, 1994. **33**(35): p. 10825-36.

38. Lyman, E., et al., *A role for a specific cholesterol interaction in stabilizing the Apo configuration of the human A(2A) adenosine receptor.* Structure, 2009. **17**(12): p. 1660-8.

39. Lam, R.S., D. Nahirney, and M. Duszyk, *Cholesterol-dependent regulation of adenosine A(2A) receptor-mediated anion secretion in colon epithelial cells.* Experimental cell research, 2009. **315**(17): p. 3028-35.

40. Zezula, J. and M. Freissmuth, *The A(2A)-adenosine receptor: a GPCR with unique features?* British journal of pharmacology, 2008. **153 Suppl 1**: p. S184-90.

41. Prosser, R.S., et al., *Magnetically aligned membrane model systems with positive order parameter: Switching the sign of S-zz with paramagnetic ions.* Journal of the American Chemical Society, 1996. **118**(1): p. 269-270.

42. Katsaras, J., et al., *"Bicellar" lipid mixtures as used in biochemical and biophysical studies.* Naturwissenschaften, 2005. **92**(8): p. 355-366.

43. Sanders, C.R., et al., *Magnetically-oriented phospholipid micelles as a tool for the study of membrane-associated molecules.* Progress in Nuclear Magnetic Resonance Spectroscopy, 1994. **26**: p. 421-444.

44. Nieh, M.P., et al., *Formation of kinetically trapped nanoscopic unilamellar vesicles from metastable nanodiscs.* Langmuir : the ACS journal of surfaces and colloids, 2011. **27**(23): p. 14308-16.

45. Park, S.H., et al., *High-resolution NMR spectroscopy of a GPCR in aligned bicelles.* Journal of the American Chemical Society, 2006. **128**(23): p. 7402-3.

46. Rasmussen, S.G., et al., *Crystal structure of the human beta2 adrenergic G-protein-coupled receptor.* Nature, 2007. **450**(7168): p. 383-7.

47. Ujwal, R. and J.U. Bowie, *Crystallizing membrane proteins using lipidic bicelles.* Methods, 2011. **55**(4): p. 337-41.

48. Park, S.H., et al., *Optimization of purification and refolding of the human chemokine receptor CXCR1 improves the stability of proteoliposomes for structure determination.* Biochimica et biophysica acta, 2012. **1818**(3): p. 584-91.

49. Grisshammer, R.K., S.K. Buchanan, and Royal Society of Chemistry (Great Britain), *Structural biology of membrane proteins*. RSC biomolecular sciences, 2006, Cambridge: RSC. xxiii, 392 p.

50. Hong, K. and W.L. Hubbell, *Preparation and properties of phospholipid bilayers containing rhodopsin.* Proceedings of the National Academy of Sciences of the United States of America, 1972. **69**(9): p. 2617-21.

51. Schubert, R., *Liposome preparation by detergent removal.* Methods in enzymology, 2003. **367**: p. 46-70.

Chapter 6

CONCLUSION AND PERSPECTIVES

Understanding of the structure-function relationship of GPCRs is paramount to the design of more effective drugs targeting these receptors. The work covered in this thesis advanced three areas of current interest in the GPCR field, as highlighted in Chapter 1:

- Structural features important for the expression, function and stability of GPCRs
- Characterization of ligand-binding kinetics
- Solubilization of GPCRs in native-like environments

6.1. Structural Features Important for the Expression, Function and Stability of GPCRs

Toward the first aim, we investigated the role that the extensive disulfide bond network has on the expression, trafficking and ligand-binding activity of human $A_{2A}R$. Cys-to-Ala mutations were conducted systematically for the cysteines in extracellular loop 1 (ECL1) and ECL2. The ECL regions are challenging to capture in GPCR crystal structures due to their flexibility; therefore, mutagenesis and functional studies continue to provide insight into the importance of these flexible regions. Our results suggest that the disulfide bond network in $A_{2A}R$ is important for restricting the topology of the ECLs. By mutating the cysteines in the ECLs, we were able to access various active conformations, with an affinity ranging from 52–150 nM.

A semi-quantitative method (Hausdorff distance ratio analysis) was implemented to characterize the various trafficking patterns observed. This analysis identified three different trafficking patterns: a higher ER retention relative to the WT $A_{2A}R$ – all the single Cys-to-Ala variants and the conserved disulfide bond variant (C77A-C166A); a similar trafficking pattern as the WT $A_{2A}R$ – C71A-C159A; and improved plasma membrane trafficking relative to the WT receptor – C74A-C146A. All the single Cys-to-Ala variants showed higher ER retention levels, likely from the interaction of unpaired cysteine with ER oxidoreductases. In contrast to the other double cysteine variants (C74A-C146A and C71A-C159A), whose trafficking to the plasma membrane improved or were comparable to the WT trafficking, C77A-C166A (site of conserved disulfide bond) had a higher level of ER localized receptor. It is unclear how the ER quality control recognizes the differences in loop structure that form upon the removal of the conserved disulfide bond, but not the removal of the other two non-conserved disulfide bonds.

Surprisingly, the results presented in Chapter 2 and Chapter 3 suggest that the conserved disulfide bond is not essential for A_{2A} receptor trafficking and activity. Our results also indicate that the disulfide bonds do not contribute to the assembly of the most stable conformation, as the removal of C74-C146 improves folding efficiency and trafficking to the plasma membrane, attributes that have been linked to conformational stability. This suggests that a widely accepted concept in the biophysical community, that disulfide bonds contribute to protein stability, may not always be the case, in particular with proteins with an extensive disulfide bond network, such as $A_{2A}R$.

Future Considerations

The C74A-C146A variant shows improved trafficking and wild-type ligand-binding affinity; it has been hypothesized that this improved trafficking is due to enhanced folding efficiency and/or conformational stability. This hypothesis could be tested by cloning this construct into pITy and expressing this variant in yeast for purification. Biophysical characterization of this variant could be conducted as described previously [1, 2] to determine thermodynamic stability.

Double disulfide bond mutations could be conducted to further test the role of an individual disulfide bond. These studies could determine which disulfide bond is critical for expression, trafficking and ligand-binding activity of $A_{2A}R$, or if more than one disulfide bond is needed for the successful expression of this adenosine receptor.

6.2. Characterization of Ligand-Binding Kinetics

In Chapter 4 we applied fluorescence anisotropy to measure the binding affinity and kinetics of ligands targeting the full-length human $A_{2A}R$. K_i values for six unlabeled ligands were determined and are in agreement with values reported in literature; values deviated only by a factor of 1-6. This indicates that the micelle-solubilized receptor retains a binding affinity comparable to the affinity of the receptor in more complex systems (i.e. membrane preparations).

Furthermore, the analytical solutions for single-site binding models were used to fit the FITC-APEC association kinetic data and the two-ligand kinetic association data. It is important to note that FA assays generally operate in the ligand depletion regime; here we validated the application of this analytic approach for characterizing the binding kinetics of $A_{2A}R$ ligands, further expanding the use of FA assays.

This analysis determined that the different affinities observed between two structurally similar ligands (NECA and adenosine) result from differences in their residence time; the high affinity of ZM 241385 can be attributed to a faster association rate than NECA and adenosine. These studies represent an important step toward validating the use of micellar solubilized $A_{2A}R$ for the characterization of unlabeled ligand-binding kinetics, and the application of FA to better understand the kinetic contributions to ligand-binding affinity.

Future Considerations

Ligand-binding measurements require the use of labeled compounds; this requirement limits these studies to a few ligands, and as a consequence the literature data are often incomplete or conflicting [3]. As can be seen from Table 4.4 in Chapter 4, the affinity constants reported in literature vary, which is not surprising as the variability in K_D may depend on the membrane or membrane-mimetic environment that the protein resides in, apart from changes in pH, temperature, and ion concentrations [4]. The FA assay developed using purified $A_{2A}R$ could be used to test the binding affinity and kinetics of all ligands known to target this receptor. This will lead to a self-consistent, ligand-binding affinity library for the human $A_{2A}R$. Furthermore, the ligand-binding kinetics of more unlabeled ligands can be measured; kinetic information of the unlabeled ligands targeting this receptor, and other GPCRs is sparse.

The molecular determinants of ligand-receptor binding kinetics remain poorly understood [5]. In combination with mutagenesis studies, structural data and molecular dynamic simulations, this *in vitro* system could aid in the rational design of drugs (with the desired binding kinetics) that target the human A_{2A} adenosine receptor.

Additionally, the Cys-to-Ala variants (in HEK 293 membrane preparations or detergent micelles) could be used to test how the different loop conformations change the ligand-binding kinetics; and relate the association and dissociation rate constants with the binding affinities, ranging from 52–150 nM.

Moving forward it is important to determine experimentally why FITC-APEC recognizes only 5.6% of the total receptor population (R_T) and characterizing if this phenomenon is observed *in vivo*. Size exclusion chromatography could be used to identify the oligomeric state of the purified receptor, and whether it is this population that is binding specifically to FITC-APEC. Also these data pointed out that B_{max} might not equal R_T. Another model suggests that antagonists recognize R_T, binding not just the R^* receptor conformation [6, 7]. To test if an antagonist binds to the total receptor population fluorescence anisotropy measurements could be conducted using a fluorescent antagonist (e.g. MRS5346, derived from SCH 442416) [8].

6.3. Solubilization of GPCRs in Native-Like Environments

Purifying GPCRs in their active conformation remains a grand challenge, and finding agents that can purify and stabilize a wide range of GPCRs is of current interest. Previous results from our group showed that the human A_{2A} adenosine receptor purified in DDM, CHAPS, and a cholesterol analog (CHS), retained its α-helical content and ligand-binding activity. Importantly, however, in the absence of CHS, both the activity and the α-helical content of the receptor were eliminated [2, 9].

We have used successfully the short hydrocarbon-chain lipid, DHPC, to solubilize and purify A_{2A} receptor in an active form and in high yields (6.2 mg per liter of culture). The DHPC purification system alleviates the need for detergents, which investigators have traditionally made great efforts to remove prior to the reconstitution

of membrane proteins into biomimetic membrane systems [10-13]. To our surprise, and unlike our previous results of a detergent purification protocol [2], DHPC retained the ligand-binding ability of $A_{2A}R$ in the absence of cholesterol.

Additionally, the present lipid purification system allowed the facile incorporation of long hydrocarbon chain lipids (DMPC). Initial characterization indicated that upon addition of DMPC/DHPC to $A_{2A}R$-DHPC the receptor retained the α-helical content and ligand-binding activity.

Future Considerations

Comparison of the three solubilization systems (i.e. DDM/CHAPS/CHS (DCC), DDM and DHPC) led to interesting observations:

- Freezing cell pellets at a consistent optical density and starting the detergent solubilization step from membrane preparations instead of crude cell lysis improved reproducibility and the purity of the purified protein.
- Ergosterol was detected in $A_{2A}R$ solubilized in DCC; no ergosterol was detected in the $A_{2A}R$-DDM and $A_{2A}R$-DHPC samples. It remains unknown if the ergosterol presence improves ligand-binding properties.
- Mitochondrial membrane proteins were identified as the main impurities in the DHPC purification. It remains unknown whether these proteins are contaminants or if their interaction with $A_{2A}R$ is physiologically relevant.
- After implementing the changes in the purification protocol, $A_{2A}R$ purified in DDM retained α-helical content, but negligible binding activity was detected within five days after purification. This suggests that α-helical retention is not indicative of the receptor activity.

$A_{2A}R$ retains ligand-binding activity in DHPC in the absence of cholesterol, while ligand-binding activity was lost in the detergent based system (DDM). However,

$A_{2A}R$ in DHPC is in a conformation with less affinity for the ligands tested in this study. Understanding the mechanistic differences between the two purification systems (i.e. the need of cholesterol in DDM micelles) will shed light on GPCR allosteric signal modulation by cholesterol and other lipids, in general. To this end, cholesterol or CHAPS/CHS could be added to the $A_{2A}R$-DHPC purification to test if the high affinity conformation is restored. Additionally, changes in ligand-binding kinetics in the presence of cholesterol, CHAPS/CHS, and ergosterol could be measured using fluorescence anisotropy.

To increase the purity of DHPC preparations, higher speed centrifugation could be used during the removal of insoluble material; also plasma membrane preparations using sucrose gradients could be conducted to remove the mitochondrial membrane proteins [14]. Further characterization of $A_{2A}R$ in DHPC/DMPC bicelles is required; initially dynamic light scattering and cryogenic transmission electron microscopy could be used to confirm that A_{2A} is reconstituted into bicelles.

Moving forward *in vivo* and *in vitro* studies will continue to be instrumental as we determine the mechanism responsible for the modulation of GPCR signaling. Continuing the investigation of the role of the disulfide bond network may enhance our understanding of the involvement of the extracellular loops in ligand-binding recognition and kinetics. Fluorescence anisotropy could be used to characterize the changes in binding affinity and kinetics as a function of the oligomerization state of the receptor and the lipid composition. Overall, the studies and assays described in this thesis will be important as we begin to understand the emerging ligand-lipid-receptor-effector relationships.

REFERENCES

1. O'Malley, M.A., et al., *Analysis of adenosine A(2)a receptor stability: Effects of ligands and disulfide bonds.* Biochemistry, 2010. **49**(43): p. 9181-9189.

2. O'Malley, M.A., et al., *High-level expression in Saccharomyces cerevisiae enables isolation and spectroscopic characterization of functional human adenosine A2a receptor.* Journal of structural biology, 2007. **159**(2): p. 166-78.

3. Zhukov, A., et al., *Biophysical mapping of the adenosine A(2A) receptor.* Journal of medicinal chemistry, 2011. **54**(13): p. 4312-4323.

4. Lauffenburger, D.A. and J.J. Linderman, *Receptors: Models for binding, trafficking, and signaling*1993: Oxford University Press.

5. Pan, A.C., et al., *Molecular determinants of drug-receptor binding kinetics.* Drug Discovery Today, 2013. **18**(13-14): p. 667-673.

6. Bennett, K.A., et al., *Pharmacology and structure of isolated conformations of the adenosine A(2A) receptor define ligand efficacy.* Molecular pharmacology, 2013. **83**(5): p. 949-958.

7. Guo, D., et al., *Functional efficacy of adenosine A2A receptor agonists is positively correlated to their receptor residence time.* British journal of pharmacology, 2012. **166**(6): p. 1846-1859.

8. Kecskes, M., et al., *Novel Alexa Fluor-488 labeled antagonist of the A(2A) adenosine receptor: Application to a fluorescence polarization-based receptor binding assay.* Biochemical pharmacology, 2010. **80**(4): p. 506-511.

9. O'Malley, M.A., et al., *Toward rational design of protein detergent complexes: determinants of mixed micelles that are critical for the in vitro stabilization of a G-protein coupled receptor.* Biophysical journal, 2011. **101**(8): p. 1938-48.

10. Park, S.H., et al., *Optimization of purification and refolding of the human chemokine receptor CXCR1 improves the stability of proteoliposomes for structure determination.* Biochimica et biophysica acta, 2012. **1818**(3): p. 584-91.

11. Grisshammer, R.K., S.K. Buchanan, and Royal Society of Chemistry (Great Britain), *Structural biology of membrane proteins*. RSC biomolecular sciences, 2006, Cambridge: RSC. xxiii, 392 p.

12. Hong, K. and W.L. Hubbell, *Preparation and properties of phospholipid bilayers containing rhodopsin.* Proceedings of the National Academy of Sciences of the United States of America, 1972. **69**(9): p. 2617-21.

13. Schubert, R., *Liposome preparation by detergent removal.* Methods in enzymology, 2003. **367**: p. 46-70.

14. Xiao, W., *Yeast protocols third edition preface*, in *Yeast Protocols, Third Edition*, W. Xiao, Editor 2014. p. V-V.

Appendix A

Primers Used for Mutagenesis and Analysis of HR Variance

Primers Used for Mutagenesis and PCR Steps

This appendix contains the primers used to create the point mutations in $A_{2A}R$ in Table A.1 and the primers used for subcloning the $A_{2A}R$ constructs into the pCEP4-CFP vector in Table A.2.

Table A.1 Primers used for the creation of the $A_{2A}R$ Cys-to-Ala constructs

Mutation	Primer Sequence (5' to 3')
C71 forward	AGCACCGGGTTCGCCGCTGCCTGCC
C71 reverse	GGCAGGCAGCGGCGAACCCGGTGCT
C74 forward	GTTCTGCGCTGCCGCCCACGGCTGCC
C74 reverse	GGCAGCCGTGGGCGGCAGCGCAGAAC
C77 forward	TGCCTGCCACGGCGCCCTCTTCATTGCCTGCTTCG
C77 reverse	CGAAGCAGGCAATGAAGAGGGCGCCGTGGCAGGCA
C146 forward	GGTTGGAACAACGCCGGTCAGCCAAAGGAG
C146 reverse	CTCCTTTGGCTGACCGGCGTTGTTCCAACC
C159 forward	CTCCCAGGGCGCCGGGGAGGGCCAAG
C159 reverse	CTTGGCCCTCCCCGGCGCCCTGGGAG
C166 forward	CCAAGTGGCCGCTCTCTTTGAGGATG
C166 reverse	CATCCTCAAAGAGAGCGGCCACTTGG

Table A.2 Primers used for subcloning the $A_{2A}R$ constructs into pCEP4-CFP.

Primer	TM °C	Primer Sequence (5' to 3')
KpnI-A_2aR forward	63.3	ATGTTGGTACCATGCCCATCATGG
XhoI-A_2aR reverse	66.8	GCCATCTCGAGGGACACTCCTGC

A PCR step was introduce prior to the DNA digestion for the pCEP4-CFP vector, in order to eliminate the stop codon at the end of the $A_{2A}R$ gene. KOD Hot Start Master Mix from EMD Millipore was used for the PCR reaction.

Analysis of HR Variance

High correlation was observed between the sample size (n) and the HR variance (p=0.03, Figure A.1C). To test that the HR variance is not correlated with the sample size (n) we selected at random 20 data points from the HR data set for each variant. With a constant sample size (n=20) the trend of the HR variance remained the same (Apendix A , Figure A.1B), having a strong correlation (p=0.0014) with the variance of the original HR data set (n≥20) (Apendix A, Figure A.1D).

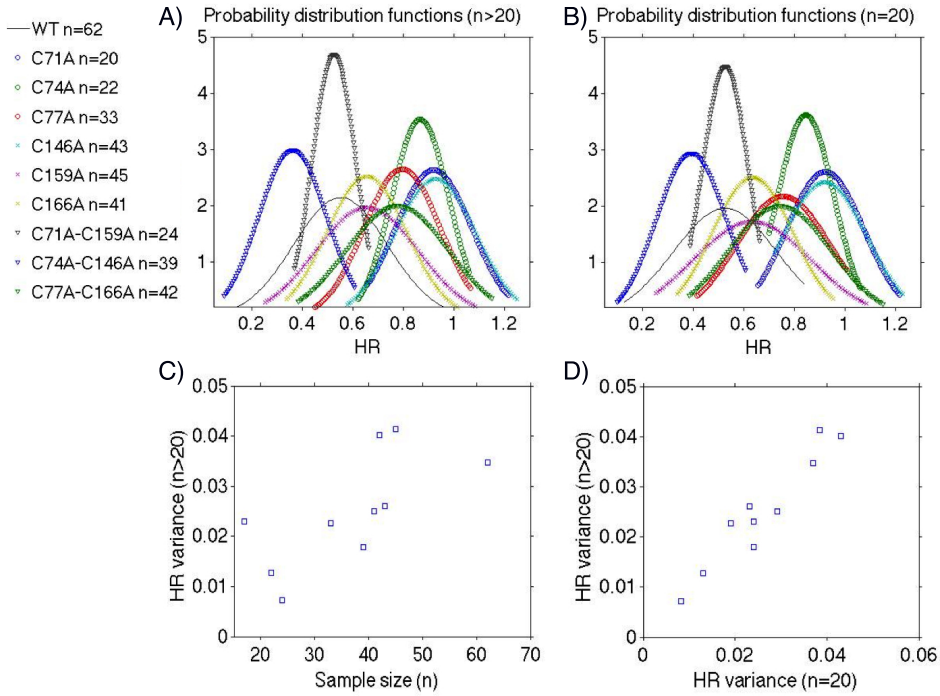

Figure A.1 Probability distribution functions and correlation between sample size (n) and HR variance for the WT receptor and Cys-to-Ala variants. A) Probability distribution function of the original HR data set (n≥20). B) Probability distribution function of randomly selected HR data (n=20). C) Correlation between sample size (n) and HR variance of the original data set (p=0.03). D) Correlation between HR variance of randomly selected data (n=20) and HR variance of the original data set (n≥20) (p=0.0014). A normal distribution was used to fit the HR data.

Figure A.2 shows the histogram of the CFP to PM pixel distances (Figure A.2A and A.2D), ER to PM pixel distances (Figure A.2B and A.2E), and the ratio of these distances (Figure A.2C and A.2F) for the WT receptor and the C71A variant. Data were fit using a normal distribution (solid red line).

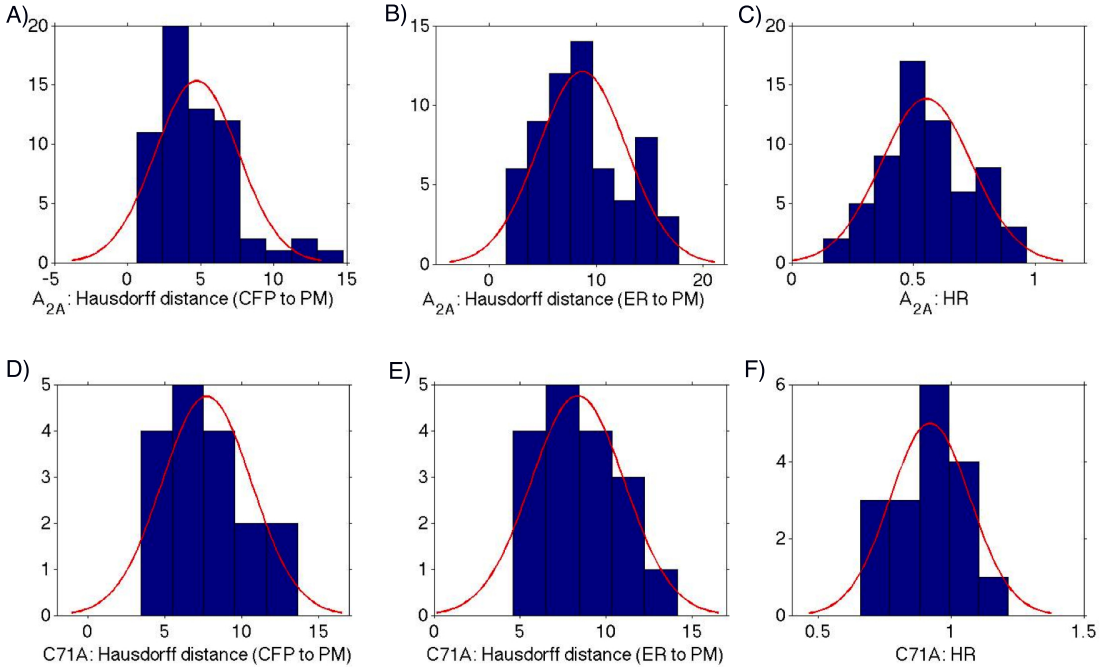

Figure A.2 Histogram and normal distribution fit for the WT receptor and the C71A variant. A and D) Histogram of the CFP to PM pixel distances. B and E) Histogram of the ER to PM pixel distances. C and F) Histogram of the HR (CFP to PM/ER to PM).

Appendix B

Matlab Functions Used to Fit Ligand-Binding Affinity and Kinetic Data

IC_{50} Fit

```
function [beta, R, xfit, yfit, yfit_reduced, r2, adjr2,
J, CovB, MSE  ] = IC50(xData, yData)
%beta(1)= log[M]
x=[xData yData];
% Set up fittype and options.
y=x(:,2);
ymax=max(y);
ymin=min(y);

Model= @(k,x)      ymin+((ymax-ymin)./(1+10.^(x-k)));
initialGuess = [-4 ];
    [beta, R, J, CovB, MSE ] =
nlinfit(x(:,1),x(:,2),Model,initialGuess);
% Fit model to data.
   n=length(x(:,2));      %#data points
   df=n-1-1 ;   %#data points  - #parameters -1

   min_x=min(x(:,1));
   max_x=max(x(:,1));

 xfit=[min_x:  0.5:  max_x]';
 xfit_reduced=x(:,1);

     yfit=  ymin+((ymax-ymin)./(1+10.^(xfit-beta(1))));
    yfit=yfit(:,1);

    yfit_reduced=  ymin+((ymax-
ymin)./(1+10.^(xfit_reduced-beta(1))));
    yfit_reduced=yfit_reduced(:,1);

    yresid=R ;        %y-yfit;
    SSresid = sum(yresid.^2);
    SStotal = (n-1) * var(y);

    r2 = 1 - SSresid/SStotal;
    adjr2=1-((1-r2)*((n-1)/df));
    end
```

```
function [beta, R, xfit, yfit, r2, adjr2, J, CovB, MSE  ]
= ExpAssociation(xData, yData)
%beta(1)= kobs

%Data can be fit to a 1-phase exponential association
equiation ymax*(1-exp(k*x))
 x=[xData yData];
% Set up fittype and options.
y=x(:,2);
ymax=mean(y(end-10:end,:));

Model= @(k,x)      ymax.*(1-exp(k(1).*x));
initialGuess = [0.005 ];
    [beta, R, J, CovB, MSE ] =
nlinfit(x(:,1),x(:,2),Model,initialGuess);

   n=length(x(:,2));      %#data points
   df=n-1-1 ;   %#data points  - #parameters -1
   min_x=min(x(:,1));
   max_x=max(x(:,1));
   xfit=[min_x:  1:  max_x]';

   yfit=ymax.*(1-exp(beta(1).*xfit)) ;
   yfit=yfit(:,1);

    yresid=R ;        %y-yfit;
    SSresid = sum(yresid.^2);
    SStotal = (n-1) * var(y);

    r2 = 1 - SSresid/SStotal;
    adjr2=1-((1-r2)*((n-1)/df));
    end


function [beta, R, xfit, yfit, r2, adjr2, J, CovB, MSE  ]
= ExpDissociation(xData, yData)
%beta(1)= koff

%Data can be fit to a dissociation equation   Y=(Y0-
NS)*exp(-K*X) + NS
% Y0 is the binding at time zero, in the units of the Y
axis.
% NS is the binding (nonspecific) at infinite times, in
```

```
the units of the Y axis.
% K is the rate constant in inverse units of the X axis.
The half-life equals the ln(2) divided by K.

x=[xData yData];
% Set up fittype and options.
y=x(:,2);
ymax=max(y);
ymin=min(y);

Model= @(k,x)      ((ymax-ymin).*(exp(-k(1).*x)))+ymin;
initialGuess = [0.005 ];
    [beta, R, J, CovB, MSE ] =
nlinfit(x(:,1),x(:,2),Model,initialGuess);
% Fit model to data.
   n=length(x(:,2));      %#data points
   df=n-2-1 ;   %#data points  - #parameters -1
   min_x=min(x(:,1));
   max_x=max(x(:,1));
    xfit=[min_x:  1:  max_x]';
    yfit=((ymax-ymin).*(exp(-beta(1).*xfit)))+ymin ;
    yfit=yfit(:,1);

    yresid=R ;        %y-yfit;
    SSresid = sum(yresid.^2);
    SStotal = (n-1) * var(y);
    r2 = 1 - SSresid/SStotal;
    adjr2=1-((1-r2)*((n-1)/df));

end
```

```
% One ligand (Labeled)
function [beta, R, xfit, yfit, r2, adjr2, J, CovB, MSE  ]
= kon_koff_LabeledLigand2(xData, yData,N,L)
%beta(1)= kon    beta(2) koff

% [xData, yData] = prepareCurveData( xData, yData );

x=[xData yData];
% Set up fittype and options.
Model= @(k,x)   ((k(1)*N*L)/(((k(1).*L)+k(2)))).*(1-exp(-
((k(1).*L)+k(2)).*x));
initialGuess = [0.00005 0.08];
    [beta, R, J, CovB, MSE ] =
nlinfit(x(:,1),x(:,2),Model,initialGuess);
% Fit model to data.
    n=length(x(:,2));      %#data points
    df=n-2-1 ;   %#data points  - #parameters -1
    y=x(:,2);
   min_x=min(x(:,1));
   max_x=max(x(:,1));

    xfit=[min_x:  1:  max_x]';
 yfit=((beta(1,1)*N*L)/(((beta(1,1).*L)+beta(1,2)))).*(1-
exp(-((beta(1,1).*L)+beta(1,2)).*xfit));
    yfit=yfit(:,1);

    yresid=R ;        %y-yfit;
    SSresid = sum(yresid.^2);
    SStotal = (n-1) * var(y);
    r2 = 1 - SSresid/SStotal;
    adjr2=1-((1-r2)*((n-1)/df));

end
```

```
     % Two ligand association competition
```

```
function [beta, R, xfit, yfit, r2, adjr2, J, CovB, MSE  ]
= kon_koff_LabeledCompetitorLigands3(xData,
yData,N,L,I,k1,k2)

x=[xData yData];
% Set up fittype and options.
Model= @(k,x)
((N*k1*L)/((0.5.*(((k1.*L)+k2)+((k(1).*I)+k(2))+sqrt((((k
1.*L)+k2)-((k(1).*I)+k(2)))^2+4*k1*k(1)*L*I)))-
(0.5.*(((k1.*L)+k2)+((k(1).*I)+k(2))-sqrt((((k1.*L)+k2)-
((k(1).*I)+k(2)))^2+4*k1*k(1)*L*I))))).*(
((k(2)*((0.5.*(((k1.*L)+k2)+((k(1).*I)+k(2))+sqrt((((k1.*
L)+k2)-((k(1).*I)+k(2)))^2+4*k1*k(1)*L*I)))-
(0.5.*(((k1.*L)+k2)+((k(1).*I)+k(2))-sqrt((((k1.*L)+k2)-
((k(1).*I)+k(2)))^2+4*k1*k(1)*L*I))))/((0.5.*(((k1.*L)+k
2)+((k(1).*I)+k(2))+sqrt((((k1.*L)+k2)-
((k(1).*I)+k(2)))^2+4*k1*k(1)*L*I)))*(0.5.*(((k1.*L)+k2)+
((k(1).*I)+k(2))-sqrt((((k1.*L)+k2)-
((k(1).*I)+k(2)))^2+4*k1*k(1)*L*I))))) + (((k(2)-
(0.5.*(((k1.*L)+k2)+((k(1).*I)+k(2))+sqrt((((k1.*L)+k2)-
((k(1).*I)+k(2)))^2+4*k1*k(1)*L*I))))/(0.5.*(((k1.*L)+k2)
+((k(1).*I)+k(2))+sqrt((((k1.*L)+k2)-
((k(1).*I)+k(2)))^2+4*k1*k(1)*L*I)))).*exp(-
(0.5.*(((k1.*L)+k2)+((k(1).*I)+k(2))+sqrt((((k1.*L)+k2)-
((k(1).*I)+k(2)))^2+4*k1*k(1)*L*I))).*x)) - (((k(2)-
(0.5.*(((k1.*L)+k2)+((k(1).*I)+k(2))-sqrt((((k1.*L)+k2)-
((k(1).*I)+k(2)))^2+4*k1*k(1)*L*I))))/(0.5.*(((k1.*L)+k2)
+((k(1).*I)+k(2))-sqrt((((k1.*L)+k2)-
((k(1).*I)+k(2)))^2+4*k1*k(1)*L*I)))).*exp(-
(0.5.*(((k1.*L)+k2)+((k(1).*I)+k(2))-sqrt((((k1.*L)+k2)-
((k(1).*I)+k(2)))^2+4*k1*k(1)*L*I))).*x)) );
initialGuess = [0.005 0.016];
    [beta, R, J, CovB, MSE ] =
nlinfit(x(:,1),x(:,2),Model,initialGuess);
% Fit model to data.
    n=length(x(:,2));      %#data points
    df=n-2-1 ;   %#data points  - #parameters -1
    y=x(:,2);
   min_x=min(x(:,1));
   max_x=max(x(:,1));

    xfit=[min_x:  1:  max_x];
    xfit=x(:,1);

yfit=((N*k1*L)/((0.5.*(((k1.*L)+k2)+((beta(1,1).*I)+beta(
```

```
1,2))+sqrt((((k1.*L)+k2)-
((beta(1,1).*I)+beta(1,2)))^2+4*k1*beta(1,1)*L*I)))-
(0.5.*(((k1.*L)+k2)+((beta(1,1).*I)+beta(1,2))-
sqrt((((k1.*L)+k2)-
((beta(1,1).*I)+beta(1,2)))^2+4*k1*beta(1,1)*L*I))))).*(
((beta(1,2)*((0.5.*(((k1.*L)+k2)+((beta(1,1).*I)+beta(1,2
))+sqrt((((k1.*L)+k2)-
((beta(1,1).*I)+beta(1,2)))^2+4*k1*beta(1,1)*L*I)))-
(0.5.*(((k1.*L)+k2)+((beta(1,1).*I)+beta(1,2))-
sqrt((((k1.*L)+k2)-
((beta(1,1).*I)+beta(1,2)))^2+4*k1*beta(1,1)*L*I)))))/((0
.5.*(((k1.*L)+k2)+((beta(1,1).*I)+beta(1,2))+sqrt((((k1.*
L)+k2)-
((beta(1,1).*I)+beta(1,2)))^2+4*k1*beta(1,1)*L*I)))*(0.5.
*(((k1.*L)+k2)+((beta(1,1).*I)+beta(1,2))-
sqrt((((k1.*L)+k2)-
((beta(1,1).*I)+beta(1,2)))^2+4*k1*beta(1,1)*L*I))))) +
(((beta(1,2)-
(0.5.*(((k1.*L)+k2)+((beta(1,1).*I)+beta(1,2))+sqrt((((k1
.*L)+k2)-
((beta(1,1).*I)+beta(1,2)))^2+4*k1*beta(1,1)*L*I))))/(0.5
.*(((k1.*L)+k2)+((beta(1,1).*I)+beta(1,2))+sqrt((((k1.*L)
+k2)-
((beta(1,1).*I)+beta(1,2)))^2+4*k1*beta(1,1)*L*I)))).*exp
(-
(0.5.*(((k1.*L)+k2)+((beta(1,1).*I)+beta(1,2))+sqrt((((k1
.*L)+k2)-
((beta(1,1).*I)+beta(1,2)))^2+4*k1*beta(1,1)*L*I))).*x))
- (((beta(1,2)-
(0.5.*(((k1.*L)+k2)+((beta(1,1).*I)+beta(1,2))-
sqrt((((k1.*L)+k2)-
((beta(1,1).*I)+beta(1,2)))^2+4*k1*beta(1,1)*L*I))))/(0.5
.*(((k1.*L)+k2)+((beta(1,1).*I)+beta(1,2))-
sqrt((((k1.*L)+k2)-
((beta(1,1).*I)+beta(1,2)))^2+4*k1*beta(1,1)*L*I)))).*exp
(-(0.5.*(((k1.*L)+k2)+((beta(1,1).*I)+beta(1,2))-
sqrt((((k1.*L)+k2)-
((beta(1,1).*I)+beta(1,2)))^2+4*k1*beta(1,1)*L*I))).*x))
);
    yfit=yfit(:,1);

    yresid=R ;        %y-yfit;
    SSresid = sum(yresid.^2);
    SStotal = (n-1) * var(y);
    r2 = 1 - SSresid/SStotal;
```

```
    adjr2=1-((1-r2)*((n-1)/df));
end
```

Appendix C

$A_{2A}R$ DHPC Purification

Reduction of $A_{2A}R$-DHPC Oligomers

To confirm that the oligomers were not disulfide-linked, purified $A_{2A}R$ were incubated with tris-(2-carboxyethyl)phosphine (TCEP). Incubating the samples with TCEP affected the mobility of $hA_{2A}R$ monomers and oligomers, as the receptor contains four disulfide bonds. However, the oligomers are still present after the incubation with TCEP, indicating that the oligomeric interactions do not involve intermolecular disulfide bonds.

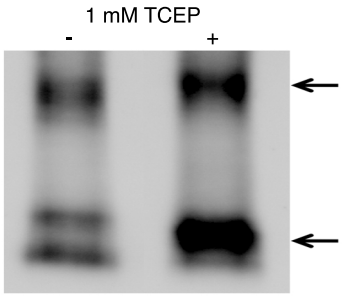

Figure C.1 Effect of TCEP on $A_{2A}R$ monomers and oligomers solubilized in DHPC. $A_{2A}R$ solubilized in DHPC was incubated with 1 mM TCEP, separated via a 10% precast stain-free polyacrylamide gel (Bio-Rad), and transferred to a nitrocellulose membrane using the Trans-Blot Turbo transfer System (Bio-Rad) for Western blot detection with an anti-A_{2A} monoclonal antibody, as described in the Material and Methods. The mobility of $hA_{2A}R$ (-) was compared with the mobility of $hA_{2A}R$ incubated with 1 mM TCEP (+). The arrows indicate the $hA_{2A}R$ monomers and oligomers.

Presence of Mitochondrial Membrane Proteins in DHPC Preparation

The main impurities observed in the DHPC preparations were identified via mass spectrometry as F1F0 ATP synthase (*a) and ADP/ATP transporter (*b). The ability of various detergents to solubilized other contaminants is commonly encountered [1].

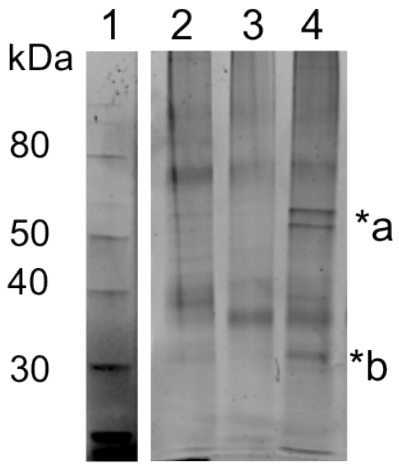

Figure C.2 $A_{2A}R$ solubilized in various micellar environments. $A_{2A}R$ protein bands were separated in 12% SDS-PAGE, stained with Sypro Ruby. Lane (1) contains MagicMark protein standard, with molecular weights indicated on the left. Lane (2) $A_{2A}R$ purified from membrane preparations using DCC (0.1% DDM, 0.1% CHAPS, and 0.02% CHS). Lane (3) $A_{2A}R$ purified from membrane preparations using DDM (0.1%). Lane (4) $A_{2A}R$ purified from membrane preparations using the short hydrocarbon chain lipid (0.8% DHPC). The main impurities were identified via mass spectrometry as F1F0 ATP synthase (*a) and ADP/ATP transporter (*b).

GC/MS Results

The CG/MS procedure was developed and conducted by Dr. Robert Standaert at Oak Ridge National Laboratory.

Sample 1, $A_{2A}R$ in DCC

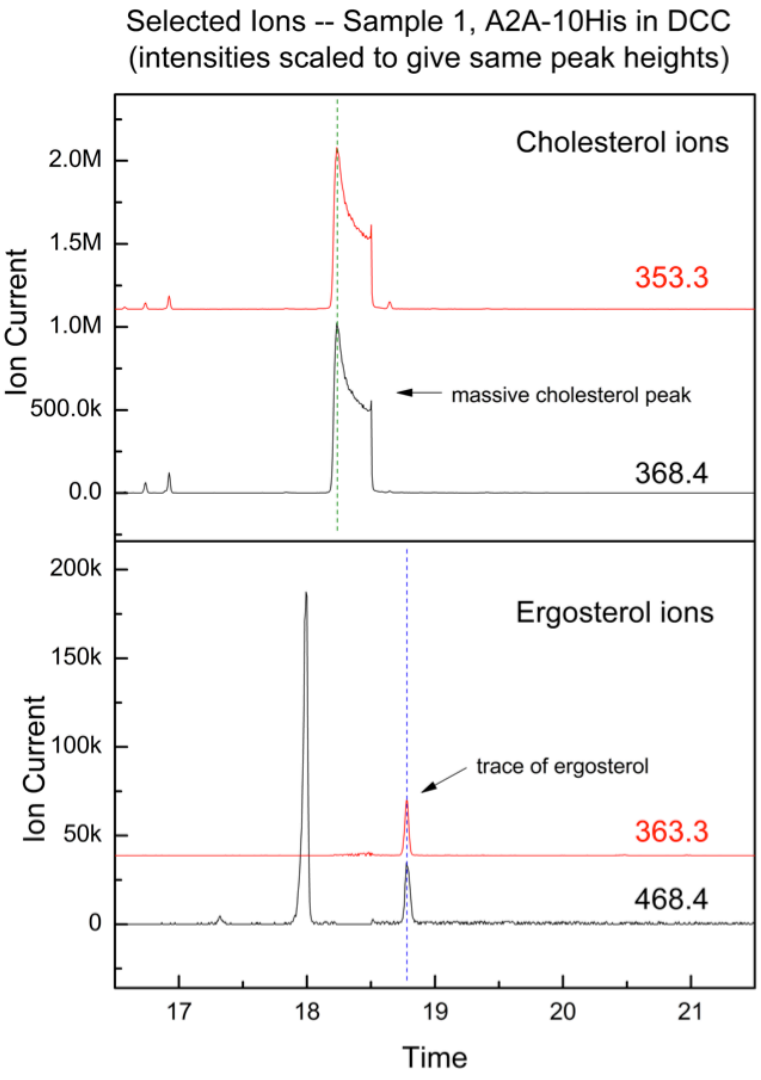

Figure C.3 GC/MS results for $A_{2A}R$ solubilized in DCC

Sample 2, $A_{2A}R$ in DDM

Note the trace of cholesterol (similar to blank) and absence of ergosterol.

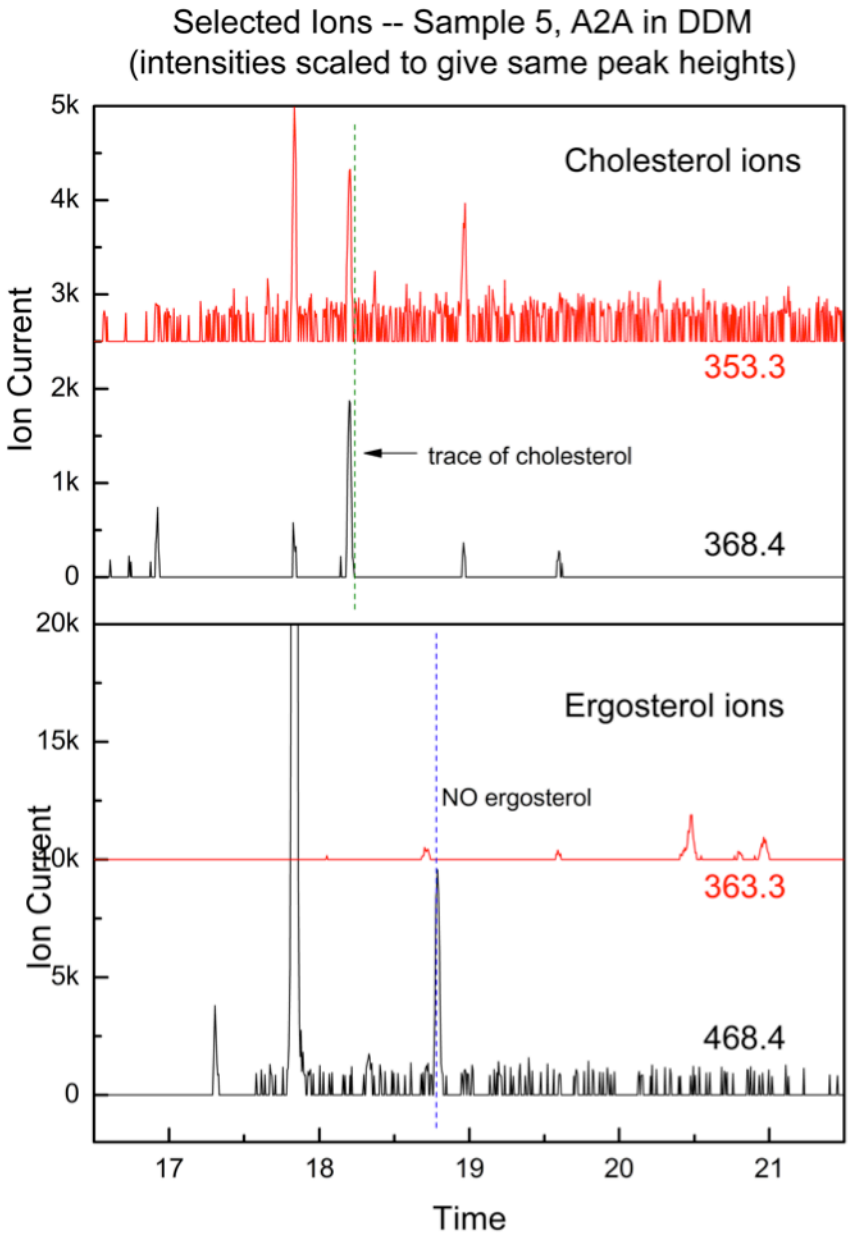

Figure C.4 GC/MS results for $A_{2A}R$ solubilized in DDM

Sample 3, $A_{2A}R$ in DHPC.

Note the trace of cholesterol (similar to blank) and absence of ergosterol.

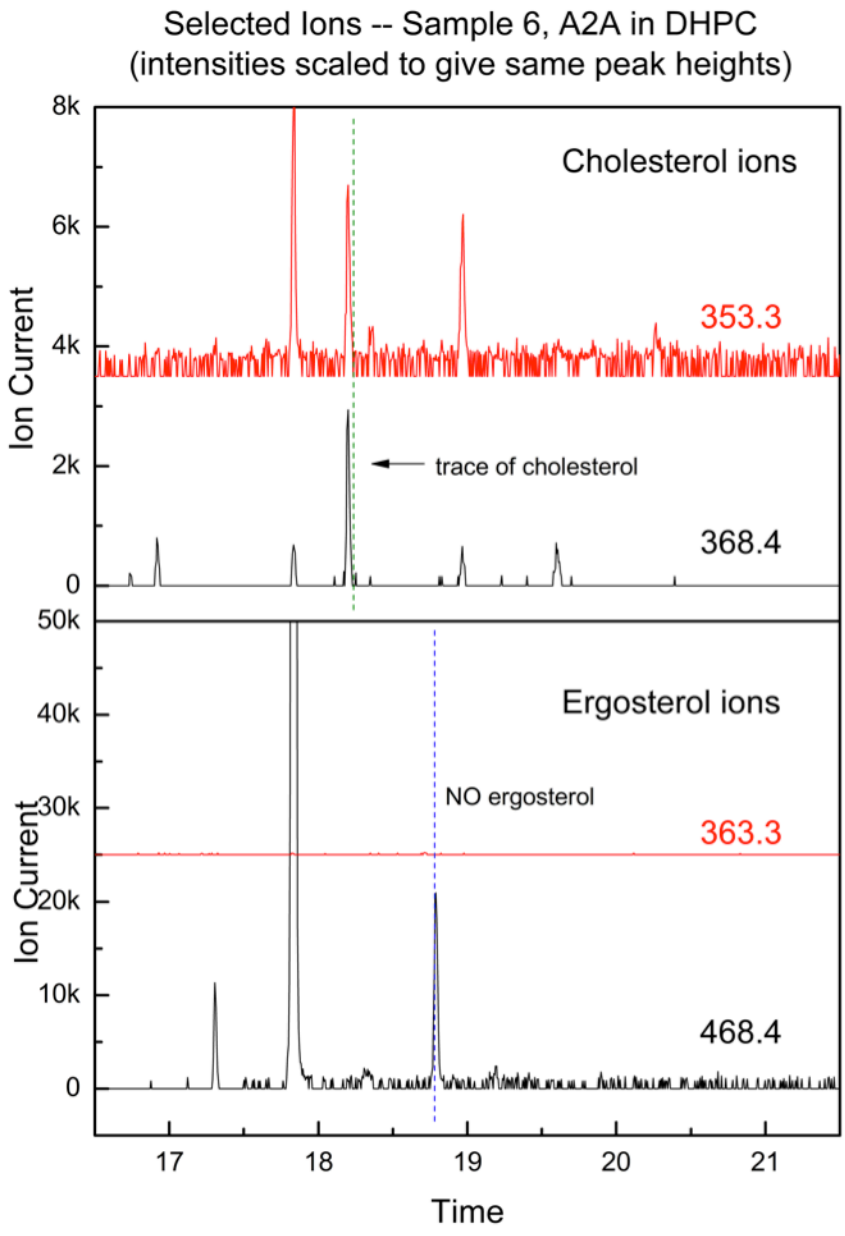

Figure C.5 GC/MS results for $A_{2A}R$ solubilized in DHPC

GPCR Crystal Structures: Solubilization and Reconstitution Systems

Table C.1 GPCRs with high-resolution X-ray crystal structures. Receptor source, expression, purification, and reconstitution systems used. The list of GPCRs with known crystallographic structures was obtained from S. H. White's website, Membrane Proteins of Known 3D Structures, http://blanco.biomol.uci.edu/mpstruc/listAll/list, as of November, 2012.

Rodopsin Source: *Bos taurus,* purified from bovine retina, COS-1 and HEK293S-GnTI$^-$ cells *Todarodes pacificus,* purified from squid retina		
Detergents used for solubilization: Heptanetriol, heptylthioglucoside, octylglucoside, octyltetraoxyethylene (C8E4), nonylglucoside, decylmaltoside, dodecylmaltoside (DDM), lauryldimethyl amine oxide (LDAO)	Some protocols involved detergent exchange to octylglucoside or C8E4 or additions prior to crystallization: • LDAO • Brain lipid extract	[2-19]
β_1-adrenergic receptor. Source: *Meleagris gallopavo*, purified from High 5^{TM} insect cells		
Detergents used for solubilization: • Decylmaltoside • DDM	Some protocols involved detergent exchange to: Octylthioglucoside, hega-10 or additions prior to crystallization of cholesterol hemisuccinate (CHS)	[20-24]
β_2-adrenergic receptor. Source: *Homo sapiens,* purified from Sf9 insect cells		
Detergent used for solubilization: • DDM • DDM with CHS	Some protocols involved detergent exchange to Lauryl maltose neopentyl glycol (LMNG) or additions prior to crystallization: • DMPC and CHAPSO • Monoolein and cholesterol, to form lipidic cubic phase (LCP) • Modified monoolein (7.7 MAG) and cholesterol, to form LCP	[25-33]
A_{2A} adenosine receptor. Source: *Homo sapiens,* purified from Sf9 insect cells and *P. pastoris* yeast cells.		
Detergents used for solubilization: • Decylmaltoside • DDM with CHS	Some protocols involved detergent exchange to: Octylthioglucoside, nonylglucoside or additions prior to crystallization of monoolein and cholesterol, to form LCP	[34-40]
CXCR4 chemokine, Dopamine D3, Sphingosine 1-phosphate, κ-opioid, Nociceptin/orphanin FQ receptors. Source: *Homo sapiens,* purified from Sf9 Histamine H1 receptor. Source: *Homo sapiens,* purified from *P. pastoris* yeast cells		
Detergents used for solubilization: DDM with CHS	Monoolein and cholesterol were added prior to crystallization to form LCP	[41-46]
M2 muscarinic acetylcholine receptor. Source: *Homo sapiens,* purified from Sf9		
Detergent used for solubilization: Decylmaltoside	Addition prior to crystallization: • LMNG • Monoolein and cholesterol, to form LCP	[47]
M3 muscarinic acetylcholine receptor. Source: *Rattus norvegicus,* purified from Sf9		
Detergents used for solubilization: DDM with CHS	Detergent exchange to LMNG, followed by addition of monoolein and cholesterol, to form LCP	[48]
μ-opioid receptor. Source: *Mus musculus,* purified from Sf9		
Detergents used for solubilization: DDM, CHAPS and CHS	Detergent exchange to LMNG, followed by addition of monoolein and cholesterol, to form LCP	[49]
δ-opioid receptor. Source: *Mus musculus,* purified from Sf9 Neurotensin receptor NTSR1. Source: *Rattus norvegicus*, purified from *Trichoplusia ni* insect cells		
Detergents used for solubilization: LMNG with CHS	Monoolein and cholesterol were added prior to crystallization to form LCP	[50, 51]

REFERENCES

1. Allen, S.J., et al., *Expression, purification and in vitro functional reconstitution of the chemokine receptor CCR1.* Protein expression and purification, 2009. **66**(1): p. 73-81.

2. Choe, H.W., et al., *Crystal structure of metarhodopsin II.* Nature, 2011. **471**(7340): p. 651-5.

3. Deupi, X., et al., *Stabilized G protein binding site in the structure of constitutively active metarhodopsin-II.* Proceedings of the National Academy of Sciences of the United States of America, 2012. **109**(1): p. 119-24.

4. Edwards, P.C., et al., *Crystals of native and modified bovine rhodopsins and their heavy atom derivatives.* Journal of Molecular Biology, 2004. **343**(5): p. 1439-50.

5. Li, J., et al., *Structure of bovine rhodopsin in a trigonal crystal form.* Journal of Molecular Biology, 2004. **343**(5): p. 1409-38.

6. Murakami, M. and T. Kouyama, *Crystal structure of squid rhodopsin.* Nature, 2008. **453**(7193): p. 363-7.

7. Murakami, M. and T. Kouyama, *Crystallographic analysis of the primary photochemical reaction of squid rhodopsin.* Journal of Molecular Biology, 2011. **413**(3): p. 615-27.

8. Okada, T., et al., *Functional role of internal water molecules in rhodopsin revealed by X-ray crystallography.* Proceedings of the National Academy of Sciences of the United States of America, 2002. **99**(9): p. 5982-7.

9. Okada, T., et al., *X-Ray diffraction analysis of three-dimensional crystals of bovine rhodopsin obtained from mixed micelles.* Journal of Structural Biology, 2000. **130**(1): p. 73-80.

10. Okada, T., et al., *The retinal conformation and its environment in rhodopsin in light of a new 2.2 A crystal structure.* Journal of Molecular Biology, 2004. **342**(2): p. 571-83.

11. Okada, T., K. Takeda, and T. Kouyama, *Highly selective separation of rhodopsin from bovine rod outer segment membranes using combination of divalent cation and alkyl(thio)glucoside.* Photochemistry and photobiology, 1998. **67**(5): p. 495-9.

12. Palczewski, K., et al., *Crystal structure of rhodopsin: A G protein-coupled receptor.* Science, 2000. **289**(5480): p. 739-45.

13. Park, J.H., et al., *Crystal structure of the ligand-free G-protein-coupled receptor opsin.* Nature, 2008. **454**(7201): p. 183-7.

14. Salom, D., et al., *Improvements in G protein-coupled receptor purification yield light stable rhodopsin crystals.* Journal of Structural Biology, 2006. **156**(3): p. 497-504.

15. Salom, D., et al., *Crystal structure of a photoactivated deprotonated intermediate of rhodopsin.* Proceedings of the National Academy of Sciences of the United States of America, 2006. **103**(44): p. 16123-8.

16. Scheerer, P., et al., *Crystal structure of opsin in its G-protein-interacting conformation.* Nature, 2008. **455**(7212): p. 497-502.

17. Shimamura, T., et al., *Crystal structure of squid rhodopsin with intracellularly extended cytoplasmic region.* The Journal of biological chemistry, 2008. **283**(26): p. 17753-6.

18. Standfuss, J., et al., *The structural basis of agonist-induced activation in constitutively active rhodopsin.* Nature, 2011. **471**(7340): p. 656-60.

19. Standfuss, J., et al., *Crystal structure of a thermally stable rhodopsin mutant.* Journal of Molecular Biology, 2007. **372**(5): p. 1179-88.

20. Moukhametzianov, R., et al., *Two distinct conformations of helix 6 observed in antagonist-bound structures of a beta1-adrenergic receptor.* Proceedings of the National Academy of Sciences of the United States of America, 2011. **108**(20): p. 8228-32.

21. Warne, T., et al., *Crystal structures of a stabilized beta1-adrenoceptor bound to the biased agonists bucindolol and carvedilol.* Structure, 2012. **20**(5): p. 841-9.

22. Warne, T., et al., *The structural basis for agonist and partial agonist action on a beta(1)-adrenergic receptor.* Nature, 2011. **469**(7329): p. 241-4.

23. Warne, T., et al., *Structure of a beta1-adrenergic G-protein-coupled receptor.* Nature, 2008. **454**(7203): p. 486-91.

24. Warne, T., et al., *Development and crystallization of a minimal thermostabilised G protein-coupled receptor.* Protein Expression and Purification, 2009. **65**(2): p. 204-13.

25. Bokoch, M.P., et al., *Ligand-specific regulation of the extracellular surface of a G-protein-coupled receptor.* Nature, 2010. **463**(7277): p. 108-12.

26. Cherezov, V., et al., *High-resolution crystal structure of an engineered human beta2-adrenergic G protein-coupled receptor.* Science, 2007. **318**(5854): p. 1258-65.

27. Hanson, M.A., et al., *A specific cholesterol binding site is established by the 2.8 A structure of the human beta2-adrenergic receptor.* Structure, 2008. **16**(6): p. 897-905.

28. Kobilka, B.K., *Amino and carboxyl terminal modifications to facilitate the production and purification of a G protein-coupled receptor.* Analytical Biochemistry, 1995. **231**(1): p. 269-71.

29. Rasmussen, S.G., et al., *Structure of a nanobody-stabilized active state of the beta(2) adrenoceptor.* Nature, 2011. **469**(7329): p. 175-80.

30. Rasmussen, S.G., et al., *Crystal structure of the human beta2 adrenergic G-protein-coupled receptor.* Nature, 2007. **450**(7168): p. 383-7.

31. Rasmussen, S.G., et al., *Crystal structure of the beta2 adrenergic receptor-Gs protein complex.* Nature, 2011. **477**(7366): p. 549-55.

32. Rosenbaum, D.M., et al., *Structure and function of an irreversible agonist-beta(2) adrenoceptor complex.* Nature, 2011. **469**(7329): p. 236-40.

33. Wacker, D., et al., *Conserved binding mode of human beta2 adrenergic receptor inverse agonists and antagonist revealed by X-ray crystallography.* Journal of the American Chemical Society, 2010. **132**(33): p. 11443-5.

34. Dore, A.S., et al., *Structure of the adenosine A(2A) receptor in complex with ZM241385 and the xanthines XAC and caffeine.* Structure, 2011. **19**(9): p. 1283-93.

35. Hino, T., et al., *G-protein-coupled receptor inactivation by an allosteric inverse-agonist antibody.* Nature, 2012. **482**(7384): p. 237-40.

36. Jaakola, V.P., et al., *The 2.6 angstrom crystal structure of a human A2A adenosine receptor bound to an antagonist.* Science, 2008. **322**(5905): p. 1211-7.

37. Lebon, G., et al., *Agonist-bound adenosine A2A receptor structures reveal common features of GPCR activation.* Nature, 2011. **474**(7352): p. 521-5.

38. Liu, W., et al., *Structural basis for allosteric regulation of GPCRs by sodium ions.* Science, 2012. **337**(6091): p. 232-6.

39. Xu, F., et al., *Structure of an agonist-bound human A2A adenosine receptor.* Science, 2011. **332**(6027): p. 322-7.

40. Warne, T., J. Chirnside, and G.F. Schertler, *Expression and purification of truncated, non-glycosylated turkey beta-adrenergic receptors for crystallization.* Biochimica et biophysica acta, 2003. **1610**(1): p. 133-40.

41. Wu, B., et al., *Structures of the CXCR4 chemokine GPCR with small-molecule and cyclic peptide antagonists.* Science, 2010. **330**(6007): p. 1066-71.

42. Chien, E.Y., et al., *Structure of the human dopamine D3 receptor in complex with a D2/D3 selective antagonist.* Science, 2010. **330**(6007): p. 1091-5.

43. Hanson, M.A., et al., *Crystal structure of a lipid G protein-coupled receptor.* Science, 2012. **335**(6070): p. 851-5.

44. Shimamura, T., et al., *Structure of the human histamine H1 receptor complex with doxepin.* Nature, 2011. **475**(7354): p. 65-70.

45. Wu, H., et al., *Structure of the human kappa-opioid receptor in complex with JDTic.* Nature, 2012. **485**(7398): p. 327-32.

46. Thompson, A.A., et al., *Structure of the nociceptin/orphanin FQ receptor in complex with a peptide mimetic.* Nature, 2012. **485**(7398): p. 395-9.

47. Haga, K., et al., *Structure of the human M2 muscarinic acetylcholine receptor bound to an antagonist.* Nature, 2012. **482**(7386): p. 547-51.

48. Kruse, A.C., et al., *Structure and dynamics of the M3 muscarinic acetylcholine receptor.* Nature, 2012. **482**(7386): p. 552-6.

49. Manglik, A., et al., *Crystal structure of the micro-opioid receptor bound to a morphinan antagonist.* Nature, 2012. **485**(7398): p. 321-6.

50. Granier, S., et al., *Structure of the delta-opioid receptor bound to naltrindole.* Nature, 2012. **485**(7398): p. 400-4.

51. White, J.F., et al., *Structure of the agonist-bound neurotensin receptor.* Nature, 2012. **490**(7421): p. 508-13.